Interaction Notes

Note 153

19 June 1973

SOME COMPUTATIONAL ASPECTS OF THIN WIRE MODELING

E. K. Miller

F. J. Deadrick

Lawrence Livermore Laboratory
University of California/Livermore, California

ABSTRACT

Some of the computational aspects which may affect the validity and applicability of a numerical solution for a thin-wire structure are considered in this paper. These include: (1) structure segmentation, (2) current expansions, (3) the thin-wire approximation, (4) matrix factorization roundoff error, (5) near-field numerical anomalies, (6) multiple junction treatment, (7) wire-grid modeling, and (8) computer time required. The discussion will be based upon results obtained from a subsectional-collocation and point-matching solution to the thin-wire integral equation, but the implications which arise are of a more general nature. Minimizing the possibly deleterious impact of the above on performing practical calculations will be discussed.

FOREWORD

Support for the work presented here was primarily provided by the Department of Transportation, United States Coast Guard. The authors are especially grateful to Mr. Walter O. Henry of the Coast Guard for his interest in this study and for making it possible. They also appreciate the co-operation of: G. J. Burke and E. S. Selden of MB Associates; Prof. B. J. Strait of Syracuse University; and Mr. W. Curtis of Boeing Aircraft Co.; who provided data and helpful information. The work was performed under the auspices of the U.S. Atomic Energy Commission.

ACKNOWLEDGEMENT

The authors would particularly like to thank Janet Brown for her many hours of diligence in preparing this manuscript.

2
Jan 9 1976

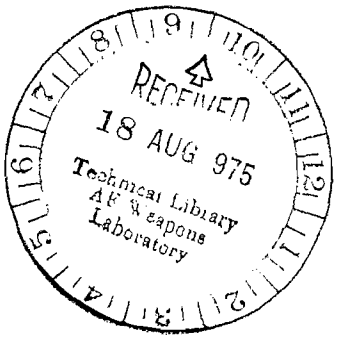

I. INTRODUCTION

Some of the computational aspects which may affect the validity and practical applicability of a numerical solution for a wire structure obtained from a moment method treatment are considered in this discussion. The results presented are, unless otherwise indicated, obtained from a sub-sectional collocation solution using point matching and a three-term current expansion of the thin-wire electric-field integral equation

$$\bar{E}^I(\bar{r}) \cdot \hat{t}(\bar{r}) = \frac{i\omega\mu_o}{4\pi} \int_{C(\bar{r})} I(\bar{r}') \left[\hat{t}(\bar{r}) \cdot \hat{t}(\bar{r}') + \frac{1}{k^2} [(\hat{t}(\bar{r}) \cdot \nabla)] [t(\bar{r}') \cdot \nabla)] \right] g \, ds' \qquad (1)$$

where

$$g = e^{-ikR}/R,$$

$$k = \omega\sqrt{\mu_o\varepsilon_o}$$

and

$$R = |\bar{r}-\bar{r}' + \bar{a}(\bar{r}')|$$

with $\hat{t}(\bar{r})$ the tangent vector to the wire at $\bar{r}$, $\bar{E}^I$ the incident field, $\bar{a}(\bar{r}')$ the wire radius at $\bar{r}'$ in the direction $\hat{t}(\bar{r}') \times (\bar{r}-\bar{r}')$ and the (suppressed) time variation $e^{i\omega t}$. The reader is referred to Harrington (1968) for the general approach and to Poggio and Miller (1970) for specific details. Where possible the findings which derive from this particular solution procedure are generalized to permit identification of the broader implications pertaining to similar numerical methods. Recommendations for avoiding possible pitfalls and more fully realizing the potential of such methods are also discussed.

II. NUMERICAL EXAMPLES

Some of the various aspects to be considered here include; A) current expansions; B) structural segmentation and boundary condition matching; C) multiple junction treatment; D) thin wire approximation; E) matrix factorization round-off error; F) near field behavior; G) wire grid modeling; and H) computer time requirements. Each of these items is discussed in turn below. The order of presentation is essentially that in which these various factors are encountered in an actual calculation.

A. Current Expansions

The type of current and charge basis function expansions used in the numerical solution is perhaps one of the most important and at the same time one of the most inconvenient factors to vary for numerical comparison. Computation of the impedance matrix elements is intimately related to the form chosen for the current variation. Thus in contrast to the relative ease with which the effects of varying the segmentation, boundary condition matching, etc., which require only minor program modifications, can be achieved, varying the basis function expansion will instead generally involve major changes. In spite of these difficulties, some studies have been performed (Richmond 1965 and Neureuther, et al. 1968), concerning the impact of using various kinds of current bases function expansions. Some of their results will be summarized below.

Before getting into specific numerical results, however, let us consider the general question of current basis function expansions appropriate for thin wire structures. We can basically divide the current expansions into two types: 1) complete domain representations and 2) sub-domain representations. A complete domain representation is one wherein the current expansion is applied over the entire wire structure. Such a complete domain representation for example, is typified by the use of a Fourier series for the current on a linear wire antenna. In this case the parameter of expansion is the number of expansion functions used in the Fourier series. The sub-domain representation is by contrast applied over sub-section portions of the entire structure. An example of this case is the pulse approximation for the currents on a linear wire antenna wherein the current on each of the N segments or pieces into which the antenna is divided is represented as constant. The distinction between the two forms becomes somewhat blurred as the segment size, and the number of constants which maybe associated with that segment, increases.

It is worthwhile to summarize some of the kinds of complete domain and sub-domain current expansions which have been or might be employed for wire antenna analysis. In Table I below are shown complete domain representations based on Fourier, MacLauren,

Chebyshev, Hermite, and LeGendre polynomial series [Richmond (1965)]. Results obtained by Richmond from using these expansions for analyzing the current excited on a linear dipole by a plane wave at broadside incidence are also shown in the Table. Richmond comments that the expansion based on the Chebyshev and LeGendre polynomials may be most promising for further investigation. For many reasons complete domain current representations have not been extensively employed in wire antenna theory.

TABLE I. Polynomial Series Current Expansions
(After Richmond, 1965)

Fourier:

$$I(z) = I_1 \cos \pi x/2 + I_2 \cos 3\pi x/2 + I_3 \cos 5\pi x/2 \quad + \quad +$$

MacLaurin:

$$I(z) = I_1 \quad + I_2 x^2 \quad + I_3 x^4 \quad + \quad +$$

Chebyshev:

$$I(z) = I_1 T_0(x) \quad + I_2 T_2(x) \quad + I_3 T_4(x) \quad + \quad +$$

Hermite:

$$I(z) = I_1 H_0(x) \quad + I_2 H_2(x) \quad + I_3 H_4(x) \quad + \quad +$$

LeGendre:

$$I(z) = I_1 P_0(x) \quad + I_2 P_2(x) \quad + I_3 P_4(x) \quad + \quad +$$

where

$$x = 2z/L$$

Coefficients for the Current I(z) for an Incident Plane Wave: $L = 0.5\lambda$; $a = 0.005\lambda$; $\theta_i = 90°$

Mode No. n	Fourier	MacLaurin	Chebyshev	Hermite	LeGendre
1	3.476	3.374	1.7589	8.2929	2.2763
2	0.170	4.037	1.5581	14.3644	2.1005
3	0.085	3.128	0.0319	4.4135	0.0655
4	0.055	4.101	0.0112	0.3453	0.0421
5	0.040	1.871	0.0146	0.0073	0.0372

Sub-domain representations seem to be more popular because they are apparently easier to use and generally speaking provide comparable accuracy with shorter calculation times. One possible explanation for this situation is that a complete domain representation in a series form such as illustrated above, requires integration over the entire wire structure for each of the N terms in the series. The sub-domain representation, however, involves integration of the term or terms used for the current representation over only a small part (one segment) of the entire structure. Furthermore by choosing the appropriate kinds of expansion functions it may be possible to perform such integrations analytically.

Before considering specific sub-domain expansions which have been employed let us consider some of the general implications of the sub-domain expansion function itself. For simplicity suppose we consider a simple isolated wire having no multiple junctions and divided into N equal length segments. Furthermore let us assume that the goal of our solution method is to obtain a numerical representation for the structure in terms of at most N samples for the currents on the structure. Let us then consider the implications of using one, two and three or more terms in the current expansion on each of the N segments.

1. <u>One Sample Per Segment</u>

The use of one expansion function per structure segment is generally realized via the pulse approximation. In this case the current on each segment is viewed as a constant, and, there being N segments, N unknowns or N sampled current values are the result, thus leading to an Nth order system for the numerical solution. The equations which are typically used in this case are obtained by point matching the boundary conditions at the centers of the structure N segments. This is achieved by the use of delta function weights. The nth segment expansion function and mth segment weight function can be represented in this case by

$$I_n(s') = A_n$$

$$W_m(s) = \delta(s-s_m)$$

where s_i is the midpoint coordinate of segment i. The convergence rate which is typically achieved using the pulse approximation for the currents can be quite slow. In Figure 1

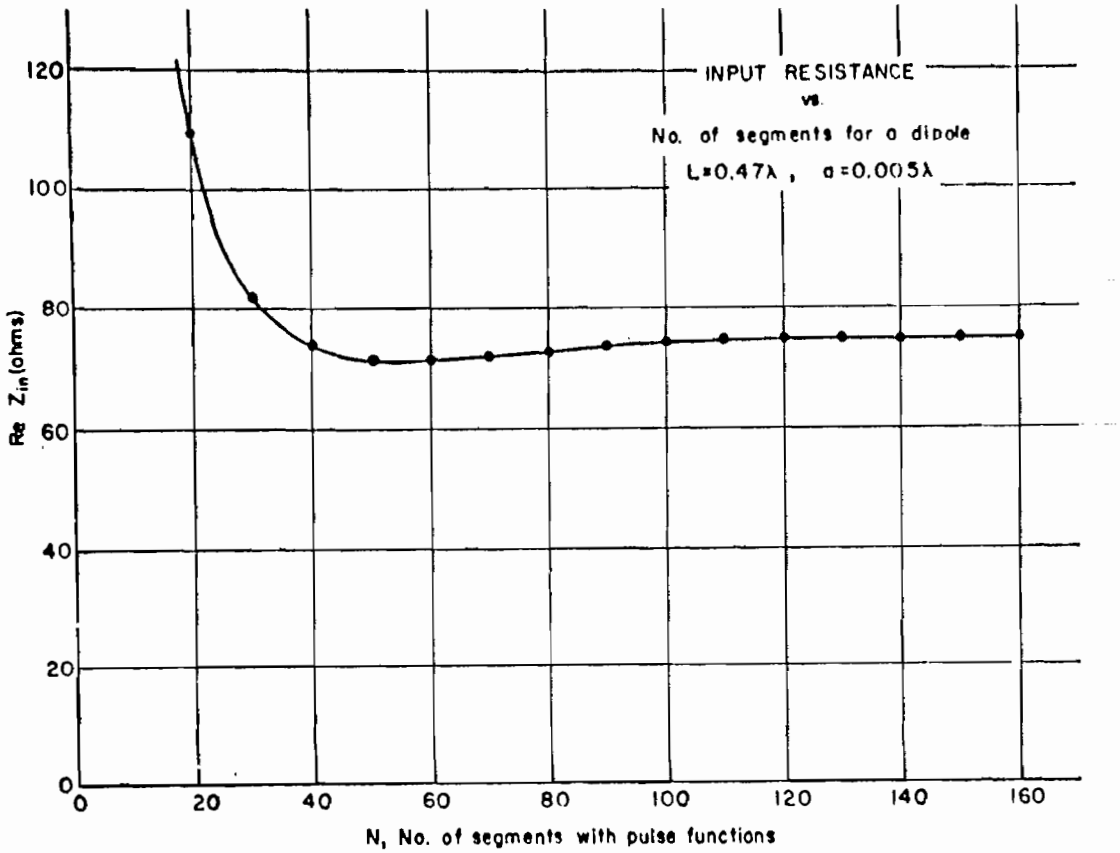

FIGURE 1a Curve showing convergence of input resistance as the number of pulse functions is increased.

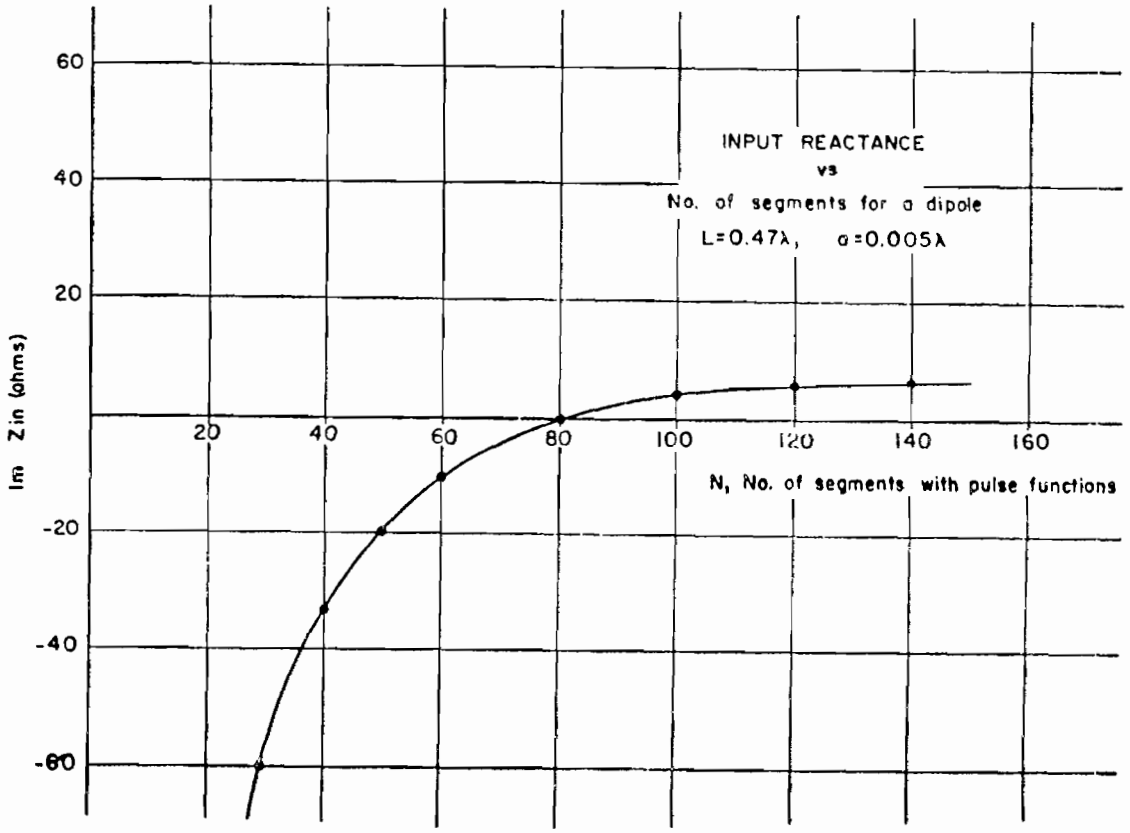

FIGURE 1b Curve showing convergence of input reactance as the number of pulse functions is increased. (After Thiele, 1970)

we present results due to Thiele (1970) which depict the input impedance of the half wave antenna as a function of N. It may be observed that a rather large number of segments is required per wave length before the input impedance stabilizes to what appears to be a useful numerical value. Further comparisons of the pulse approximation with other kinds of current expansions will be given below. The results of Figure 1 should not be taken to indicate however, that the pulse approximation is not a useful one for antenna analysis. What must be considered is not only the current expansion itself but the specific integral equation form and the weight functions used in reducing the integral equation to a linear system.

2. Two Functions Per Segment

There are understandably a considerable number of functions which might be employed in a two term expansion on each structure segment. Some of those which have been investigated include the piecewise linear, and piecewise sinusoidal forms employed by Chao and Strait (1970) and Richmond (1969) respectively. But note that the use of two terms per segment implies that two constants per segment are associated with the current expansion. For an N-segment structure this leads to 2N unknowns. Additional effort is thus required to reduce the system to the order of N unknowns in the final matrix representation for the structure. The most obvious procedure to employ for this purpose is that of matching currents at each of the N-1 segment junctions which exist on the N segment structure. This reduces the number of unknowns to N+1. With the two additional conditions that the current on the two open ends of the wire must vanish N-1 unknowns are then obtained for the N structure segments. These N-1 unknowns can be taken as the current amplitudes at the N-1 junctions of the N segments. For closed structures having N segments (a wire loop for example), N unknowns are obtained.

Since there are only N-1 unknowns on an open ended structure having N segments the method of matching boundary conditions on the N segments is no longer so obvious as for the case previously considered. We might derive N equations by computing the electric field at the centers of each of the N segments but we then have an over determined system for the N-1 unknowns. This could be reduced to an N-1 system by the method of regularization which is frequently employed in numerical methods. However, this procedure requires an N^3 operation before even obtaining the matrix from which we compute the antenna admittance via a subsequent inversion or fractorization. It could consequently be rather time consuming and inefficient. Instead we might consider computing the field values at the centers of the N segments by then performing a course integration which

involves adding each of these N equations together a pair at a time, and generate finally an N-1th order linear system. This is in fact essentially what Chao and Strait (1970) do in their use of the piecewise linear current approximation except that they compute the field at two points per segment rather than at a single point at the segment center. Richmond on the other hand employs Galerkin's method whereby he integrates the electric field on the antenna using as weight functions sinusoidal terms which are the same as those employed for the current expansion itself. The Chao and Strait approach it should be noted is also essentially a Galerkin's method since the weight functions employed for the boundary condition matching are the same piecewise linear forms as used for the current expansion. Note that it may not be advisable to compute the fields at the N-1 segment junctions because it is at these points that the current distribution has discontinuous derivatives which can result in poorly behaved field values (as discussed further below).

The expansion functions (linear and sinusoidal) and weight functions employed for the two term case are as listed below

$$I_n(s') = A_n \left[\frac{\sin k(s'-s_n+\Delta_n/2)}{(s'-s_n+\Delta_n/2)} \right] + B_n \left[\frac{\sin k(s'-s_n-\Delta_n/2)}{(s'-s_n-\Delta_n/2)} \right]$$

or equivalently

$$I_n(s') = I_n \left[\left[\frac{\sin k(s'-s_n+\Delta_n/2)}{(s'-s_n+\Delta_n/2)} \right] U_n(s'-s_n) + \left[\frac{\sin k(s'-s_{n+1}-\Delta_{n+1}/2)}{(s'-s_{n+1}-\Delta_{n+1}/2)} \right] U_{n+1}(s'-s_{n+1}) \right]$$

Also

$$W_m(s) = U_n(s-s_n) \left[\frac{\sin k(s-s_n+\Delta_n/2)}{(s-s_n+\Delta_n/2)} \right] + U_{n+1}(s-s_{n+1}) \left[\frac{\sin k(s-s_{n+1}-\Delta_{n+1}/2)}{(s-s_{n+1}-\Delta_{n+1}/2)} \right]$$

where Δ_i is the length of segment i and

$$U_n(s'-s_n) = \begin{cases} 1/\sin k\Delta_n & -\Delta_n/2 \le s'-s_n < \Delta_n/2 \\ 1/\Delta_n & \\ 0 & \text{otherwise} \end{cases}$$

3. Three Term Current Expansions

The most often used current representation employing three terms per structure segment is the so called sinusoidal expansion which involves a constant, sine and cosine term on each of the structure segments. This particular form was evidently first employed by Yeh and Mei (1967) and Andreason and Harris (1968). Obviously since there are N total segments on the structure, 3 N constants are associated with the current distribution. In order to reduce the system to on the order of N unknowns, approximately 2 N conditions on the current expansion must be derived.

Two approaches have been employed for this particular sinusoidal current expansion. One involves interpolation of the current on a given segment to its junction with the neighboring segments where the current amplitudes and derivatives are matched. Since there are N-1 junctions this procedure results in 2N-2 boundary conditions. A final two boundary conditions which require that the current be zero at the open ends of the wire then leads to a total of 2 N conditions on the current expansion functions. Thus N unknowns for the sampled current values on the structure can be identified for the subsequent linear system solution. For convience the N current samples generally used are the current values at the centers of each of the N structure segments. Note that since the current expansion on a given segment involves relating the three coefficients in its expansion with those of the segments connected to either of its ends, that a 2N by 2N linear system of equations is obtained from the 2N linear wire or circular loop and hence easily solveable. However, for general structures where there are multiple segments some additional complications can arise. Consideration of this point is deferred to Section V below.

An alternative approach for determining the 2 N equations required for reduction of the 3N system to Nth order was suggested by Yeh and Mei (1967). It involves writing the current on a given segment in terms of the current samples at the centers of its neighboring segments. This procedure also generates two equations for each of the structure segments. Furthermore the equations thus derived involve only the center current samples on the segments to which a given segment is connected. It is thus possible to solve for the expansion coefficients in terms of the unknowns (the center current samples) which will appear in the reduced Nth order system on a segment-by-segment basis. This procedure then bypasses the requirement for solving a 2 Nth order interpolation matrix prior to generation of the Nth order linear system. However, it is not as physically meaningful as

the first method suggested, and furthermore permits both current discontinuities and slope discontinuities at the junctions of adjacent segments. This possibility can give rise to rather poorly behaved fields along the structure as will be discussed below.

Another current expansion that might be considered for the three constant case is that of polynomial expansion involving constant, linear and quadratic terms. Such expansions, generally speaking, have not been as widely pursued as the sinusoidal expansion for at least two reasons: 1) the currents used in the sinusoidal expansion permit analytic intergration of all but one of the six field terms required per segment; 2) the sinusoidal expansion involves the kind of current behavior found on long wires and transmission lines where traveling wave currents exist. Since the basis functions used should resemble as closely as possible the actual current variation on the structure, it is obvious that the sinusoidal expansion is desirable from this viewpoint. However, in the limit of short structure segments we can conclude that the polynomial approximation to second order is essentially equivalent to the sinusoidal expansion since the latter also contains terms of second order for small argument.

A summary of the three term current expansions and associated weight functions is included below.

$$I_n(s') = A_n + B_n \left[\sin k(s'-s_n) \right] + C_n \left[\cos k(s'-s_n) \right]$$
$$\left[(s'-s_n) \right] \quad \left[(s'-s_n)^2 \right]$$

and

$$W_m(s) = \delta(s-s_m)$$

4. Four or More Expansion Functions Per Segment

There has evidently been little or no effort made to continue this sequence of current approximations by using four or more expansion functions per segment. The increased complexity which results from the need to obtain more relations between neighboring segment expansions, the selection of points for boundary condition calculations, etc. indicate generally that rather than using a single segment with four, five or more expansion functions, it may be preferable to instead use a segment of half the length with three expansion functions on each of the two halves, an essentially equivalent procedure. This basic approach has been found, for example, to work well

in developing adaptive numerical quadrature schemes wherein the number of integrand sample points per interval is limited to some maximum such as three or five and the increased sample densities required for rapidly varying parts of the intergrand are realized by using more intervals, rather than by employing longer intervals with greater numbers of integrand of abscissa samples and higher order quadrature rules per interval (Miller, 1971). We thus conclude our consideration of higher order of current expansion at this point.

While extensive examples demonstrating the relative desirability of the various current expansions discussed above are not available, some comparisons have been made and are included here to demonstrate the effects of varying the current expansion function used for a given application. In Figure 2 is shown the real part of the input admittance of a linear dipole as obtained from Hallen's and Pocklington's integral equation using various kinds of current expansions due to Neureuther et al. (1968). On this figure are shown the computed input conductance as a function of the number of segments per antenna for constant, linear, quadratic and sinusoidal current expansions in Hallen's integral equation and the sinusoidal current expansion for the Pocklington equation. We see as might be expected, that for the Hallen integral equation, the results tend to improve with the change from the linear to quadratic to the sinusoidal current forms but the sensitivity to the kind of current expansion used is not great. This is as expected since the Hallen integral equation contains only a lower order spatial variation in its kernel and therefore is not too sensitive to the differentiability of the current expansion employed for the solution. In the case of Pocklington's equation however, where a second order derivative appears on the Green's function, this is not the situation so that in proceeding from a constant or pulse approximation for the current to the sinusoidal expansion, considerably improved results are obtained (compare with Figure 1 for example).

Results somewhat similar to those of Neureuther et al. are presented in Table II again for a straight wire, but for the scattering case, and for wire lengths of 5.422, 11.2 and 14.57 wavelengths. Also varied in this calculation is the number of segments used to model the wire (for the 5.422 λ case). Both the backscatter cross section σ (in units of λ^2) and the matrix fill time are shown. The latter is for a CDC-6600 computer and includes the time reduction made possible by the matrix symmetry exhibited by a straight wire.

The relative agreement of the three methods can be seen to be very good, even in the case where N = 10 for the 5.422 λ wire so that $\Delta \sim \lambda/2$. The Hallen integral equation results however change less as the segment lengths become longer than do those obtained from the Pocklington equation. Matrix fill times for the Hallen pulse current expansion and the Pocklington three term expansion are comparable.

TABLE II. COMPARISON OF POCKLINGTON'S AND HALLEN'S INTEGRAL EQUATION SOLUTIONS

	Pocklington's Equation 3 Term		Hallen's Equation Pulse		Hallen's Equation 3 Term	
No. Of Segments	Integration Time (Sec) W/Sym.	σ/λ^2 (dB)	Time (Sec) W/Sym.	σ/λ^2 (dB)	Integration Time (Sec) W/Sym.	σ/λ^2 (dB)
5.422λ						
35	~ 0.3	8.131	0.37	7.784	0.76	7.864
30	~ 0.25	8.119	0.31	7.788	0.65	7.868
25	~ 0.2	8.109	0.26	7.809	0.54	7.879
20	~ 0.2	8.131	0.20	7.927	0.42	7.974
15	~ 0.18	8.283	0.15	8.075	0.32	8.094
10	~ 0.17	8.899	0.11	8.015	0.23	7.965
11.2λ						
70	0.8	11.710	0.86	11.755	----	-----
14.57λ						
100	~ 1	21.448	1.34	21.248	2.7	21.965

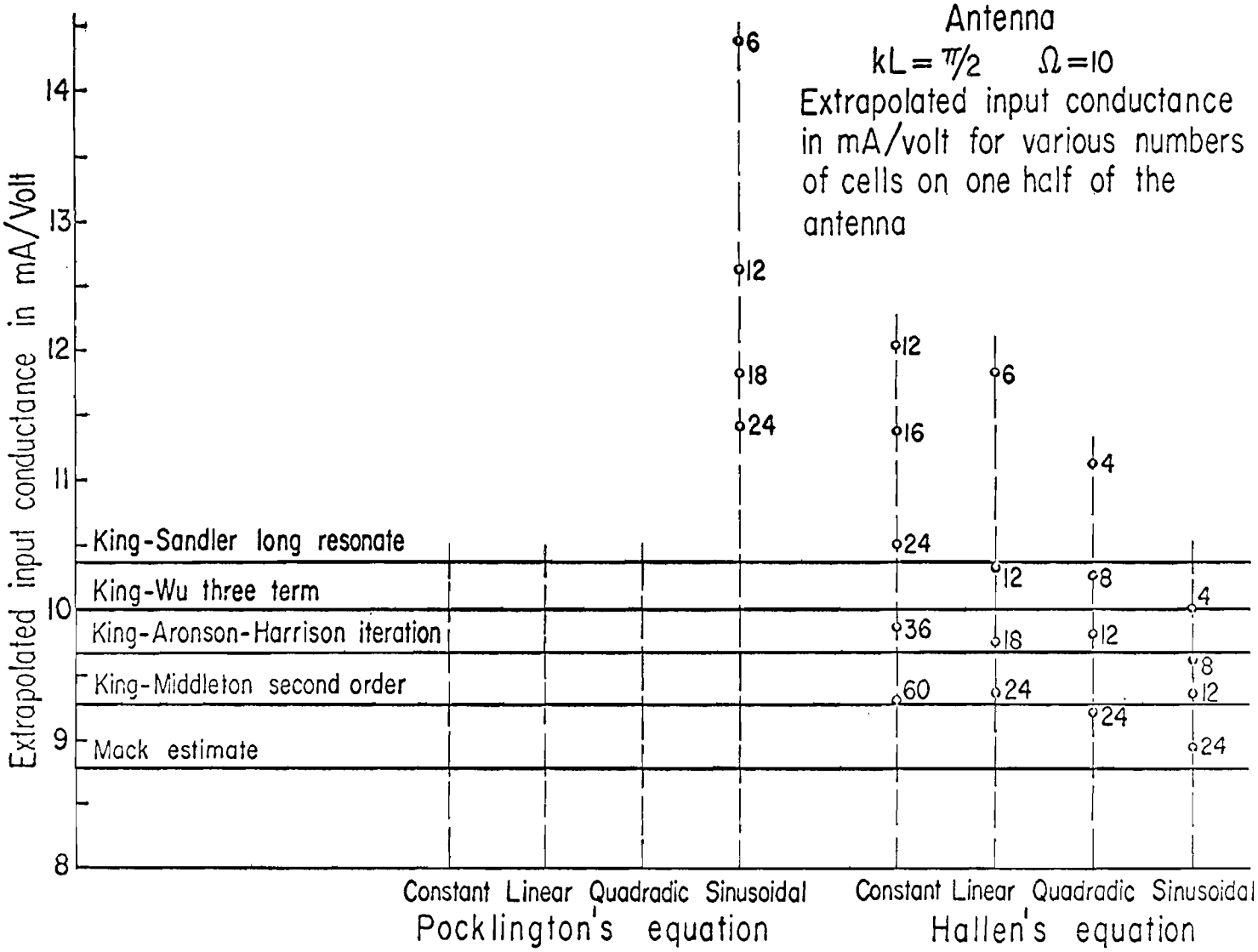

FIGURE 2 Calculated comparison of rates of convergence for various expansion functions (after Neureuther, 1968).

For other geometries, however, the Pocklington approach will generally be more efficient in this regard.

In Figures 3 and 4 are shown some computed results which compare the pulse and sinusoidal current expansions for solutions to Pocklington's integral equation for two separate scattering calculations. In the first the backscatter cross section for axial incidence on two coaxial circular rings is shown as a function of frequency.

This result was obtained from the Pocklington integral equation using both the pulse approximation and the three term expansion for the current. Obviously the three term current expansion provides much more accurate results for the same total number of current sample values in the integral equation. The pulse approximation, while not being accurate and actually missing the anti-resonance in the back-scatter cross section will produce more accurate results as the number of unknowns is increased, but obviously at the expense of increased computer time as well.

The other backscatter example, shown in Figure 4, depicts the radar cross section two dipoles crossed at an angle of 60° for a plane wave incident perpendicular to the dipole plane. In this case results are shown as a function of the number of segments on the two dipoles, again for the pulse approximation and the three term expansion. The results obtained for the latter converge with relatively few unknowns compared with the pulse approximation results which change rapdily and monotonically as a function of number of segments. The latter result has not converged to a stable value even with the maximum of 120 segments on the two dipoles. While we cannot state which result is the more accurate because we have no corroborating experimental data, it is obvious that the three term expansion provides more stable numerical results and hence might be reasonably expected to be more accurate than the more rapdily changing pulse approximation calculation.

Two things should be kept in mind however, when comparing calculations such as these. First, it is not only the current representation which is important to the overall numerical accuracy but the integral equation itself, from which the current solution is obtained, which is vitally important. For example, the results in Figure 2 show that the Pocklington integral equation with the pulse approximation provides very inaccurate results compared with the Hallen integral equation using the pulse approximation. Therefore generalizations on the basis of calculations derived from one kind of integral equation should be cautioned against. Second, a factor which is also very important, at least in practical applications, is the computer time required to obtain a given numerical accuracy. Obviously an approximation for the currents which is easier to integrate and which thus requires less computer time might be preferable to a more accurate current repre-sentation which requires more extensive computation to obtain the

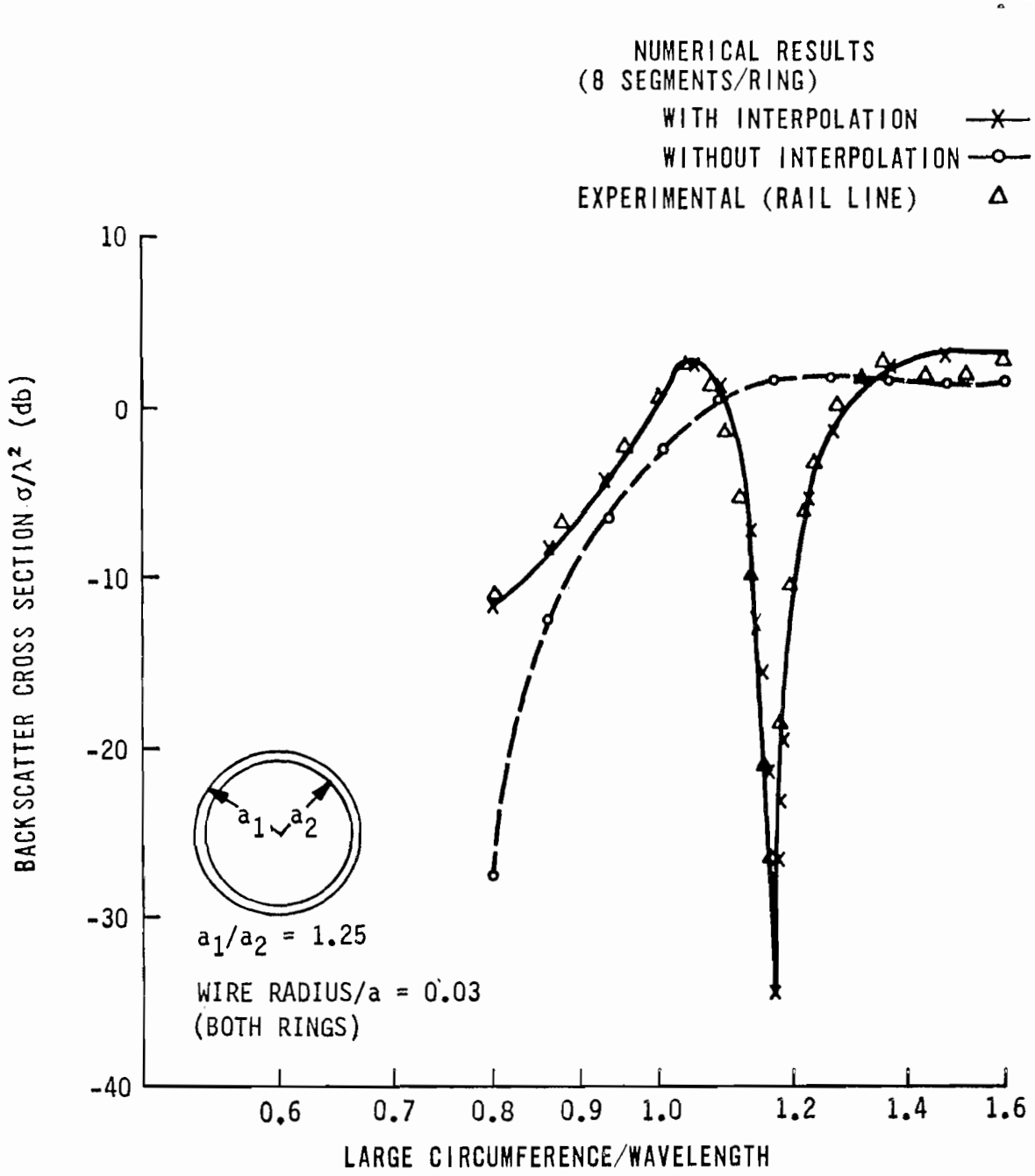

FIGURE 3 Frequency variation of the axial-incidence, backscatter rcs of two coaxial, coplanar rings showing the effect of sinusoidal current interpolation(after Poggio and Miller, 1970).

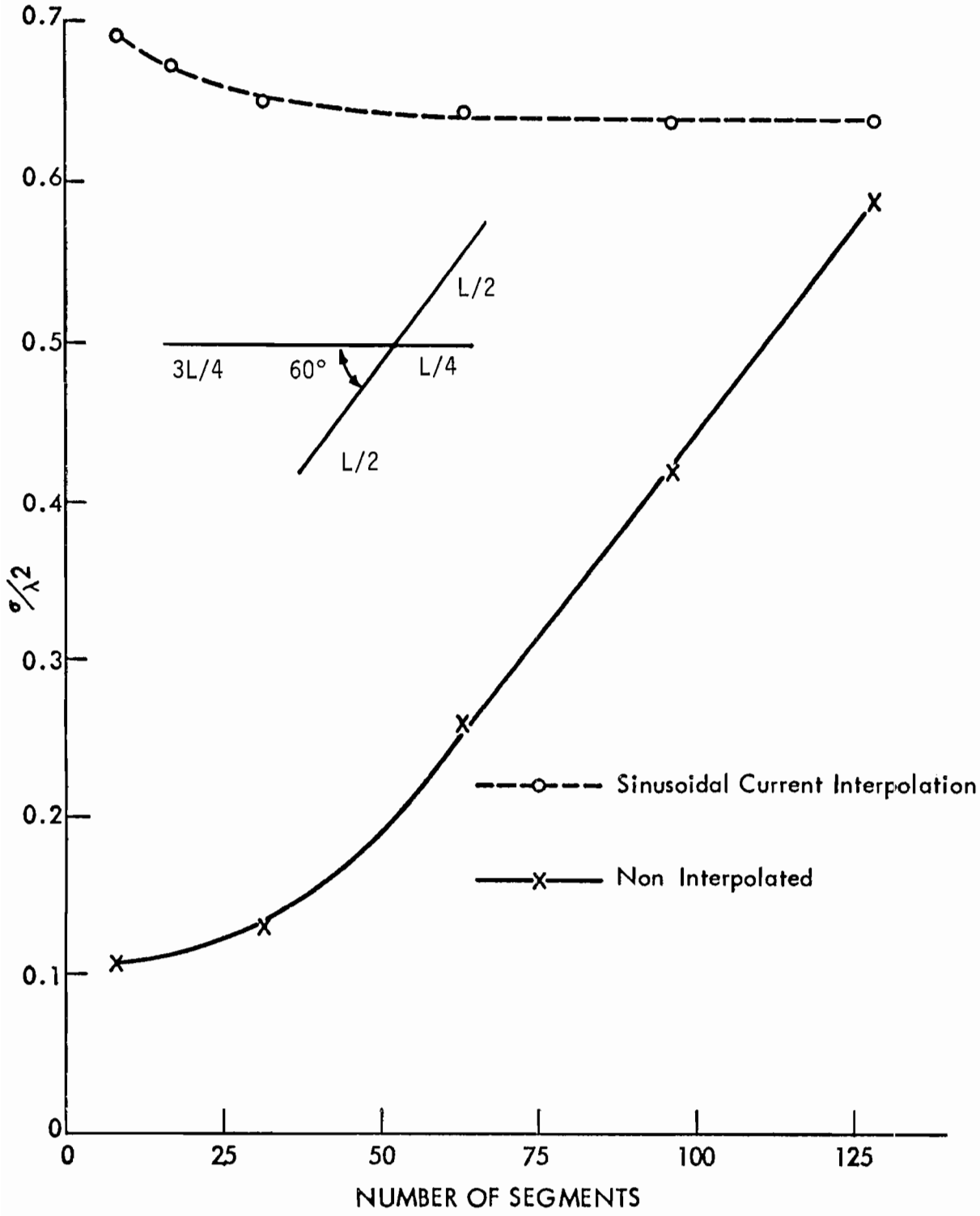

FIGURE 4 Backscatter rcs for skewed dipoles (after Poggio and Miller, 1970).

impedance matrix. Therefore the overall computation time to obtain a desired accuracy is perhaps ultimately more important than the number of current samples alone required for a given computational accuracy. The question of actual computer time requirements will not be discussed here but is deferred to Section H below.

B. Structural Segmentation and Boundary Condition Matching

There are two general aspects which must be considered when employing a moment method treatment for the solution of Maxwell's equations in integral-equation form. First, the current basis function expansion to be used and the possible segmentation of the structure into a set of approximate subdomains must be considered. This question was discussed in the previous section in connection with various kinds of current expansions which have been employed for wire structure analysis. Second, we must specify the way in which the boundary conditions on the field are to be numerically satisfied over the structure surface. These two questions are not unrelated since it is often convient to refer the current expansion and the boundary condition match points to the same set of coordinates on the structure. In employing subsectional collocation for example, we actually collocate the field match points and the current sample points. Even where the boundary condition matching is more general as in the approximate Galerkins method employed by Chao and Strait (1970) in connection with the piecewise linear current expansion, the field match points are referred in a fixed way to the current segment. Thus, when we speak of developing a numerical model for a wire structure we must simultaneously consider the impact of approximating the current distribution in an acceptable way as well as matching the boundary conditions on the total field along the structure. In the subsections which follow, we consider first the convergence rate of the numerical solution as a function of the number of segments for a variety of wire structures. We next discuss the impact of structure segmentation on boundary condition matching in the source region of antennas, and conclude with the effect of impedance loading on boundary condition matching.

1. Structural Segmentation

The development of a suitable numerical model for a given wire structure is of vital importance in obtaining efficient and accurate numerical results. For simpler structures such as the straight wire, circular ring, etc. there is not too much judgement required on the user's part. What is primarily required is a determination of the sample density necessary per unit wave length on the structure, at which point the development of a numerical model is straightforward and rather obvious. When however, the structure being considered is more complicated, a Rhombic antenna for example, or conical spirals and other more general kinds of antennas, the parameters of the numerical model to be used are no longer so clearly defined.

Some rule of thumb guidelines have been developed however, for a spectrum of representative structures encountered in practical applications. Such studies, one of which is summarized in Figures 5a and 5b due to Miller et al. (1971) have shown that, on the order of 6 to 20 samples per wave length are required to achieve an accuracy on the order of 10% or better in computed radar cross section results, antenna input impedance, etc. In addition it has been found that where practicable the segments on a structure ought to have as nearly equal lengths as possible. In actual application this is quite frequently not achieveable, for example, the feed region in a complicated antenna may be very small relative to the antenna size. Clearly one would not like to use small segments over the entire structure since this increases the computer time quite drastically. What is required in that case is some compromise, possibly using smaller segments near the feed region and letting the segments become longer as the distance from the feed region increases. However, this is too broad a question to answer in general and cannot be resolved without considering the specifics of a given problem.

2. Boundary Condition Matching

The use of equal length segments is intutitively acceptable and apparently mathematically desirable too for most problems. By matching the boundary conditions at segment centers (using sub sectional collocation) or some equivalent approach, the use of equal length segments ensures that the boundary match points are equally spaced along the structure as well. However, there is no necessity for collocating match points and segment centers. If the condition on the field match points is relaxed to allow the match points to be located at evenly spaced points along the structures while varying segment lengths are used to accomodate more rapid current variations in the vicinity of junctions and sources, possibly a more efficient numerical procedure might be developed. This kind of approach has not been investigated to any significant extent however. Care must be exercised in considering this more general approach incidentally; since field match points should not be located near discontinuities in the current or its derivative.

Besides the requirement that the total tangential field be zero at points on the structure away from the source, it is vitally important in performing antenna calculations to properly introduce the exciting field in the calculation. This is generally associated with the one (or more) segments on the structure which act as the source region. Such source segments thus serve to induce currents over the entire structure. Before computation of the antenna input admittance or impedance is possible however, the voltage associated with the source must be established. If all

Structure	Diagram	P	N_{ref}	σ_{ref}/λ^2
1. Straight Wire		0.477	96	2.60799×10^{-1}
2. Circular Ring		1.05	96	7.28953×10^{-1}
3. V Dipole	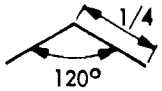	0.5	96	3.82747×10^{-1}
4. Equiangular, Planar Trifin	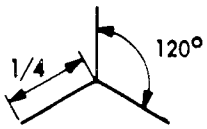	0.75	120	4.72534×10^{-1}
5. Planar, Log-Periodic Zig-Zag	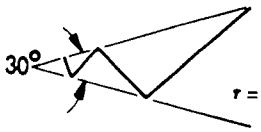	0.94	75	1.00809×10^{-1}
6. Crossed, Equal Length Dipoles	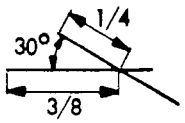	1.0	96	2.85001×10^{-1}
7. Equiangular Quadrafin	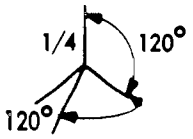	1.0	120	5.11386×10^{-1}
8. Squirrel Cage	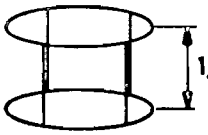	4.1	128	6.33890×10^{-1}
9. Conical Spiral	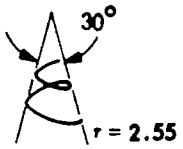	~1.0	96	1.16791×10^{-1}
10. Helix	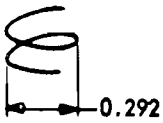	2.0	96	3.88346×10^{-2}

All Dimensions in Wavelengths
Total Wire Length = P
Expansion Factor = r (Log-Periodic Structures)
Wire Radius = 5×10^{-4}

FIGURE 5a Structures evaluated in segmentation study (after Miller, et al. (1971)).

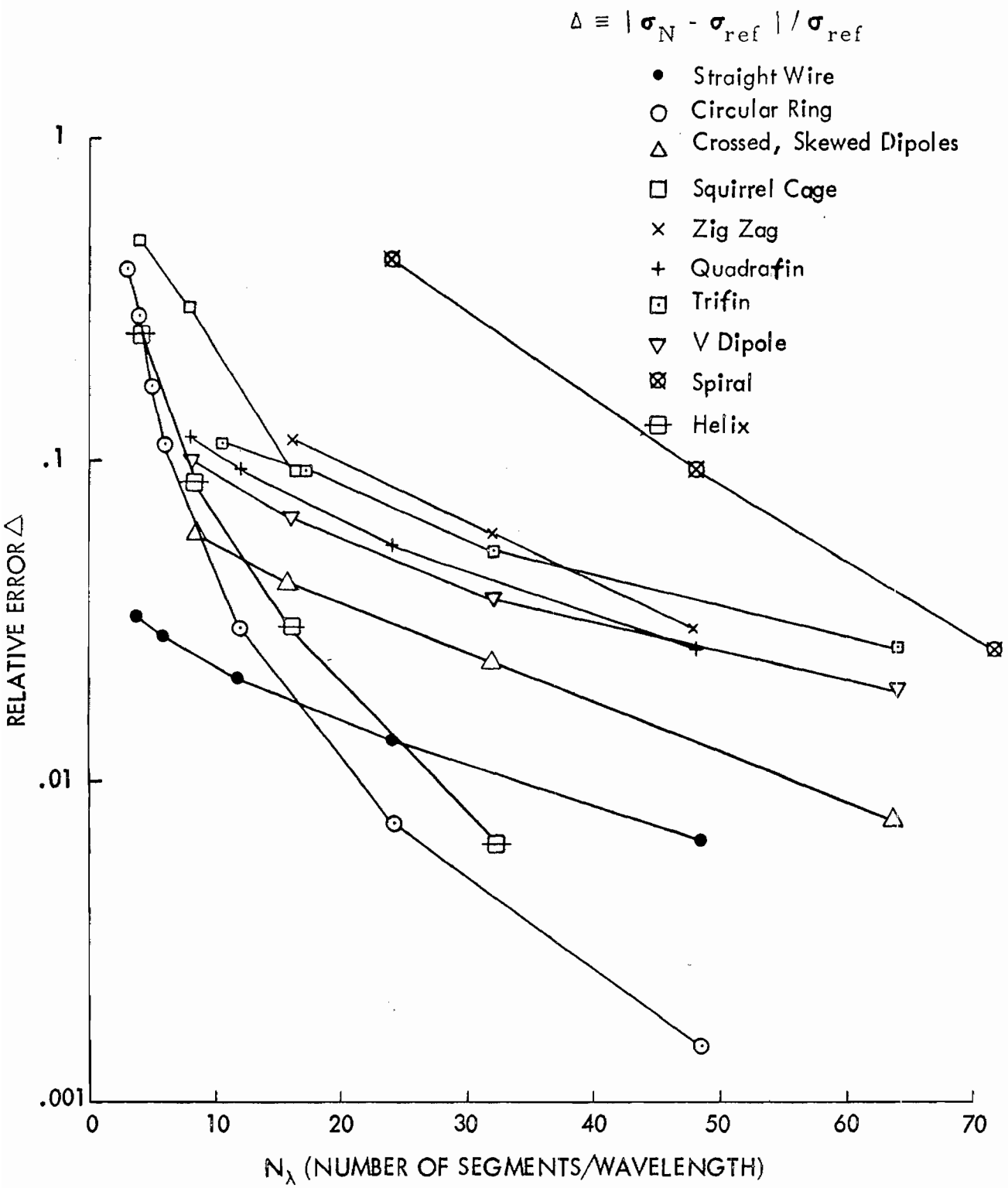

FIGURE 5b Relative error vs segments/wavelength for various structures (after Miller, et al. (1971)).

equal length segments are used in the structure it is generally accurate to consider the applied voltage on a given source segment equal the product of this segment length and the electric field value at its center. This however is an approximation which may not always be satisfied and which may furthermore be extremely sensitive to the structure segmentation.

As an example of the potential problem associated with structure segmentation and boundary condition matching we present in Table III some results obtained from a systematic variation of the model employed 21 equal length segments on the dipole with the center segment serving as the source. The tangential electric field on the source segment is taken as the negative voltage divided by the segment length, i.e. $E = -V/\delta$. For convenience we let V equal 1 volt.

Three variations from the nominal model were studied. In the first the center, or feed, segment was systematically shortened relative to the remaining 20 segments on the antenna so that the ratio R of the feed segment length δ to the length Δ of the remaining 20 equal length segments varied from 1 to 1/64 with the results shown in Part A of Table III. There we see that the input admittance defined by $Y = I_{feed}/(-E\delta)$ rapidly changes as a function of R, thus generating some skepticism as to the accuracy of the numerical results. While the dependence of the input susceptance of an antenna upon the feed region geometry is well known (Miller, 1967) it also is equally well known that the conductance should be relatively independent of the feed region geometry, contrary to the present results. Therefore, we conclude that something has been made invalid as a result of varying the feed segment length relative to the uniform segment lengths on the remainder of the antenna.

A part of the explanation may be due to the fact that the actual antenna input voltage is no longer really one volt. Recall that a tangential field is used as an exciting source, with the subsequent driving voltage derived by multiplying the field strength by the length of the excited segment. Since we have no control over what happens to the electric field between the match points on the antenna, we might suspect that by changing the feed segment relative to the others, the field variation between the segments has changed in a way which has caused the driving voltage defined as above, to be incorrect.

One possible way to maintain more control over the feed region field variation is to use segments on either side of the feed segment which are equal in length to it, so that the field becomes zero at one segment on either side of the applied

TABLE III. SEGMENT-LENGTH VARIATION FOR CENTER-FED DIPOLE

$\Omega = 15$
$N = 21$
$Y = I_{feed}/(-E^{I}\delta)$

A. Single Variable Feed Segment of Length δ

$$L = \frac{\lambda}{2} = (N-1)\ \Delta + \delta$$

$R = \delta/\Delta$	Y Millimhos
1	9.55 - i 5.16
1/2	11.74 - i 6.31
1/4	14.13 - i 7.57
1/8	15.99 - i 8.55
1/16	17.98 - i 9.60
1/32	23.53 - i 12.56
1/64	41.36 - i 22.08

B. Three Variable Length Segments at Center

$$L = \frac{\lambda}{2} = (N-3)\ \Delta + 3\delta$$

$R = \delta/\Delta$	Y Millimhos
1	9.55 - i 5.16
1/2	9.57 - i 5.13
1/4	9.67 - i 5.16
1/8	10.13 - i 5.39
1/16	11.45 - i 6.08
1/32	14.06 - i 7.45
1/64	16.19 - i 8.57

C. Two Variable Length Segments (n = 5,17)

$$L = \lambda/2 = (N-2)\ \Delta + 2\delta$$

$R = \delta/\Delta$	Y Millimhos
1	9.55 - i 5.16
1/2	9.57 - i 5.16
1/4	9.57 - i 5.16
1/8	9.57 - i 5.16
1/16	9.57 - i 5.16
1/32	9.57 - i 5.16
1/64	9.57 - i 5.16

electric field itself. The results of this parameter variation are shown in Part B of Table III where the center three segments on the antenna now have the length δ and the remaining 18 segments the length Δ. The results are again shown as a function of $R = \frac{\delta}{\Delta}$. In this case we find that as R becomes smaller, the input admittance remains relatively stable until R reaches a value of 1/32 or so. Beyond that point, there is again found the variation of input admittance previously demonstrated in Part I of the Table.

Finally, in Part C of Table III we examine the influence of placing variable length segments away from the feed region. The positions chosen are five segments from each end or the dipole. Again we denote the lengths of the shortened segments by δ and the remaining segment lengths by Δ with $R = \delta/\Delta$. The input admittance in this case is relative insensitive to the variation of R. This is significant in that it shows that unequal length segments located near, or in, the feed region have a much more profound influence on the calculated input admittance of an antenna than segments of unequal length located farther away.

It has been mentioned that the reason for this variation in the input admittance as a function of the source segment length may be that the applied field no longer results in a one volt source across the center of the antenna. The possibility that this is the case may be studied by integrating the electric field along the antenna in the vicinity of the source segment. We therefore present results in Table IV corresponding to those of Table III but where the input admittance is now defined to be the ratio of the feed point current divided by the integrated electric field, i.e., $Y = I_{feed}/-\int E d\ell$. Part A again corresponds to the case of a single variable length segment and Part B to three variable length segments. In contrast to the previous case where significant variations of input admittance were found as R became smaller we now find that the input admittance remains relatively insensitive to R. The integrated voltage value used to define the input admittance changes in such a way as to compensate for the input current variation, and thereby yields a nearly constant input admittance value. It should be noted that the integration range extends over approximately the center third of the antenna, and is terminated when the last segment integrated changes the voltage value by less than one percent.

This is an interesting and potentially useful result. While in practical cases we would naturally want to avoid the additional expense involved in integrating the electric field along the antenna to obtain a valid input admittance, at the same time knowledge that this might be a method whereby the input admittance

TABLE IV. SEGMENT VARIATION FOR CENTER-FED DIPOLE

$\Omega = 15$
$N = 21$
$Y = I_{feed}/(-\int E(s')ds')$

A. Single Variable Feed Segment of Length δ

δ/Δ	$V = -\int E(s')ds'$ Volts	Y Millimhos
1	1.000 + i 0.015	9.46 - i 5.31
1/2	1.227 + i 0.019	9.48 - i 5.29
1/4	1.476 + i 0.022	9.49 - i 5.27
1/8	1.670 + i 0.027	9.49 - i 5.27
1/16	1.876 + i 0.030	9.50 - i 5.27
1/32	2.456 + i 0.039	9.50 - i 5.27
1/64	4.321 + i 0.069	9.49 - i 5.26

B. Three Variable Length Segments at Center

δ/Δ	$V = -\int E(s')ds'$ Volts	Y Millimhos
1	1.000 + i 0.015	9.46 - i 5.31
1/2	1.001 + i 0.021	9.45 - i 5.32
1/4	1.006 + i 0.022	9.49 - i 5.33
1/8	1.052 + i 0.023	9.51 - i 5.33
1/16	1.187 + i 0.026	9.53 - i 5.33
1/32	1.454 + i 0.031	9.55 - i 5.33
1/64	1.675 + i 0.037	9.55 - i 5.33

could be obtained is worthwhile. Furthermore we know that calculations for radiation pattern, etc. which may not depend on knowing the input power or input admittance of the antenna could also be valid. It might therefore be concluded that for reasonably simple antennas useful input impedance and admittance data can be obtained by first deriving the current distribution and then obtaining the equivalent driving voltage from an integral of the electric field, procedure essentially equivalent to the classical emf method. Actual field variations along the antenna are shown below in Section F.

It is also worthwhile to determine the influence of segment length variations on the calculated input admittance for the antenna where the structure has a multiple junction. An antenna consisting of a straight center section and two outward point V loads having a 60° included angle symetrically located on each end of the center section was studied. In the nominal configuration this antenna had a total of 39 equal length segments; 3 on the center and 9 on each of the four arms. Two segment length variations were investigated for this particular structure. In the first, results of which are summarized in Table V, Part A the segment lengths on the center portion of the antenna were systematically shortened by using 5, 7, 9, etc. segments in place of the original 3. Corresponding input admittance results are indicated also in Table V, Part A where the variation of the input admittance obtained from an assumed applied voltage of one volt is seen to be significant as the number of center segments, and hence the ratio R, is varied. In Part B are summarized the results wherein only the center segment was shortened by replacing it with 3, 5, 7, etc. segments and exciting the center of those segments. Results obtained here also exhibit a variation in input admittance but not as marked as the previous case, indicating perhaps that unequal length segments at the multiple junction play a significant role in the admittance variation.

This study was repeated by defining the input admittance as a ratio of the feed current to the integral of the applied electric field in the vicinity of the source region. Results obtained

TABLE V. SEGMENT LENGTH VARIATION FOR CENTER-FED DIPOLE WITH V END LOADS

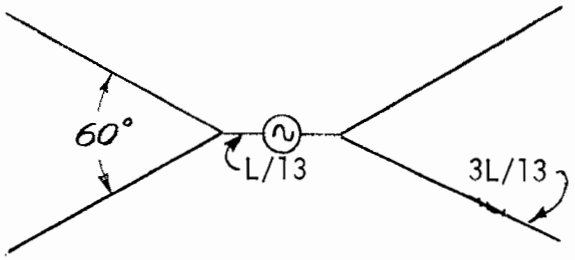

$\Omega = 2 \ln L/a = 15.4096$

$\frac{a}{\lambda} = 2.798 \times 10^{-4}$

$\frac{L}{\lambda} = 0.75 = (N-M)\Delta+M\delta$

$Y = I_{feed}/(-E^{I}\delta)$

A. M Equal Length Segments on Center Section *

δ/Δ	N	M	Y Millimhos
3/3	39	3	19.7 + i 12.2
3/5	41	5	23.1 + i 10.0
3/7	43	7	27.7 + i 4.2
3/9	45	9	28.5 - i 5.9
3/11	47	11	22.21 - i 14.36

B. Divisions of the Center Segment Into M Equal-Length Parts

δ/Δ	N	M	Y Millimhos
1	39	1	19.7 + i 12.2
1/3	41	3	19.6 + i 12.4
1/5	43	5	19.6 + i 12.4
1/7	45	7	19.7 + i 12.5
1/9	47	9	19.8 + i 12.5
1/11	49	11	19.8 + i 12.5

*Results obtained by employing Curtis' (1972) charge treatment for the junction together with the 3 term current vary only slightly over the δ/Δ range shown.

are summarized in Table VI. In a manner similar to the linear dipole example discussed above we find that the applied voltage, shown in Table VI does vary systematically as the feed region geometry is changed, and in a way which leads to the relatively stable value of input admittance as found for the linear dipole. These results indicate that integrating the electric field to define the antenna input admittance is apparently a valid procedure for general geometries. Note that the necessity for doing so is evidently sensitive to the multiple junction treatment used, as the admittance variation found here does not occur in results obtained by Curtis (1972) and Strait (1973), nor in time domain calculations which exploit the junction symmetry [Landt (1973)], which are furthermore obtained using $V = -E\delta$ rather than an integral definition of V.

There are it should be noted, other procedures whereby the exciting field or source can be introduced in the antenna calculation. One of those which have been developed and which is being applied to practical antenna problems is due to Andreason and Harris (1968) who introduce the exciting voltage at a segment junction. This is done by specifying a relationship between the current derivative discontinuity (charge) and the applied voltage, in terms of a bicone antenna model for the junction (Schelkenoff, 1952).

Another alternative to the tangential electric field source is to specify the current at the input segment to be of unit amplitude, permitting all other structure currents to be evaluated in the usual way. The antenna input impedance itself then must be found as above, from an integral of the resultant electric field over the antenna in the vicinity of the source current. This procedure has the disadvantage of course in requiring an expensive electric field integration.

3. Impedance Loading

Not all wire structures that are of practical concern can be considered to be perfectly conducting. There are two ways in which the effects of finite wire conductivity may become important. The first and most obvious occurs when the wire does indeed have a finite conductivity or where the skin depth is large enough compared to the wire diameter that the assumption of vanishing electric field along the wire is no longer strictly valid. This particular situation can be characterized as equivalent to a distributed load along the wire. The second occurs due to impedance loads located at discrete points along the wire. These might be included to modify the structure's resonant characteristics or to provide matched operation, e.g. the load on the end of a two wire transmission line. In the latter case then, the effect of the lumped impedance load is confined to a particular localized point(s) on the wire structure.

TABLE VI. SEGMENT LENGTH VARIATION FOR CENTER-FED DIPOLE WITH V END LOADS

$a/\lambda = 15$

$$\frac{L}{\lambda} = 0.75 = (N-M)\,\Delta + M\delta$$

$$Y = I_{feed}/(-\int E(s')ds')$$

A. M Equal Length Segments on Center Section

δ/Δ	N	M	$-\int E(s')ds'$	Y Millimhos
3/3	39	3	1.25 - i 0.26	13.13 + i 12.46
3/5	41	5	1.30 - i 0.48	13.39 + i 12.35
3/7	43	7	1.27 - i 0.89	13.06 + i 12.51
3/9	45	9	0.92 - i 1.33	13.02 + i 12.47
3/11	47	11	0.34 - i 1.44	13.18 + i 12.74

B. Division of the Center Segment Into M Equal-Length Parts

δ/Δ	N	M	$-\int E(s')ds'$	Y Millimhos
1/1	39	1	1.25 - i 0.26	13.13 + i 12.46
1/3	41	3	1.25 - i 0.25	13.21 + i 12.58
1/5	43	5	1.25 - i 0.25	13.08 + i 12.54
1/7	45	7	1.25 - i 0.26	12.94 + i 12.33
1/9	47	9	1.25 - i 0.26	13.16 + i 12.67
1/11	49	11	1.27 - i 0.26	13.05 + i 12.54

Either of these two cases is suited for treatment via the perfectly conducting wire integral equation (1) presented above by a suitable modification of the boundary condition matching along the wire. In the context of the point matching solution to the integral equation we generalize the boundary conditions by allowing for the additional effect of the voltage drop at each match point, in terms of the particular value of impedance located there. A distributed impedance load will in general then be modeled using a non-zero load impedance for each segment of the wire structure. In the case of lumped loading, on the other hand, only a few segments will have an associated impedance.

In either case then, the integral equation (1) may be modified to give

$$\bar{E}^I(\bar{r}) \cdot \hat{t}(\bar{r}) = \frac{i\omega\mu_0}{4\pi}\int_{C(\bar{r})} I(\bar{r})\left[\hat{t}(\bar{r}) \cdot \hat{t}(\bar{r}') + \frac{1}{k^2}\left[(\hat{t}(\bar{r}) \cdot \nabla)\right]\left[t(\bar{r}') \cdot \nabla)\right]\right] g\, ds'$$

$$- Z_L(\bar{r})\, I(\bar{r}) \qquad (1)'$$

where the Z_L I term added to the right hand side of the integral equation accounts for the effects of the added voltage drop associated with the non-perfect conductivity of the wire at $\bar{r}$. Note that the loads introduced here are what can be termed self loads. Mutual impedances which might characterize transformers coupling different parts of the structure can also be considered but for this discussion we confine ourselves to the self-impedance type load term only. In the two sections which follow we first consider the particular steps involved in applying the concept of impedance loading to imperfectly conducting and dielectric coated thin wires which we characterize as distributed loading, and conclude with a discussion of lumped impedance loading.

a. Distributed Impedance Loading

Our treatment of distributed impedance loading due to either finite wire conductivity or the presence of a dielectric sheath will follow the basic development presented by Cassidy and Feynberg (1960). Their approach was based on the treatment of a dipole scatterer. Here we will generalize the procedure

to the case of a wire structure excited as either an antenna or scatterer, and allow for the presence of a dielectric layer as well as for finite conductivity of the wire itself.

The basic procedure followed by Cassidy and Feynberg is to decompose the incident and scattered fields of a TM wave normally incident on a thin circular cylinder into the usual Fourier harmonics. By further assuming that the cylinder is small compared to all relevant wave lengths involved, only the zero order terms are then significant. Finally by relating the tangential electric and magnetic fields on the surface of the cylinder it is possible to define a surface impedance, which can in principal then be used in the wire integral equation to account for the finite conductivity of the circular wire. The formula presented by Cassidy and Feynberg for the case they considered is for a wire of radius w given by

$$z_s = \frac{i\eta_w}{2\pi w} \frac{J_0(k_w w)}{J_0'(k_w w)} = z_w \qquad (2)$$

with $k_w = k_0 \sqrt{\varepsilon_{rw}}$ and $\eta_w = \eta_0 \sqrt{\varepsilon_{rw}}$ the wave number and impedance respectively of the wire whose complex relative permitivity is ε_{rw}. The prime on the Bessel function of order zero, J_0 denotes differentiation with respect to the argument. Cassidy and Feynberg validated the results of this approach by comparing their calculations with experimental data for scattering from fine platinum wires with generally good agreement between experiment and theory.

By further extending the procedure above to allow for the effect of a thin dielectric layer of radius s on the circular cylinder and to subsequently define the surface impedance in terms of the tangential E and H at the surface of the dielectric-free space interface, it is possible to obtain a more general impedance formula which accounts for the effects of both finite wire conductivity and a sheath upon the scattering or radiating properties of a thin wire. The resulting expression, obtained in precisely the same manner as that discussed above for the uncoated wire, is

$$Z_s = Z(k_w, k_s) - Z(k_w, k_0) + Z_w \qquad (3)$$

where

$$Z(k_w,k_a) = \frac{i\eta_a}{2\pi s} \quad \frac{W(s,w') - W(s,w)(\eta_a/\eta_w)(J_w'/J_w)}{W(s',w') - W(s',w)(\eta_a/\eta_w)(J_w'/J_w)}$$

with

$$W(s^*,w+) = H_0^{(1)*}(k_a s)H_0^{(2)+}(k_a w) - H_0^{(1)+}(k_a w)H_0^{(2)*}(k_a s)$$

$$J_w = J_0(k_w w)$$

$$J_w' = J_0'(k_w w)$$

and the superscripts * and + corresponding to the primes denoting differentiation with respect to the argument. The sheath wave number and impedance are k_s and η_s respectively.

Note that the above expression is normalized with respect to the ratio of tangential E to H at the surface of the dielectric sheath when the sheath permitivity is allowed to approach that of the external medium. This is required since for non-zero sheath thicknesses, a non-zero value of sheath impedance would otherwise be obtained were the sheathless ratio of E to H not subtracted from the final results. Note in addition that the above formula exhibits the proper behavior as the sheath thickness becomes zero or the sheath permitivity becomes that of free space, becoming in each case Z_w, the impedance of the uncoated wire.

The above approach provides what appears to be a viable approach for including sheath and finite conductivity effects on the radiation and scattering properties of wire structures. The basic procedure has not been well validated however, because of the difficulty of obtaining corroborating experimental results. However the surface impedance approximation has been widely applied in similar problems involving two and three dimensional structures with generally good results when the assumptions necessary for the concept of a surface impedance to be validated are satisified. For a more general discussion of surface impedance see Senior (1960) or Mitzner (1967).

Alternative analyses for treating dielectric coated thin wires have also been examined. Richmond (1972) has considered the possibility of modeling the sheath in terms of the radially directed displacement current which is produced in the sheath by the radial-electric field. The electric field in turn can be related to the change density along the wire, and is thus derivable from the current distribution via the continuity equation. By using a Green's function in the integral equation appropriate to the external medium outside the wire-sheath combination, the sheath displacement currents can then be written in terms of the dielectric contrast between the sheath and the external medium and the sheath radial-electric field.

Similar problems have also been treated in connection with antennas immersed in a plasma where the ion sheath which forms about the body at floating potential in plasma is modeled as an effective capacitor between the antenna and the external medium. For short cylindrical antennas it is possible to express the input impedance of the antenna as a linear combination of the plasma impedance and sheath impedance (Balmain, 1969). A confocal sheath in the prolate spheriodal geometry has also been found useful (Lytle 1968). Thiele (1969) has used a treatment based on the actual current distribution in a finitely conducting wire to determine conductivity effects on scattering.

b. Lumped Impedance Loading

The approach for handling lumped or distributed impedance loads on a wire structure are not significantly different insofar as the numerical reduction of the integral equation itself is concerned. In either case a modified right hand side is obtained which involves the voltage drop on the particular structure segments whose impedance is non-zero. For the case of self impedance loads, only the diagonal elements in the impedance matrix are changed from the no-load case. This matrix can of course be subsequently solved by the usual method to allow for the effect of the specific loading arrangement.

However, the rational for specifying the value of impedance loads due to sheath and finite conductivity effects and for actual impedance loading are quite different. For the former, a procedure for determining the effective impedance load in terms of the physical parameters of interest, such as wire conductivity, sheath thickness, and sheath permittivity is required. For the latter, the impedance values need not be derived but are merely specified. There may thus be less uncertainty associated with the modeling of lumped impedances.

An additional factor which affects the nature of lumped impedance loading analysis is that only a few of the structure segments will generally be involved. It is possible to more efficiently perform a parameter variation involving the lumped impedance elements than would be true of distributed loading. Consider, for example, the case where a single structure element is loaded. The matrix version of the integral equation, written as

$$Z_{ij}\ I_j = E_i - \delta_{iL}\ Z_i\ I_i;\ i,j = 1,\ldots,N \tag{4}$$

where δ_{iL} is the Kroenecker delta function and L is the segment loaded with impedance Z_L may be seen to be modified only by the self impedance entry for the observation equation involving the loaded segment. We can therefore solve for the loaded structure current $I^{(L)}$ in terms of the unloaded solution $I^{(U)}$ as

$$I_i^{(L)} = Y_{ij}\ E_j - \delta_{jL}\ Z_j\ I_j^{(L)} \tag{5}$$

$$= I_i^{(U)} - Y_{ij}\ \delta_{jL}\ Z_j\ I_j^{(L)}$$

so that the effect of the impedance load can be summarized

$$I_L^{(L)} = \frac{I_L^{(U)}}{1 + Y_{LL}\ Z_L};\ i = L \tag{6}$$

$$I_i^{(L)} = I_i^{(U)} - Y_{iL}\ Z_L\ I_L^{(L)};\ i \neq L$$

Consequently, once a solution for the unloaded structure has been obtained it is possible to study the effect of loading by simply modifying the unloaded current as shown above. This avoids the necessity of reinverting or refactoring the impedance matrix for each new parameter case of interest which is required in the case of distributed loading. In general, when i = L,...,M of the structure

segments contain impedance loads, the procedure above for the single loaded segment can be generalized to obtain

$$I_i^{(L)} = \tilde{Y}_{ij}\, I_j^{(U)} \qquad i, j, = 1,\ldots,M \qquad (7)$$

$$I_i^{(L)} = I_i^{(U)} - Y_{ij}\, Z_j\, I_j^{(L)} \qquad i = M+1,\ldots,N$$

$$j = i,\ldots,M$$

where

$$\tilde{Y}_{ij} = [\delta_{ij} + Y_{ij}\, Z_j]^{-1}$$

Thus so long as M is much much less than N it is more efficient to develop a solution for the impedance loaded structure in terms of the unloaded solution and the auxilliary matrix $\tilde{Y}$ of order M.

Lumped impedance loading is of interest in connection with transmission lines, antennas connected to receivers, size reduction of radar scatterers through reactive loading, etc. While the calculations are readily enough performed, it is of considerable value to determine the validity of the lumped impedance term in the integral equation. Unfortunately, there are relatively few cases where independent solutions exist or where valid experimental data can be obtained. There is one case, that of the two wire transmission line however, which is amenable to solution via the thin wire electric field integral equation and where analytic solutions are expressable in terms of impedance loads connected to the line. This is the case we will use to validate the impedance load feature of the integral equation solution.

Consider a two wire transmission line having characteristic impedance Z_0 and terminated by load impedance Z_L. We are able to obtain an expression for the current and voltage at the load in terms of the load impedance and as function of distance from the generator as

$$I_L = \frac{V_g}{Z_L + Z_0}\, e^{ikd} \; ; \; V_L = Z_L\, I_L$$

assuming the transmission line is excited by a matched impedance generator of voltage V_g. The voltage and current along the line may furthermore be expressed as

$$I(s) = I_L \cos ks + i\,(V_L/Z_o)\sin ks$$

$$V(s) = V_L \cos ks + i\, I_L Z_o \sin ks \qquad (8)$$

with s representing the distance from the load.

Let us check this well known analytic result with a model based on the thin wire electric field integral equation. We can develop a thin wire model for the two wire transmission line in a rather obvious way. For convenience, we will use segments on the line equal to the line separation. Our model for the transmission line is included below (Figure 6a). We may obtain solutions for various values of load impedance for direct comparison with the analytic solutions given by equation (8) above.

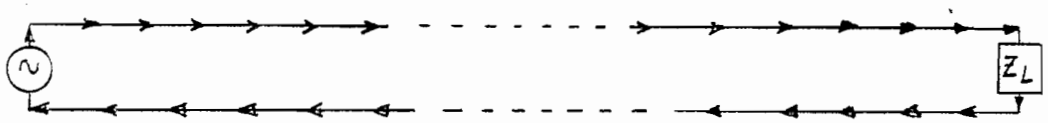

FIGURE 6a Numerical model of transmission line.

Plots of the current amplitude along the line obtained from the integral equation solution and compared on the same graph with the analytic solutions are shown in Figures 6b, 6c, and 6d, for various values of load impedance. There is seen to be excellent agreement between the integral equation solution and the analytic expression, independent of the load impedance value itself. However, because the line is considered to be of finite width in our model, the variation of the current along the line may be slightly shifted because of the added distance which the load size itself represents.

It is also of interest to determine the current on the line when rather than using a load impedance of high value to simulate the effect of an open circuit, we omit the segment representing the load in the integral equation model. Results obtained from this viewpoint are shown in Figure 6e below. Except for a slight shift in current variation along the line, there is no essential difference between this result and that obtained when a lumped load was used to simulate the effects of an open circuit.

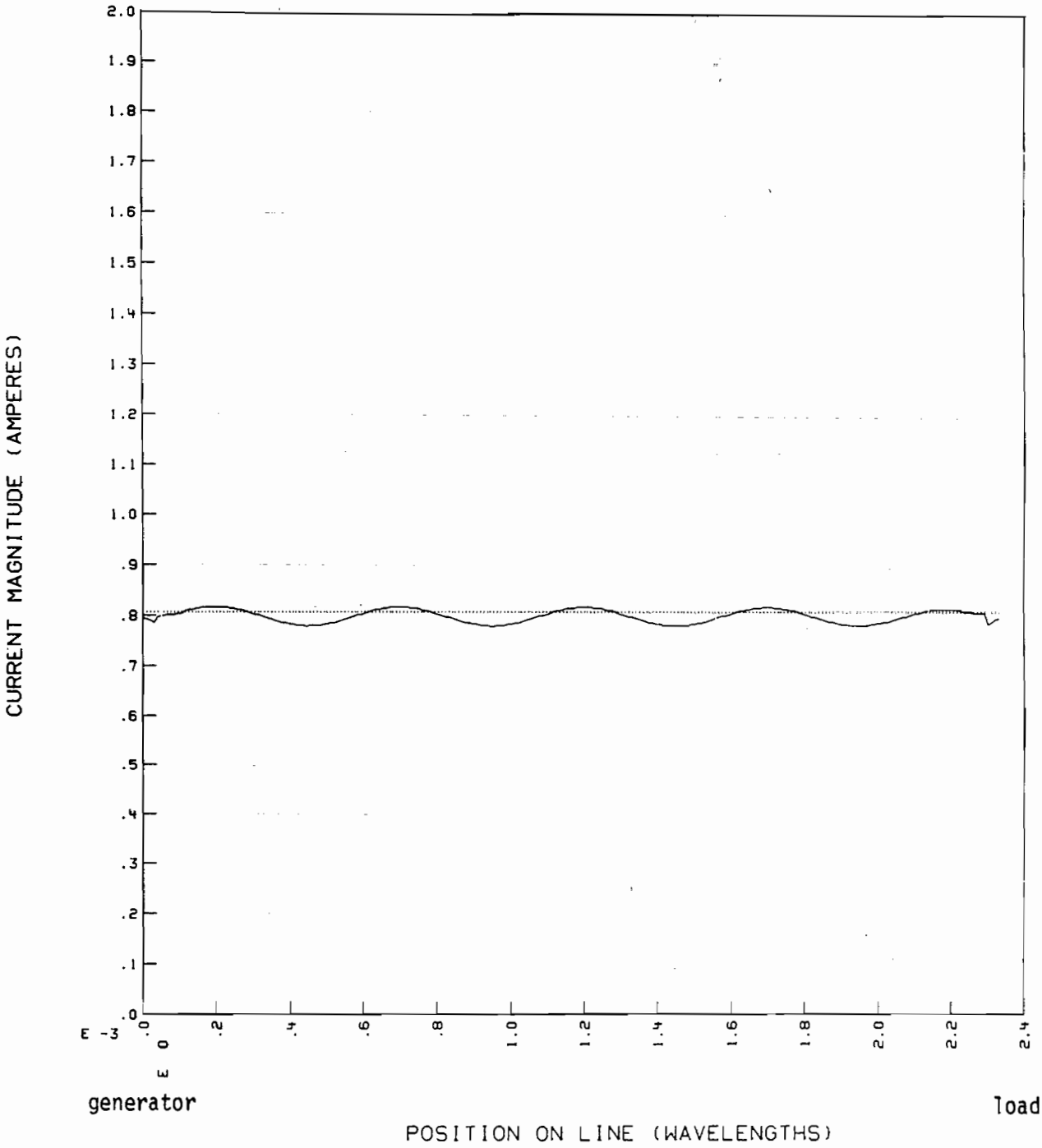

600 OHM TRANSMISSION LINE--MATCHED LOAD -----EFIE .....ANALYTIC

FIGURE 6b

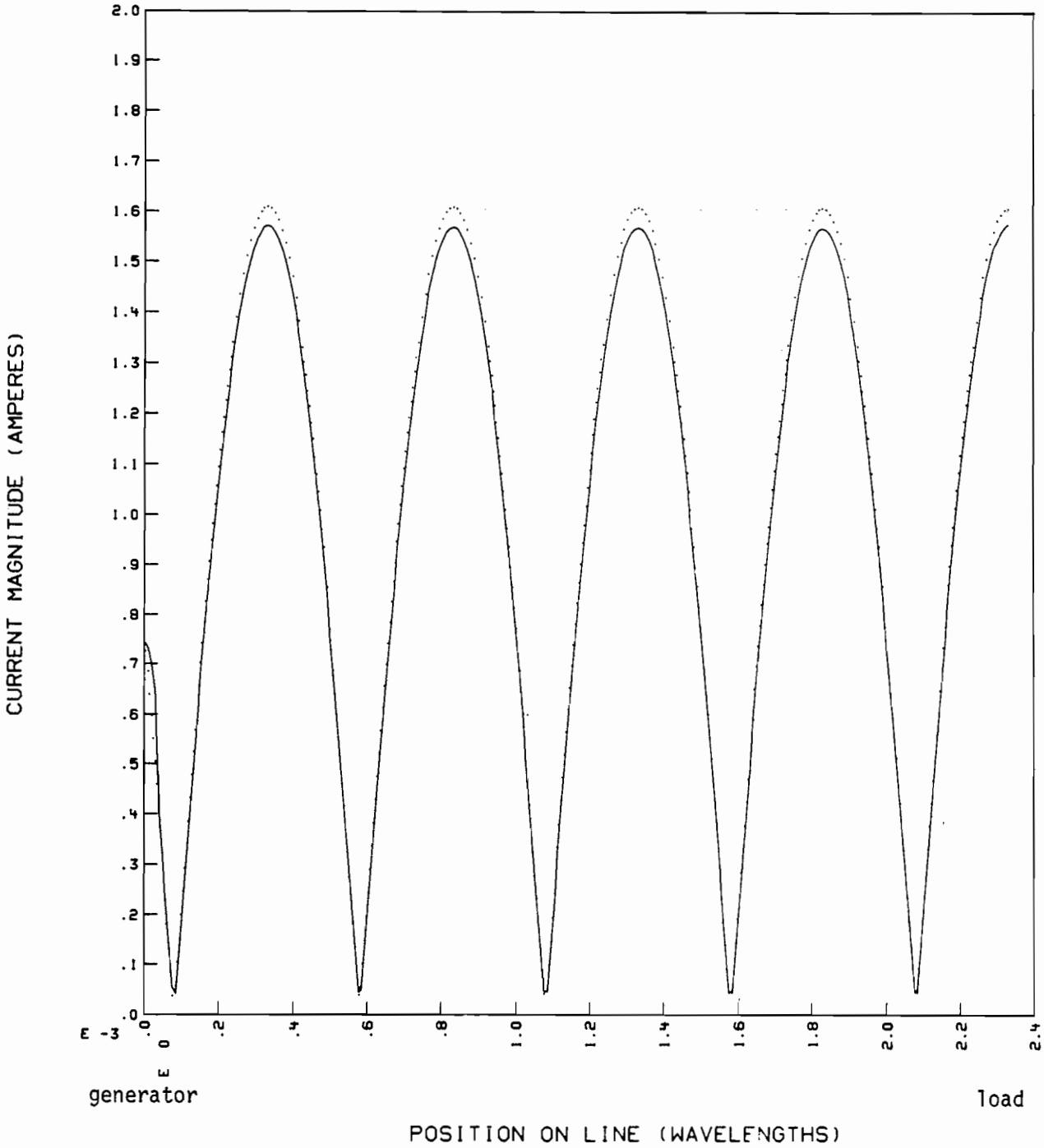

600 OHM TRANSMISSION LINE--SHORT CIRCUIT -----EFIE .....ANALYTIC

FIGURE 6c

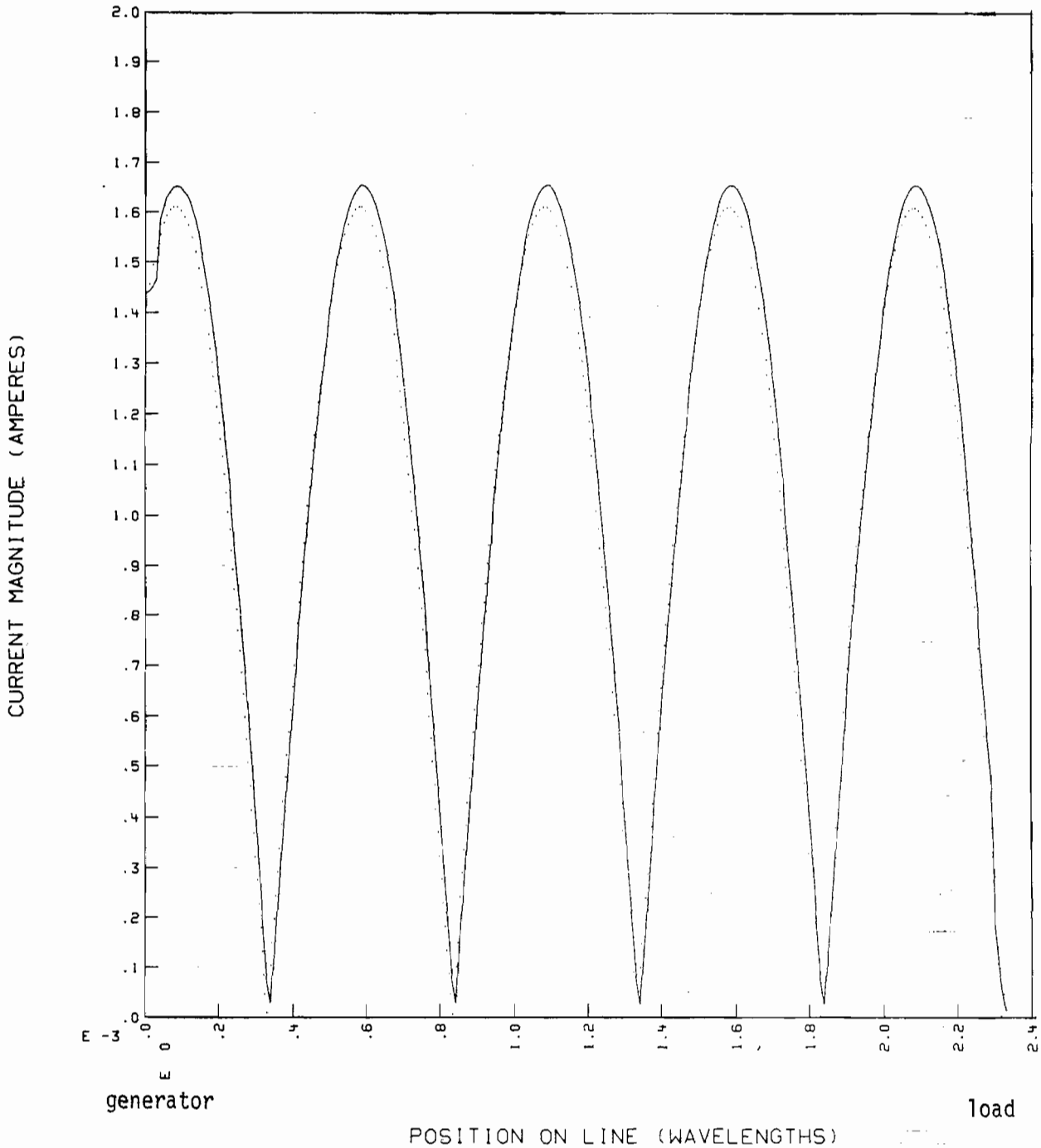

600 OHM TRANSMISSION LINE--OPEN CIRCUIT -----EFIE .....ANALYTIC

FIGURE 6d

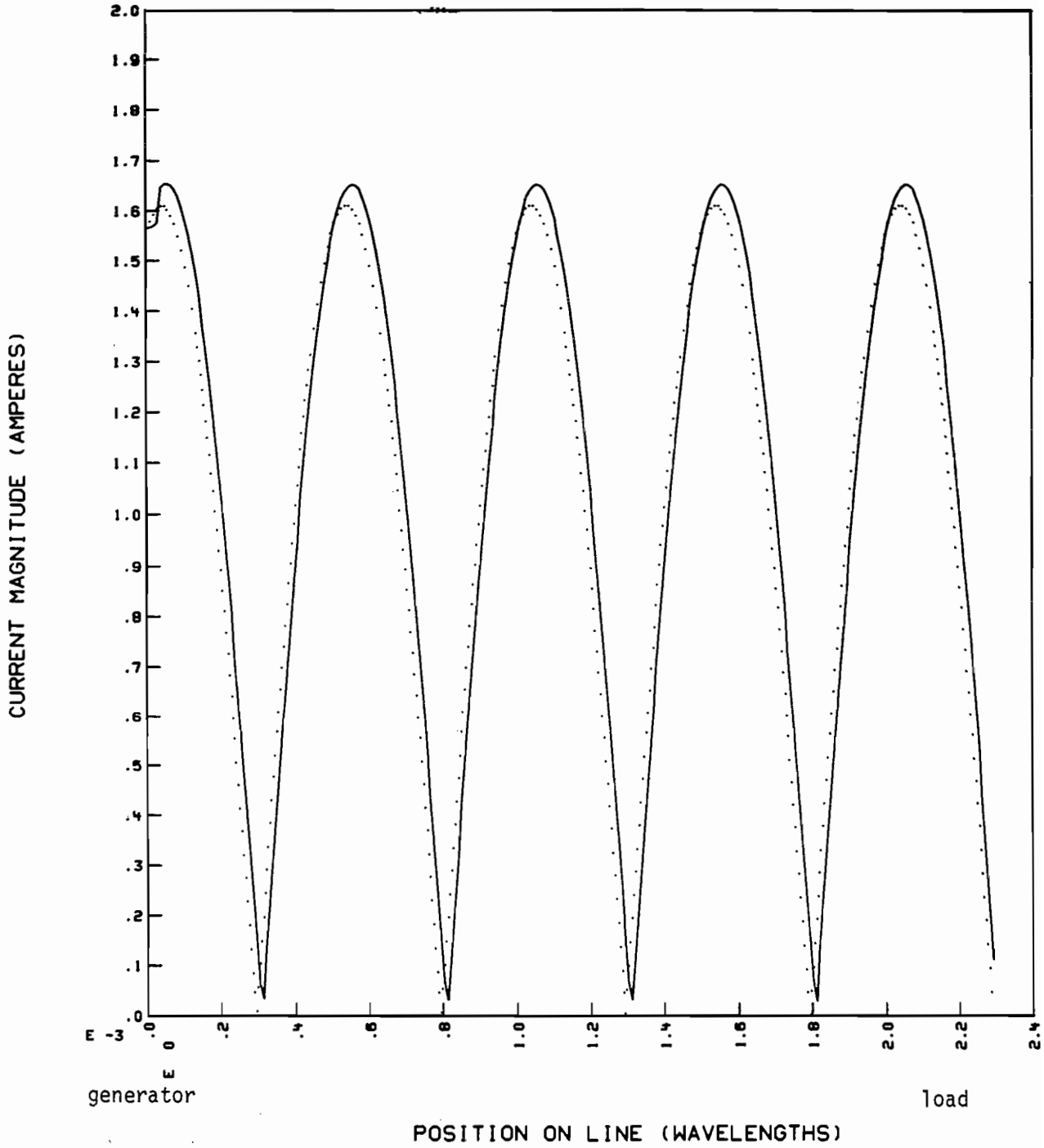

600 OHM TRANSMISSION LINE OPEN CKT (SEG REMOVED) -----EFIE .....ANALYTIC

FIGURE 6e

This brings us to the practical application of impedance loading for modeling insulators. In many low frequency antenna problems insulators are employed to electrically isolate the antenna from its support structure, to make the guy wire system electrically small to minimize re-radiation, etc. In either case it is of interest to know the effective voltage drop which appears across these insulators for design optimization and to permit realistic maintenance schedules. Various alternatives are available to us to determine the actual insulator voltage drop. We might for example, use an impedance load of high value at the point of the insulator location and determine the voltage drop across the insulator from the product of the current times the insulator impedance value along the loaded segment. Or perhaps we might use the value of electric field at the center of the segment and multiply this by the segment length to approximate the insulator voltage drop. Alternatively we might, as in the case of the open circuit transmission line above, leave a physical gap in the structure at the insulator's position and then subsequently compute the electric field along the location of the missing insulator to obtain a voltage drop. The voltage drop along the insulator could also be approximated by the product of the field value at the center times the insulator length.

There are obvious advantages to being able to employ the lumped impedance load insulator model. Perhaps most important is the fact that once the solution has been obtained for the structure, the voltage across the insulator can be readily approximated in terms of the current on the insulator impedance. Furthermore the effect of varying the insulator impedance values on the structure characteristics can be readily assessed to determine the effect of a deteriorating insulator on the structure's electromagnetic characteristics. Such information would be especially valuable for determining when maintenance schedules should be set up. It is however, not clear that a value for the insulator voltage drop obtained in this way will be entirely valid because in our model the current will essentially vanish or become small at the point of the load itself but in general will be non-zero over the rest of the load as demonstrated by the transmission line results already presented.

While the gap insulator model may on the other hand represent a more realistic version for the insulator, evaluation of the insulator voltage drop will require additional field computation(s) which are less efficient than the current determination and thus more time consuming.

In order to assess the relative advantages of modeling insulators via physical gaps versus lumped impedance loads we have performed the following computations. The first pertains to the two wire transmission line model already discussed while the second set applies to the case of a linear dipole antenna. Several insulator voltage drop values are presented.

The results of the calculations are presented in Table VII. Part A is for a 600 ohm transmission line mode, for which we know the true analytic results for the voltage across the terminating load resistor. It can be seen that we essentially obtain the correct result whether we integrate the tangential electric field across the loaded segment, or multiply the current evaluated at the center point location of the loaded segment times the load resistance value.

Part B of Table VII is for a linear half wavelength dipole with two symmetrically located insulators centered 1/8 wavelength from each end. The insulators were modeled in three ways: (1) with lumped resistive loading on segments 5, 6, and 16, 17, (2) with the loaded segments replaced by a physical gap, and (3) with a 1 segment long physical gap, such that the gap end points coincide with the current match points of the first.

We see from the results presented in Part B of Table VII that we can obtain an approximate measure of the integral of the tangential electric field across a gap insulator by simply computing the IR drop for the resistively loaded segments. A comparison of the results obtained by the loaded segment method versus the 1 and 2 segment physical gap insulator model, shows the result to be somewhat conservative, however. If the end points of the gap insulator model are made to correspond to the current match points for the resistively loaded case, we also find very little perturbation in the antenna's input impedance between the two models. Figures 7a through 7c show the total and tangential electric fields along the antenna in the vicinity of the insulator region for each of the models analyzed. Figures 7d through 7i show the real and imaginary currents along half of the dipole used for each of the cases.

Table VII Insulator Models

A. 600 Ohm 2-Wire Transmission Line

Termination	$\int E(s')ds'$	$I_L R_L$
Matched Load (R_L=600Ω)	0.46 Volts	0.48 Volts
Open Circuit (R_L=10^{10}Ω)	0.97 Volts	1.03 Volts
Short Circuit (R_L=0Ω)	0.002 Volts	0. Volts

B. Half Wavelength Dipole with Insulators

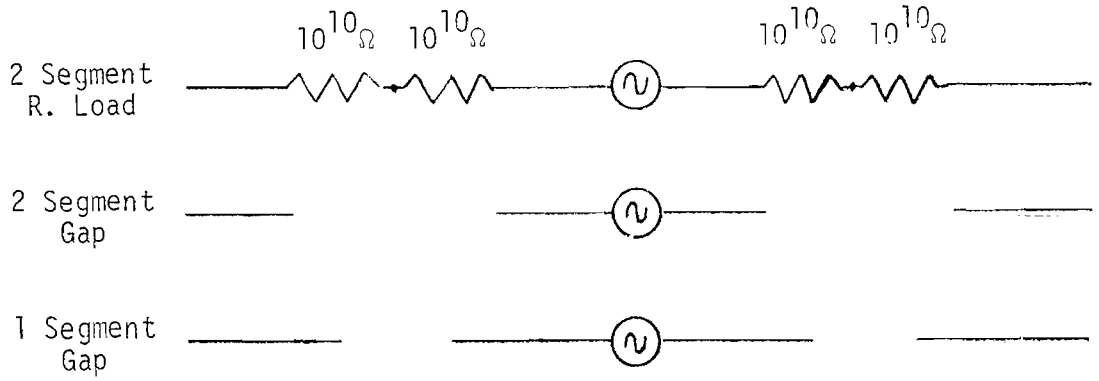

	2 Segments Loaded	2-Segment Gap	1-Segment Gap
$\int E(s')ds'$	: 321 Volts	113 Volts	105 Volts
$I_L R_L$	: 192 Volts	———	———
$E_{T_{Mid}} L_g$	: 192 Volts	37 Volts	36.4 Volts
Z_{in}	: 12.1-i678 OHMS	10.0-i761 OHMS	12.8-i663 OHMS

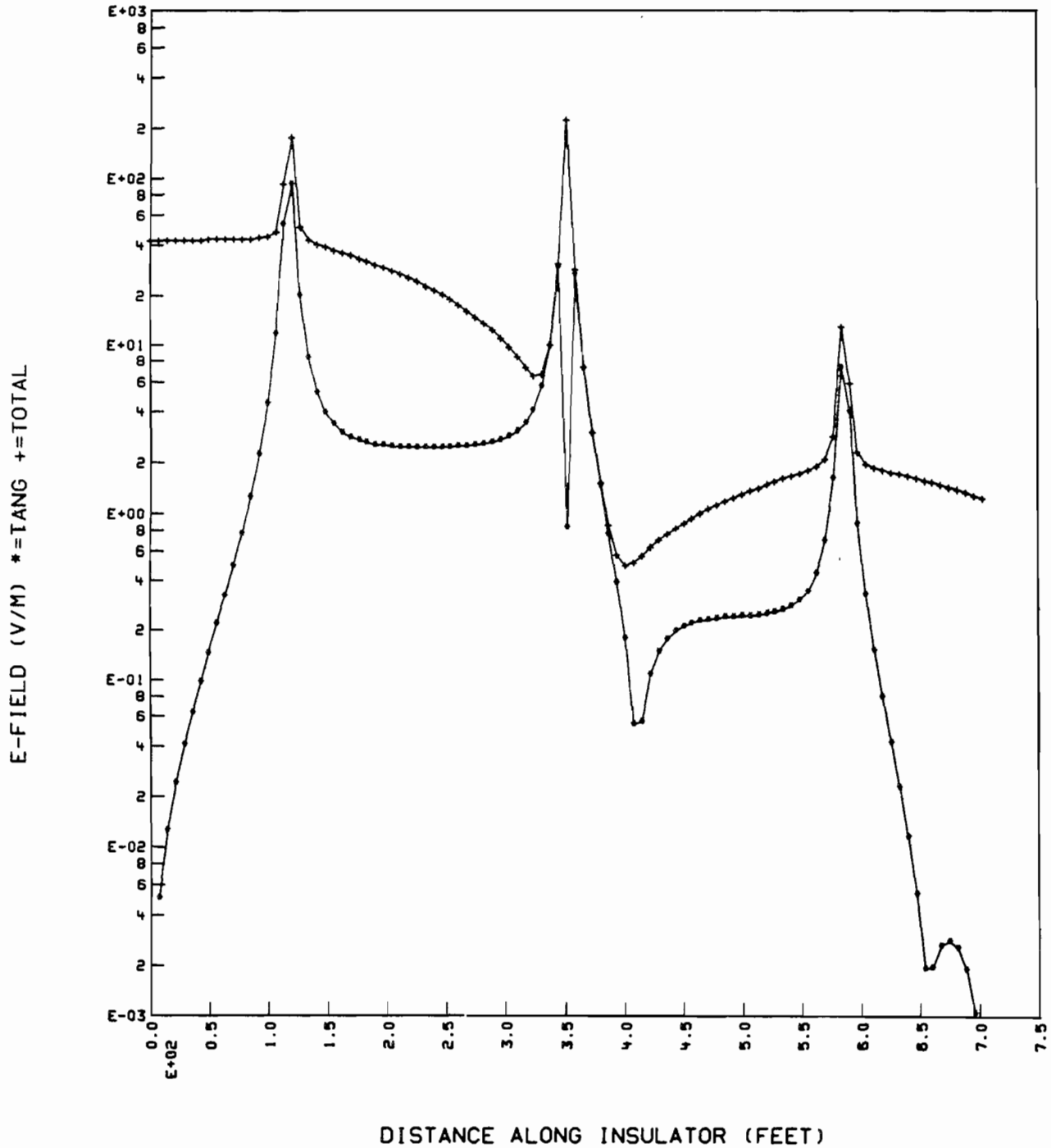

2-SEGMENT GAP--EACH SEG LOADED BY 1.E+10 OHMS--INPUT PWR=1 WATT

FIGURE 7a

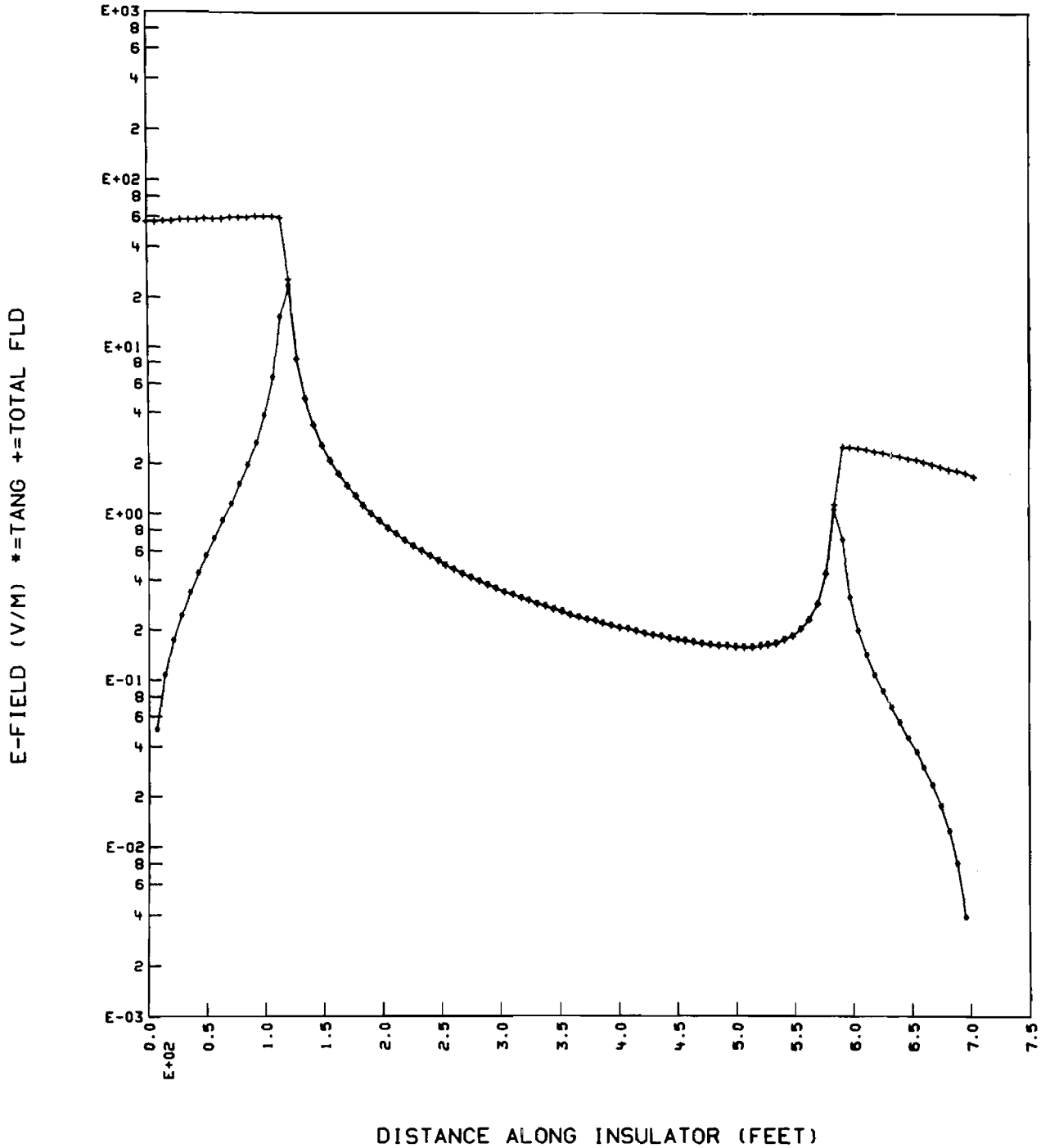

2-SEGMENT GAP INSULATOR MODEL (SEGMENTS REMOVED) INPUT=1-WATT

FIGURE 7b

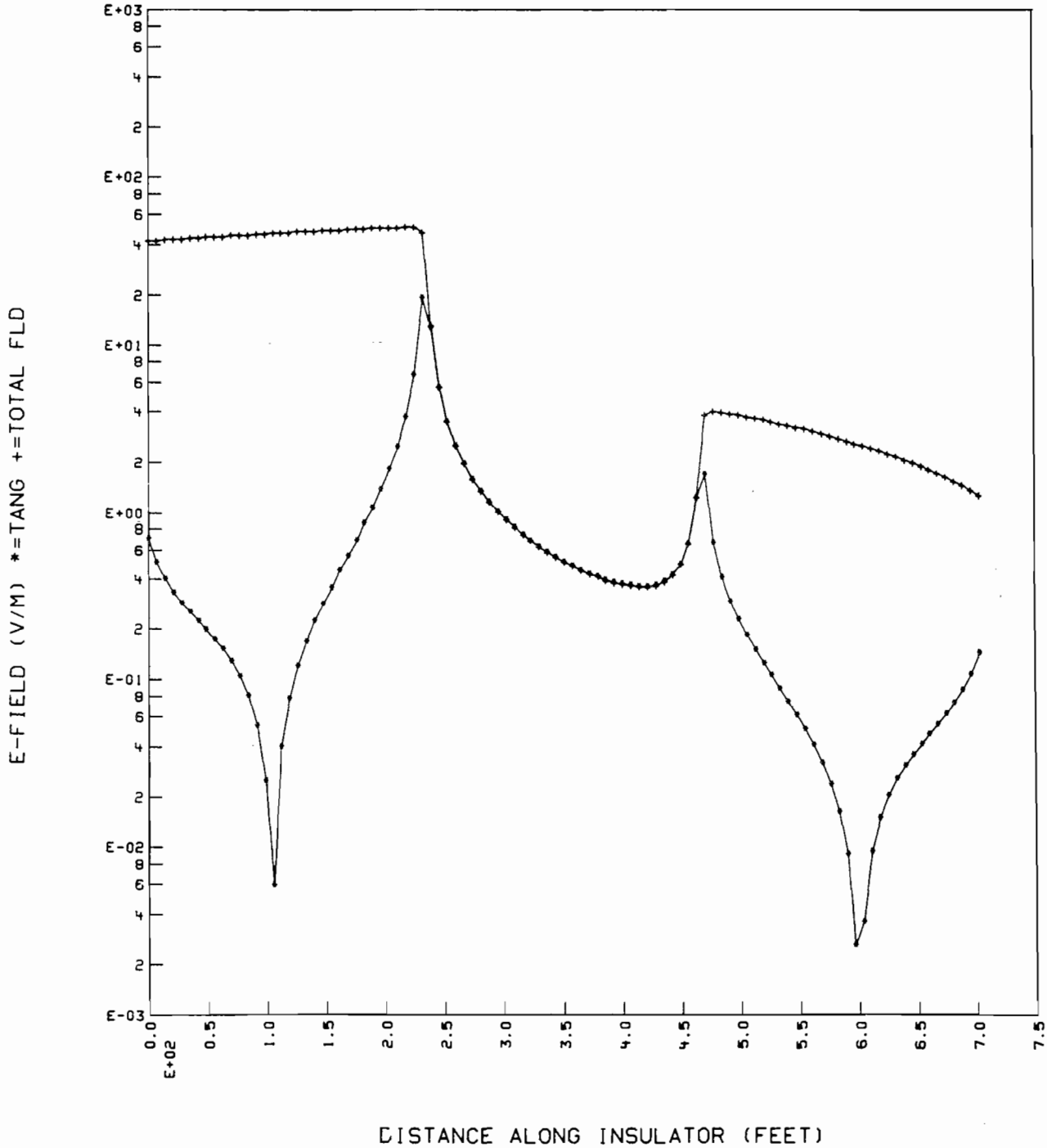

1-SEGMENT GAP INSULATOR MODEL (SEGMENT REMOVED) INPUT=1-WATT

FIGURE 7c

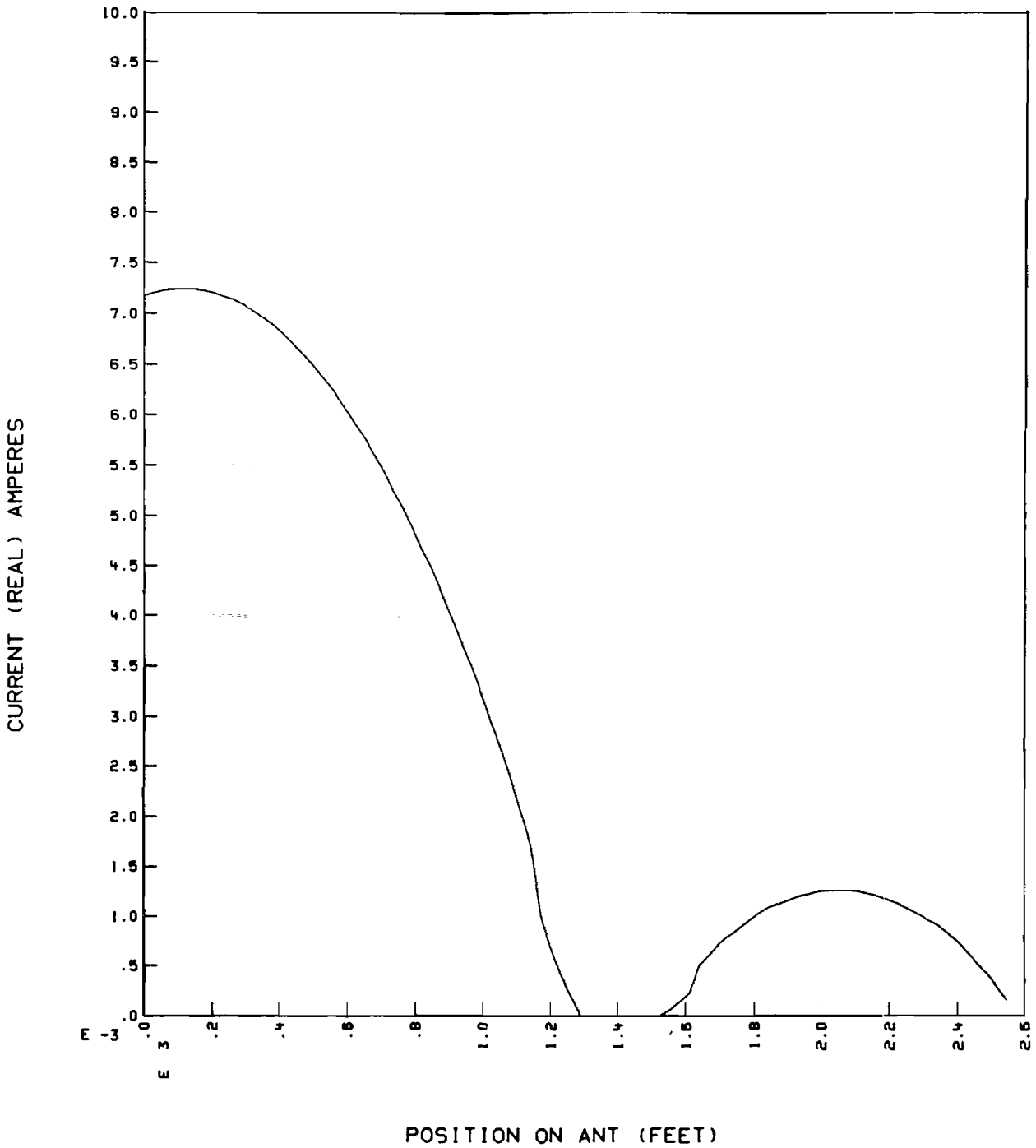

2 SEGMENTS EACH LOADED WITH 1.E+10 OHMS--CURRENTS NORMALIZED TO 1-WATT

FIGURE 7d

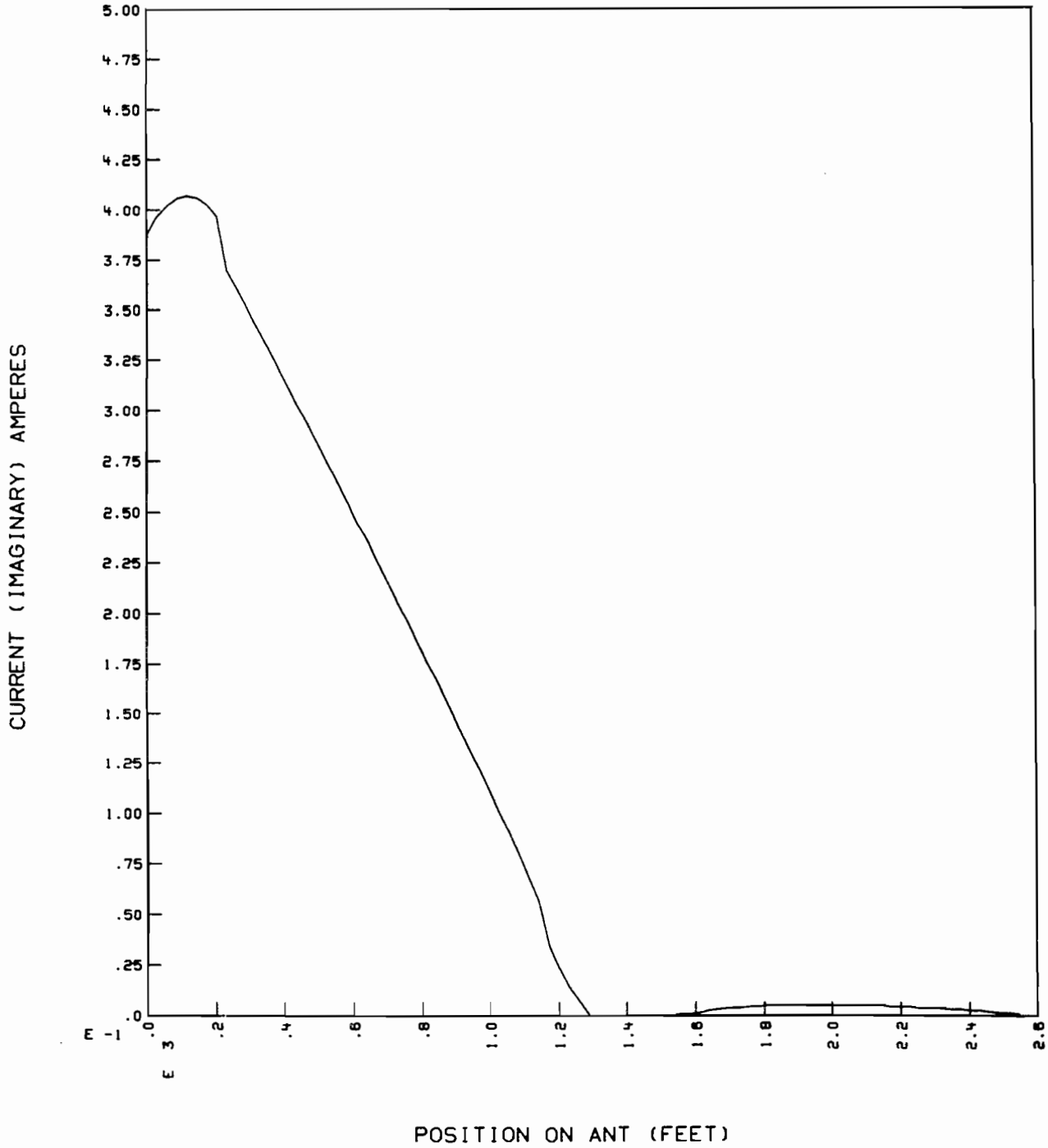

2 SEGMENTS EACH LOADED WITH 1.E+10 OHMS--CURRENTS NORMALIZED TO 1-WATT

FIGURE 7e

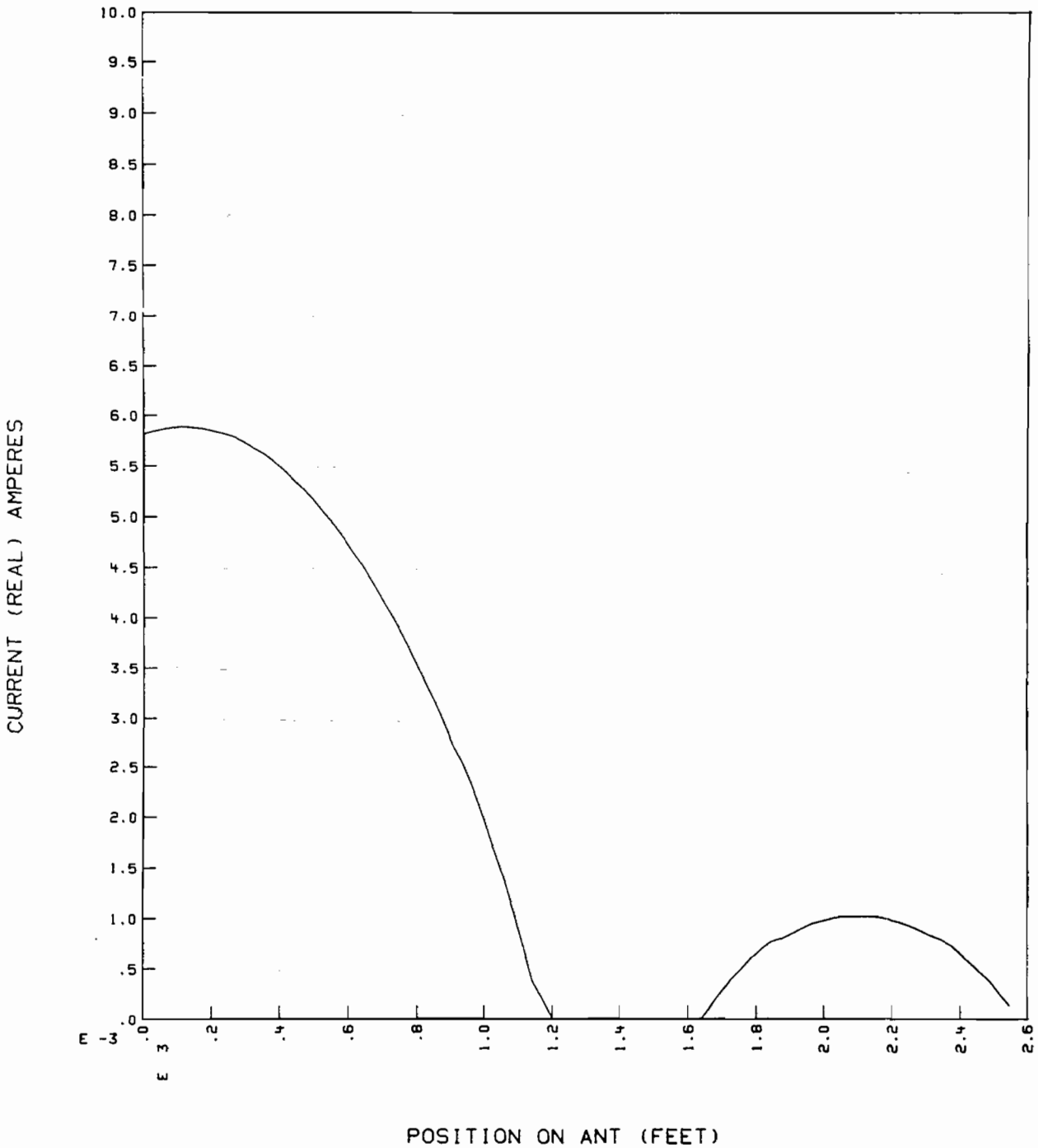

2-SEGMENT GAP INSULATOR MODEL (SEGS REMOVED) CURRENTS NORMALIZED TO 1-WATT

FIGURE 7f

(Compare with Figure 7d)

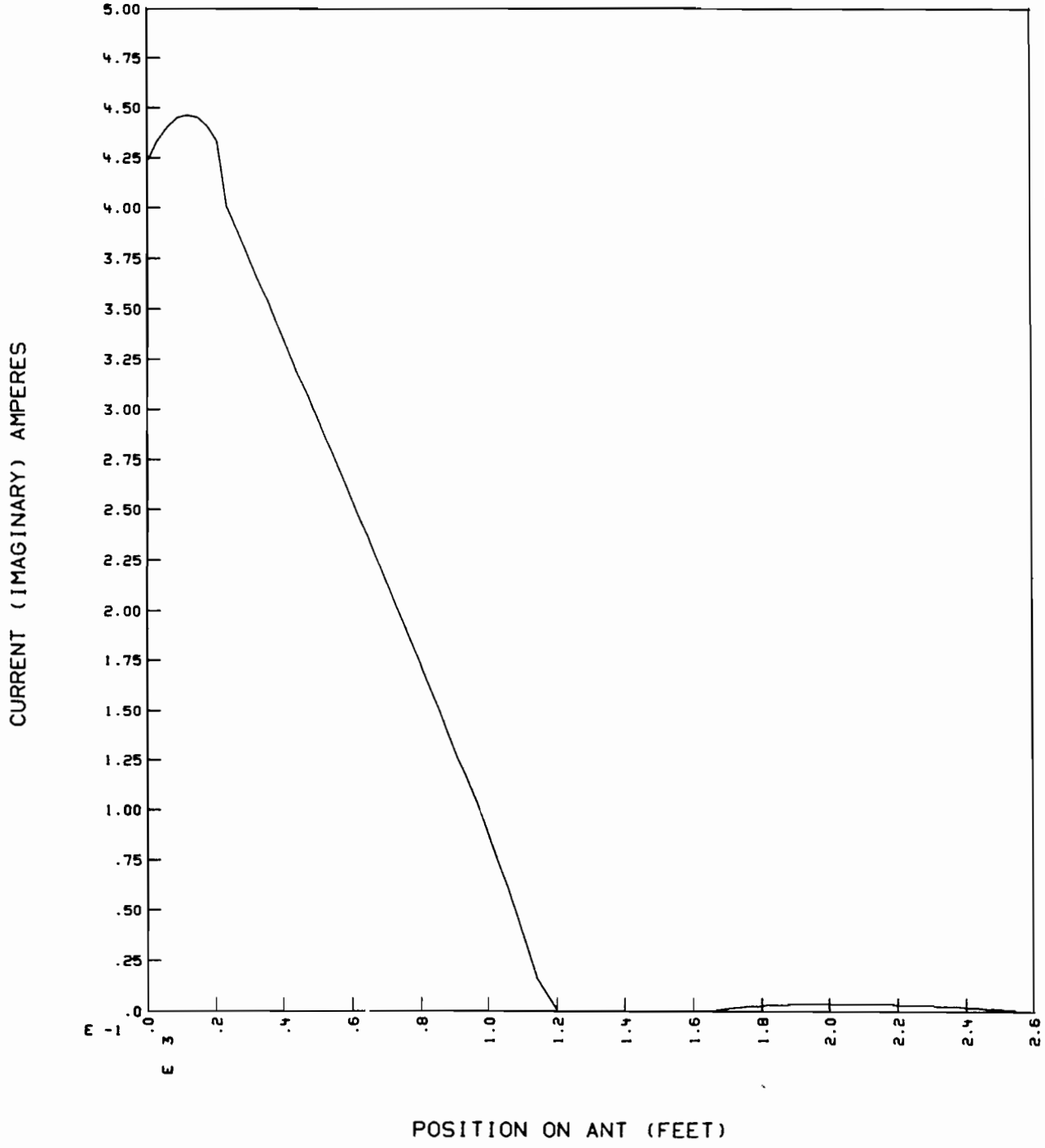

2-SEGMENT GAP INSULATOR MODEL (SEGS REMOVED) CURRENTS NORMALIZED TO 1-WATT

FIGURE 7g

(Compare with Figure 7e)

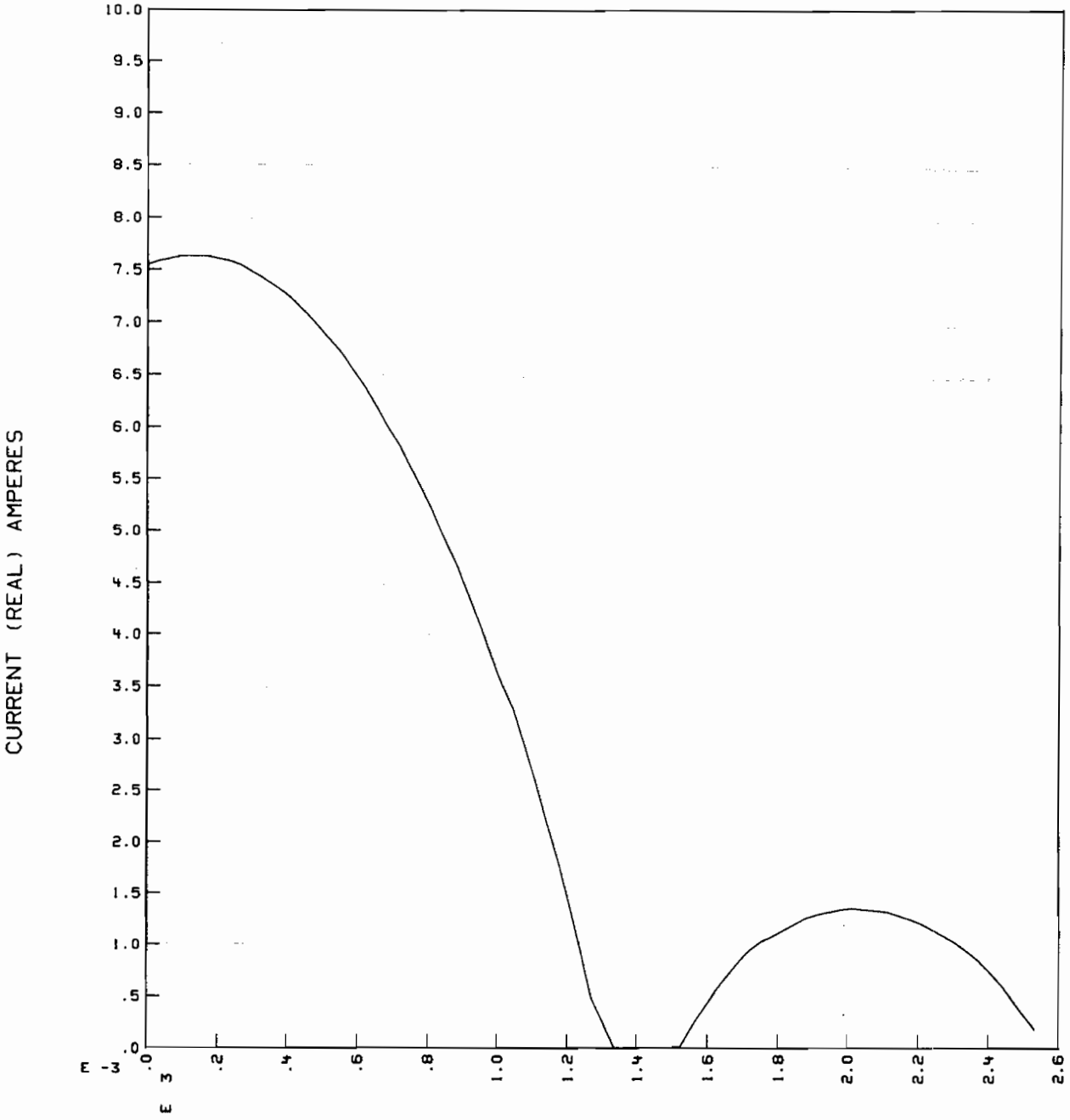

1-SEGMENT GAP INSULATOR MODEL (SEG REMOVED) CURRENTS NORMALIZED TO 1 WATT

FIGURE 7h (Compare with Figure 7d)

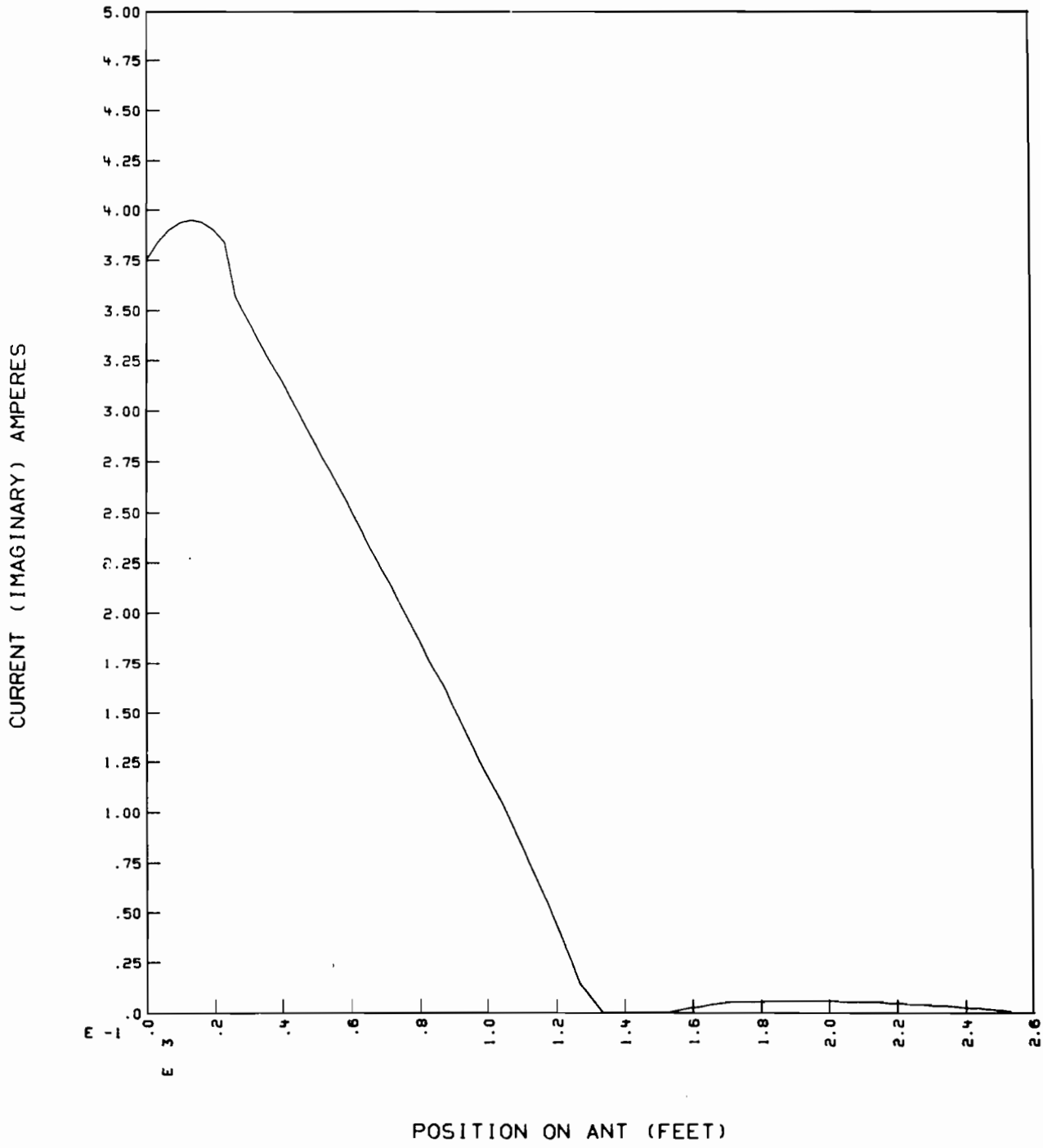

1-SEGMENT GAP INSULATOR MODEL (SEG REMOVED) CURRENTS NORMALIZED TO 1 WATT

FIGURE 7i (Compare with Figure 7e)

C. Multiple Junction Treatment

The current expansion discussed in Section A above considered the case of simply connected structures having two wire junctions only. When junctions of three or more wires must be treated, special methods may be required. In this section we briefly outline some of the procedures which may then be used.

Clearly the kind of approach used to handle the multiple junction will depend on the current expansion itself. For example, the pulse approximation for a current can be used everywhere on the structure with no special treatment of the multiple wire junction itself required, at least for the Pocklington integral euqation. The two term current expansion (piecewise linear, piecewise sinusoidal, etc.) require somewhat more care in their extension to the multiple junction. Chao and Strait (1970) report a procedure based on the generalization of the two term piecewise linear current expansion, whereby the junction is viewed as an overlap of open ended wires. The procedure basically leads to M-1 additional current unknowns at the junction of M wires. This method formally allows for variable length segments at the junction and has not been found to be sensitive to segment length discontinuities such as those previously discussed in connection with the three term current expansion and the V-wire antenna solution [Strait, (1973)].

The piecewise sinusoidal representation employed by Richmond (1969) has evidently not as yet been applied to multiple junctions. However because of its close similarity to the piecewise linear expansion employed by Chao and Strait it appears that the piecesise sinusoidal expansion could be applied to multiple junctions in much the same way.*

It should be noted in this regard that the procedure developed by Chao and Strait for multiple junctions depends essentially upon two factors for its success: 1) the current expansion involves functions which are zero at opposite ends of the given wire segment. Therefore overlapping the segments in the fashion suggested by Chao and Strait means that the current at the junction of two segments overlapped by another open-ended segment is unaffected when the end of the overlap segment coincides with the junction. 2) The procedure used is based upon a Galerkins method and involves the electric field integrated over two segments to obtain one equation in the linear system. Because of this the overlapping of segments does not result in the redundant equations which would be the case were a point matching procedure applied in this particular way.

Alternative multiple junction schemes have been reported by Andreason and Harris (1968) et al. and Gee et al. (1971). Both treatments utilize the three term current expansion, but differ in their treatment

*Prof. Richmond has recently provided the authors with multiple junction results obtained in a similar, though perhaps more elegant, fashion.

of two wire junctions in that the former use matching of current amplitude and derivative at segment ends whereas the latter employ an extrapolation to adjacent segment centers. For the multiple junction case, Andreason and Harris employ the concept of a gap current associated with the end of each wire and an associated driving voltage as well. By matching the discontinunity in current derivative on a given wire with the sum of the current derivatives on the connected wires, the effective applied voltage between a given wire and ground can be specified.

The approach used by Gee et al. (1971), on the other hand treats the multiple junction by extrapolating the current from one segment across the multiple junction to the sum of the sampled values of the M-1 currents of the other segments at the junction. This procedure has been found to work quite satisfactorily, for most cases to which it has been applied, but as shown above may encounter problems at multiple junctions of unequal length segments. It is not entirely clear whether the difficulty there is due to the feed point problem of determining the applied electric field or to invalidation of the interpolation process as the junction segment length discontinunity ratio increases. It appears from some recent results that the latter is the cause of the problem.

An alternative approach has been suggested by Curtis (1972). He employs the general treatment developed by Chao and Strait (1970) in terms of the electric field explicitly derived from the vector and scalar potentials, and employs a pulse current approximation for the current representation. At the junction he represents the current derivative (charge) in the usual way via finite differences involving the current samples. However, he makes the assumption that the total charge on the wires originating from a common junction is distributed among the wires according to the ratio their surface areas. The total charge is computed from the total current on all junction wires. A similar approach has been described by Sayre (1973).

While several different methods have been thus derived to treat the multiple junction problem there is relatively little data to compare their particular attributes. Therefore it is not now possible to say which of these approaches may involve a more physically realistic modeling of the wire current at multiple junctions, although results for the V-dipole indicate the procedure used by Chao and Strait, and Curtis to be reliable.

D. The Thin Wire Approximation

There are two potential problems which one may encounter using the thin wire approximation. One of these is its unsuitability for application to wires more than a small fraction of a wave length in

diameter. This is caused by the fact that in deriving the thin wire kernel the azimuthal variation of the current around the wire is ignored as well as the azimuthal variation of the kernel in the integral equation itself. Both are replaced by the mean values.

The other potential problem which arises from using the thin wire approximation is based on the numerical method used for solving the integral equation. The problem involves the use of segments whose lengths are shorter than several wire diameters. In this case, the nature of the integral equation kernel may produce non physical current oscillations near junctions and source regions which are numerically generated. We will discuss each of these problems in turn below.

Experimental checks on the maximum size of a wire which may be regarded as thin can be rather readily performed. One might, for example, compare the computed cross section of a circular wire scatterer with that which is measured, as a function of the wire size relative to the wave length. When the wire size becomes appreciable compared to the wave length, the computed and measured results will begin to depart in a significant fashion thus establishing a definite upper limit on wire size for the thin wire approximation to be valid.

However it is also possible to accomplish this without resorting to absolute comparison between measured and calculated results. One could instead measure the backscatter cross-section aspect-dependance of a thin wire strip, i.e. for edge-on or broadside incidence, as a function of strip width relative to the wave length. A measurement of this kind can be related to the thin wire approximation in that a static solution for the strip can be shown to approximate the static solution for a wire diameter of half the strip-width. Experiments conducted along this line have demonstrated that the wire strip is aspect insensitive for wire diameters on the order 2/10 wavelengths. Therefore an experimental upper limit on the order of 2/10th wavelengths for the wire diameter may be postulated in the scattering mode.

The question of segment size relative to the wire diameter can only be resolved of course via numerical computations. We have determined the input admittance and current distribution on a rather fat ($\Omega = 8$) half wave antenna as a function of the number of segments. Results obtained are summarized in Table VIII and Figure 8. We present in Table VIII the computed input admittance for this antenna as a function of the ratio of the wire radius (a) to the segment length (Δ). The input admittance results which are obtained exhibit a conductance which is insensitive to this ratio, but the susceptance may be seen to vary dramatically and become obviously invalid as this ratio is increased. The reason for this occurrance is dramatized by the current distributions of Figure 8 where the real current is

TABLE VIII SHORT SEGMENT ADMITTANCE

$L/\lambda = 0.5$ Dipole

$a/\lambda = 0.00916$

$\Omega = 8$

$Y_{King} \sim 10.6 - i\ 3.6$

N	a/Δ	$Y = I_{feed}/(-E\delta)$
21	0.38	$7.7 - i\ 3.3$
81	1.48	$7.5 + i\ 0.97$
181	3.32	$7.2 + i\ 343.2$

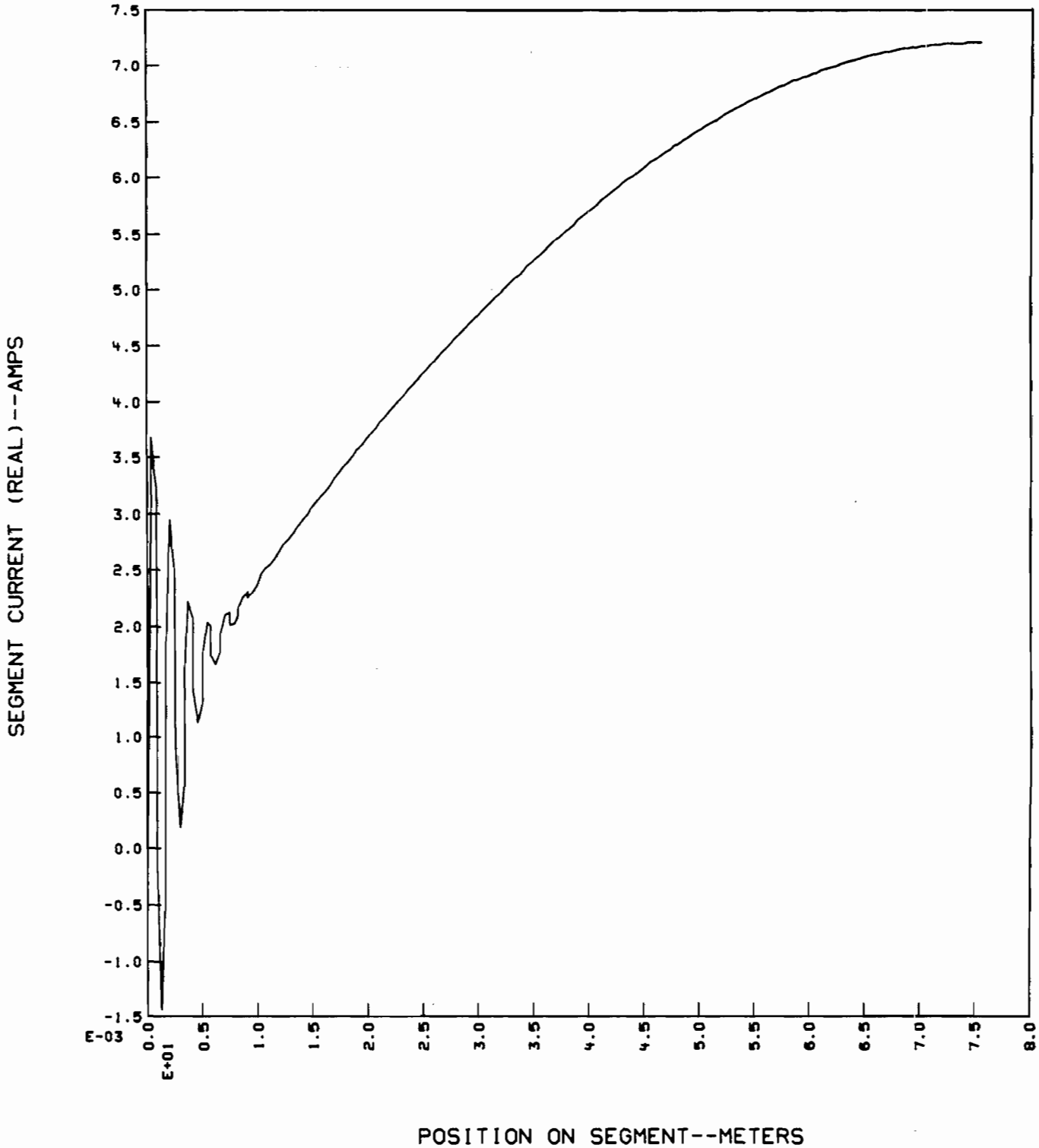

FIGURE 8a Current on a half wavelength dipole modeled with short segments (Ω = 8, 181 segments, frequency = 1 MHz).

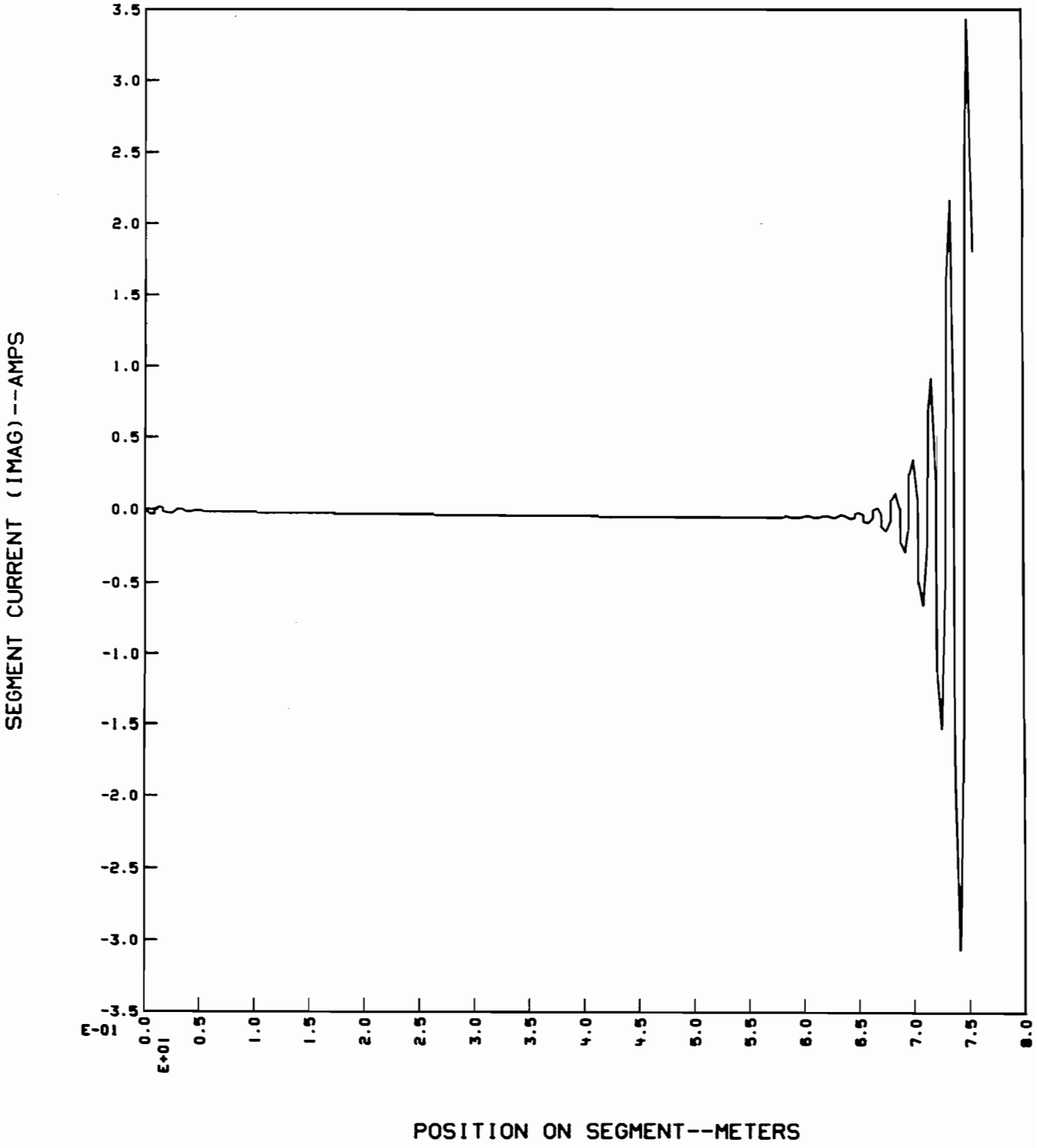

FIGURE 8b Current on a half wavelength dipole modeled with short segments (Ω = 8, 181 segments, frequency = 1 MHz).

seen to exhibit an oscillation at the end of the antenna. The imaginary current also exhibits an oscillation near the end of the antenna, but in addition one much more pronounced near the feed region itself. These results are for the extreme case of 181 segments or an $\frac{a}{\Delta}$ ratio of 3.32. The imaginary current oscillation near the feed region is seen to have values on an order of 100 times larger than the mean current away from the feed region. Obviously any attempt to define an input susceptance on the basis of a current that varies so rapdily near the feed region is questionable at best. However, if one smoothly extrapolates back to the feed region from the antenna current away from the oscillatory portion, one does obtain in all cases a reasonably stable and consistent input susceptance. Therefore while the current distribution itself contains obviously invalid behavior it is still possible to derive what seem to be valid admittance results. Furthermore the antenna radiation pattern is essentially unaffected by the oscillatory current since the current oscillation naturally tends to cancel out and thus disappear from the far field calculation itself.

Thus while one should be alert to the potential problems involved in using what are sometimes termed pancake shaped segments, i.e. segments shorter than a wire diameter or so in length, it is still feasible to obtain useful calculated data if one is careful to define input admittance in terms of an extrapolated current.

E. Matrix Factorization Roundoff Error

It is sometimes surprising to those unfamiliar with the matrix treatment of electromagnetic problems that linear systems on the order of several hundred unknowns are routinely solved with a computer. Of course, one expects that matrices of this large order would be prone to severe numerical limitations because of the inevitable roundoff which occurs as the matrix is solved by factorization or inversion and a solution is subsequently obtained.

In order to demonstrate in a controlled way the result of matrix roundoff error on the final numerical result a series of computations has been performed for various types of wire structures. Results of these calculations are summarized in Figure 9. There we plot the error in calculated input impedance for several cases as a function of the number of bits in the elements of the impedance matrix. Two structures are shown. One is a straight wire having 7, 21, and 121 segments. The other involves two different versions of the sectionalized LORAN transmitting antenna, having 237 unknowns and 240 unknowns respectively. The initial impedance matrix is computed for all cases in the usual fashion. A modified matrix is then obtained by systematically truncating each matrix (mantissa) word entry and retaining the number of bits indicated on the plot. The truncated matrix is then factored to obtain the antenna current distribution and input impedance. The error in the input impedance is then defined relative to the value obtained for the non-truncated case.

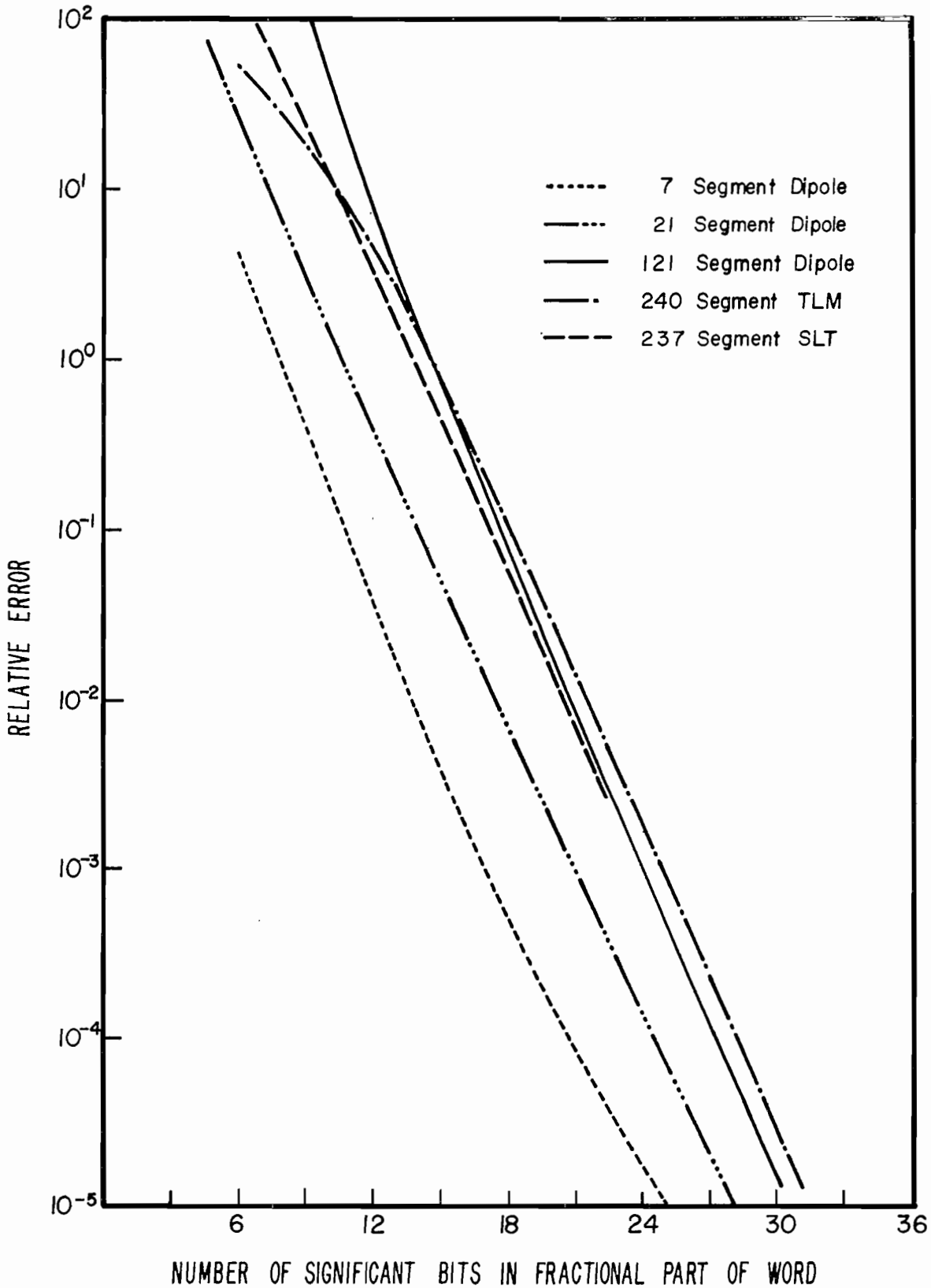

IMPEDANCE ERROR VS COMPUTER WORD SIZE

FIGURE 9

As expected, the solution accuracy increases as the number of bits in the matrix word size is increased. The relationship is essentially a logarithmetic one, i.e. the numerical accuracy is exponentially related to the number of bits in the impedance matrix coefficients. Furthermore, as is also expected, the accuracy decreases as the number of unknowns, or linear system size, increases.

The data shown on this figure may be roughly summarized in the following equation

$$E = E_0 \exp [-sd]$$

where E_0 is a reference error and d is a structure dependent coefficient with s the number of bits in the matrix elements. Using the data shown d may be given the approximate value 0.77.

On the basis of these calculations we can conclude that it is possible to treat antenna problems having at least 200 unknowns using word sizes on the order of 21 bits or more, if 10% accuracy is the minimum acceptable. This is a rather agreeable finding since it indicates that roundoff errors on most modern computers, which have word sizes generally exceeding 21 bits, would not be of paramount importance. We cannot extrapolate these results to general matrix solutions since a matrix which is ill-conditioned may be extremely more sensitive to roundoff error than those considered here. However, this finding is useful for our purposes since most problems we might expect to encounter would have similar kinds of matrices and therefore generally exhibit the kind of behavior found here.

F. Near Field Behavior

The basis for all numerical modeling via integral equations in electromagnetics is the computation of fields due to current and charge sources. Presumably then if one obtains a valid solution as measured by the accuracy of input admittance, radar cross section, etc. it must have required the calculation of numerically valid fields in originating the impedance matrix itself. Yet the demonstrated accuracy of input admittance, radar cross section, etc. is no guarantee that the overall solution can be accepted as being physically realistic or correct. As a matter of fact, various aspects of the calculated results may be obviously invalid, but without a negative impact on the overall usefulness of the calculation. One example of this is demonstrated above in connection with the oscillatory nature of the imaginary part of the antenna current near the source region. Another example of this possibility is demonstrated here where we pay particular attention to the near fields in the vicinity of the antenna.

The near fields around antennas are of significant interest with respect to corona discharge assessment, determining insulator voltage requirements, EMP vulnerability assessment, etc. Consequently, we have a legitimate interest in their behavior. However, inaccurate artifacts may be introduced into the field calculation by peculiarities associated with the current basis function expansion as shown by the following results derived from the examples of Section C above. In Figures 10a-10d we plot the field strength along a linear antenna for some of the cases considered in Section C. The real and imaginary components of the tangential electric field along the antenna are shown in Figure 10a and Figure 10b the corresponding radial electric field components for the nominal case of 21 equal length segments. The integral of the real electric field along the source segment together with that along the adjacent two or three segments is approximately equal to $-E^I\delta$, or 1 volt. Note however, the electric field variations associated with each segment junction due to the discontinuity in current amplitude permitted at these points using the three term current expansion and current extrapolation to the adjacent segment centers. Radial field variations are also associated with the segment junction current discontinuity.

To demonstrate more clearly the tangential field variation along the antenna we present the magnitude of the tangential and radial electric fields on a log plot in Figure 10c. There we see that the electric field is a rather rapidly varying function along the antenna but that the magnitude of the field discontinuities associated with the segment ends is generally small compared to the source region field except near the ends of the antenna.

For comparison purposes, field plots corresponding to those already shown are presented for two additional cases in Figures 10d and 10e. The results of Figure 10d differ from those which precede it only in that the current amplitude and derivative in the latter case are matched at segment junctions as opposed to the extrapolation to adjacent segment center used for the former. A much smoother and smaller error field is seen to be the result.

In Figure 10e we modify the approach used to obtain the data of Figure 10d in two ways: 1) the antenna has 20 rather than 21 segments; and 2) the exciting source is introduced as a slope current discontinuity rather than a tangential electric field. The relationship used for a source between segments n and n + 1 is

$$\frac{i}{2}\left[Z_0(\delta_n, a_n) \left.\frac{d\, I_n(s)}{d(ks)}\right|_{S=s_n+\delta_n/2} - Z_0(\delta_{n+1}, a_{n+1}) \left.\frac{d\, I_{n+1}(s)}{d(ks)}\right|_{s=s_{n+1}-\delta_{n+1}/2} \right] = V$$

where

$$Z_0(\delta, a) = \frac{\eta_0}{\pi}\left[\ell n \frac{2\delta}{a} - 1 \right]$$

is the impedance of a bicone whose length (δ) and radius (a) correspond to the parameters of the two segments across which the voltage is applied. The near fields which this source model produces are essentially identical (except for the segmentation change) from those just presented in Figure 10d except in the source region where the slope-discontinuity source is much narrower and in fact resembles a delta function.

To conclude these nominal geometry results, we present in Figure 11f the current distributions for the three cases just discussed, all for sources which are intended to be one volt (i.e., $-\delta E^I = 1$ for the tangential field sources, and V = 1 for the slope discontinuity source). The general current behavior for all three cases can be observed to be essentially the same except in the vicinity of the source itself. There we find that the current slope variation changes significantly. The distribution for the current extrapolation model only poorly approximates the slope discontinuity associated with a delta source. When segment junction current amplitude and slope matching are used, the current distinction more nearly approaches a slope discontinuity in the region despite causing a tangential electric field source. Finally, as expected, the slope discontinuity source itself provides the most realistic appearing current variation near the source. Note that the current amplitude differs slightly in the latter csse from the former two, due to the fact that the integrated tangential electric field which results in this model with V set equal to one, is actually about 0.9 volts. This indicates a need for more accurately characterizing the feed region geometry in terms of a bicone description so that the proportionality between the voltage and current slope discontinuity is numerically accurate.

In Figure 12 we present results similar to Figure 10a for the case where the feed segment is 1/16 that of the other antenna segments, i.e., R = 1/16. The feed region electric field is now about 16 times larger than that of Figure 10a, and in addition the electric fields associated with the segment ends are now significantly large three segments or more away from the feed. It is the integral of these fields which provides the effective voltage drop used to define the input admittance in Table IV. Therefore while these segment-end fields could logically be regarded as errors because they represent electric fields which do not match the boundary condition on the total tangential electric field along the antenna, surprisingly enough their integral provides a stable value for the antenna input admittance, as discussed above. In Figure 13 a result similar to Figure 10a is plotted for the real component of tangential field for the case where the three center segments are 1/8 of the remaining 18 segments on the antenna, i.e. R = 1/8. In this case the region of non-zero electric field is seen to be confined more closely to the center of the antenna and allows therefore the effective feed voltage to be obtained from the electric field at the center feed

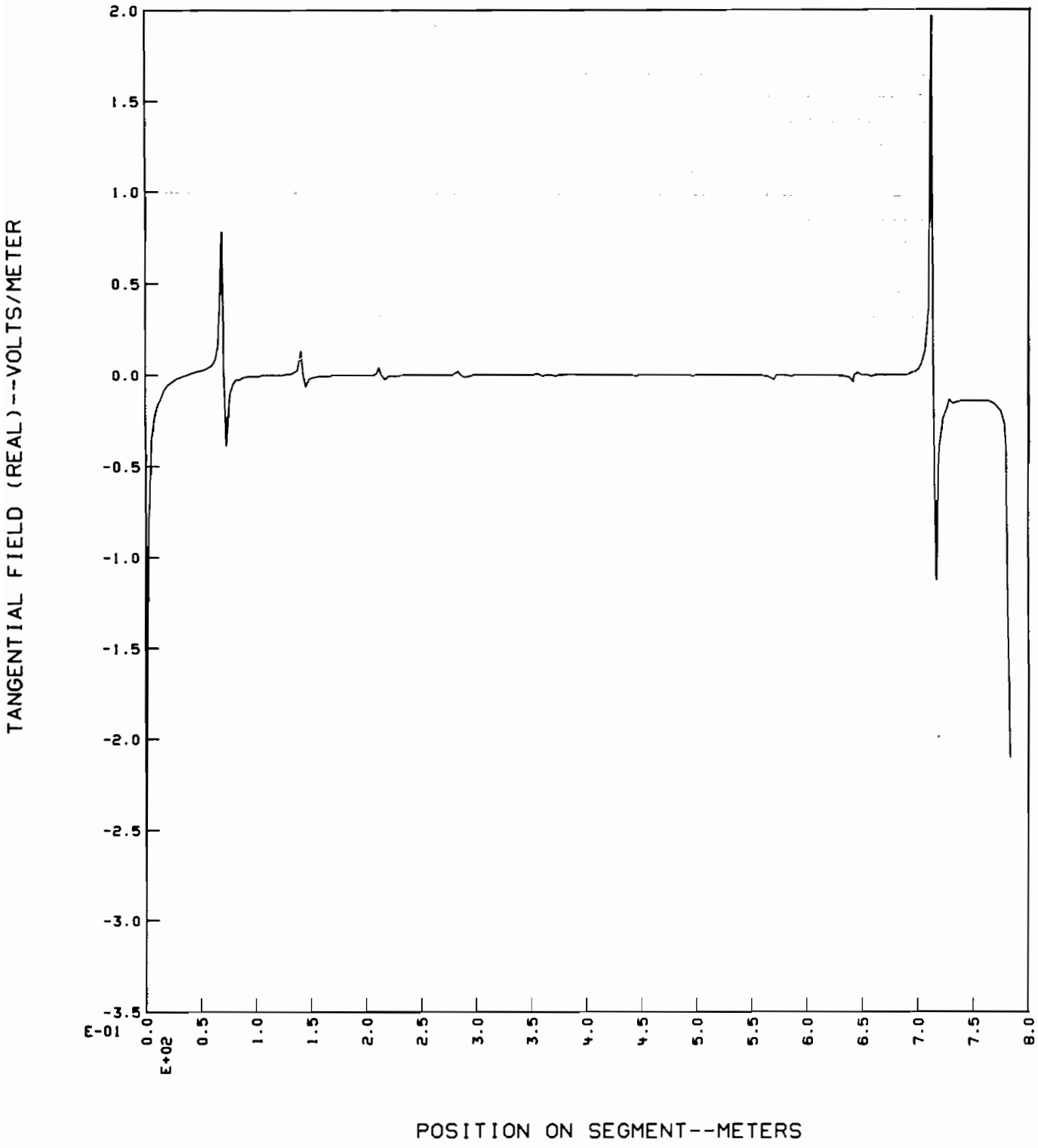

FIGURE 10 a Tangential electric field along half of a half-wavelength dipole (Ω = 15, N - 21 segments).

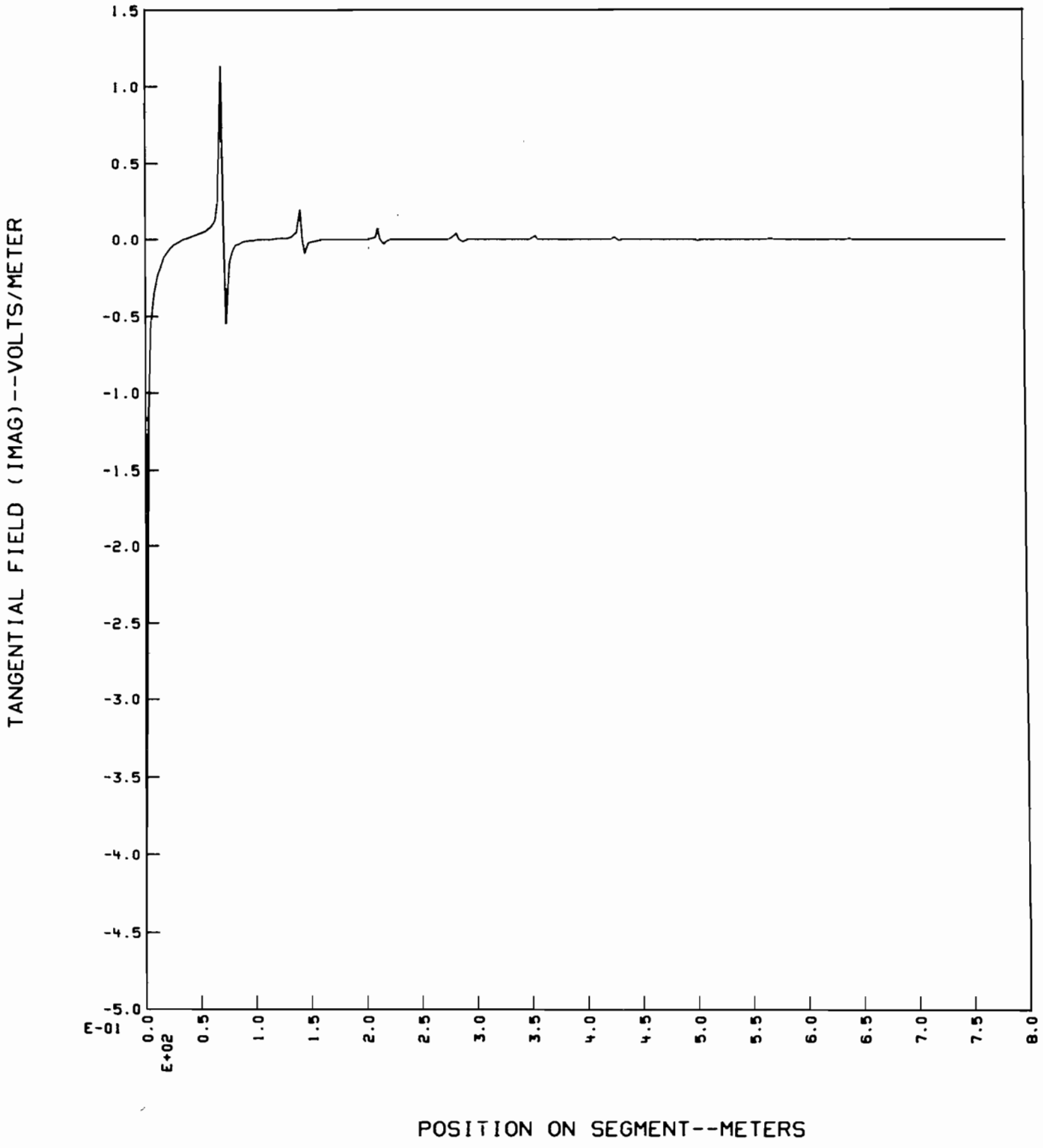

FIGURE 10a' Tangential electric field along half of a half-wavelength dipole (Ω = 15, N = 21 segments).

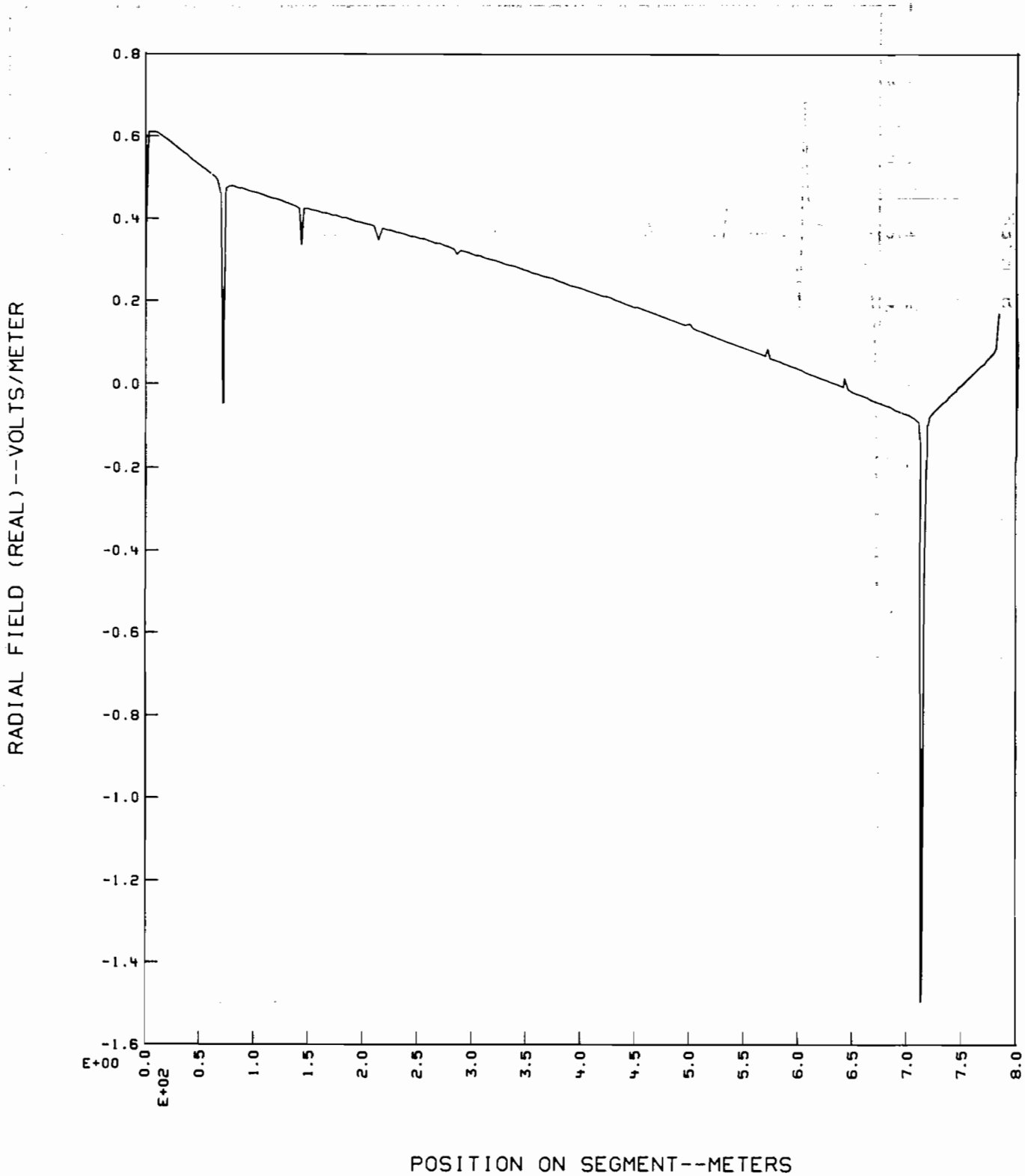

FIGURE 10b Radial electric field along a dipole (Ω = 15, N = 21).

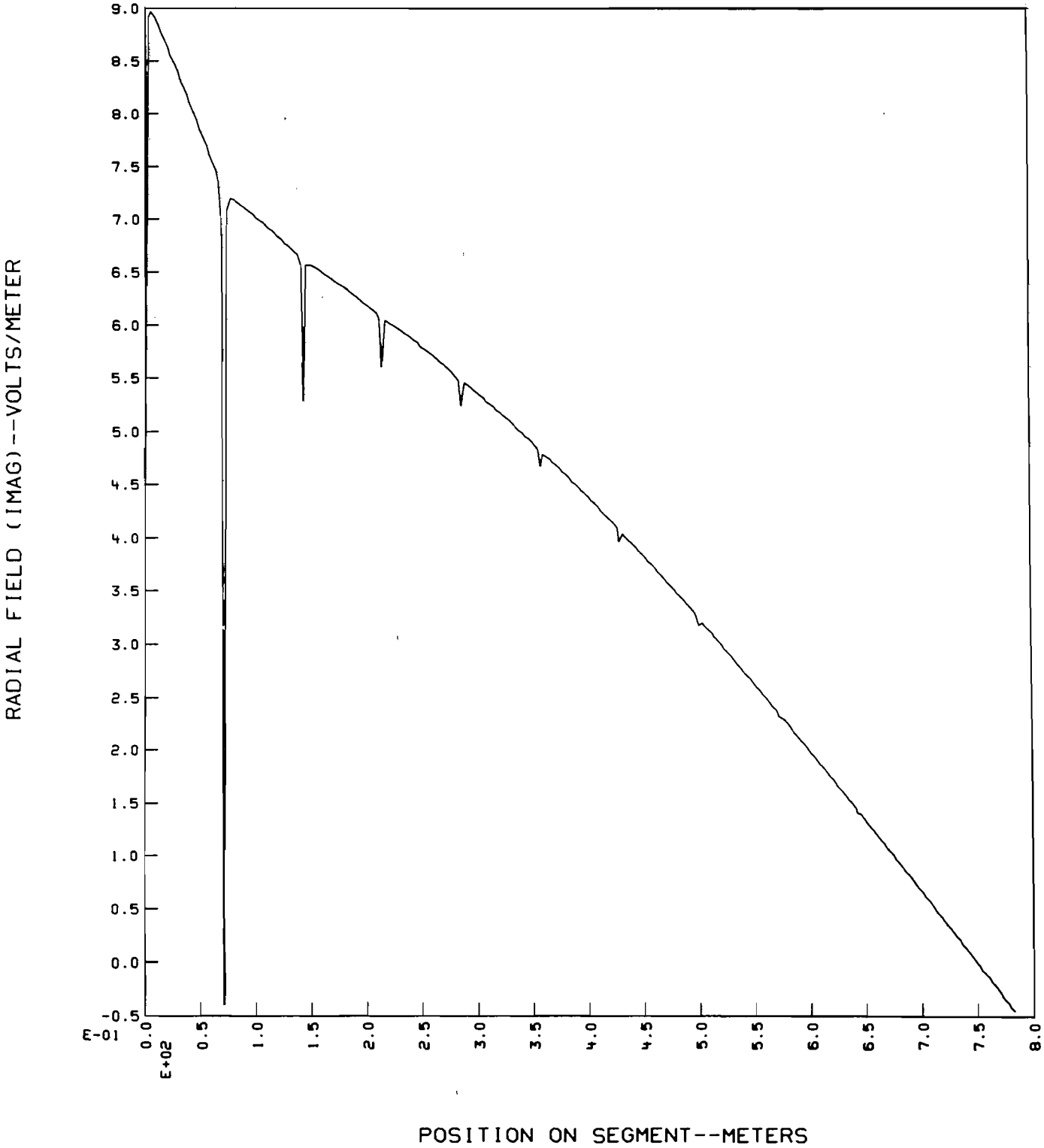

FIGURE 10b' Radial electric field along a dipole (Ω = 15, N = 21).

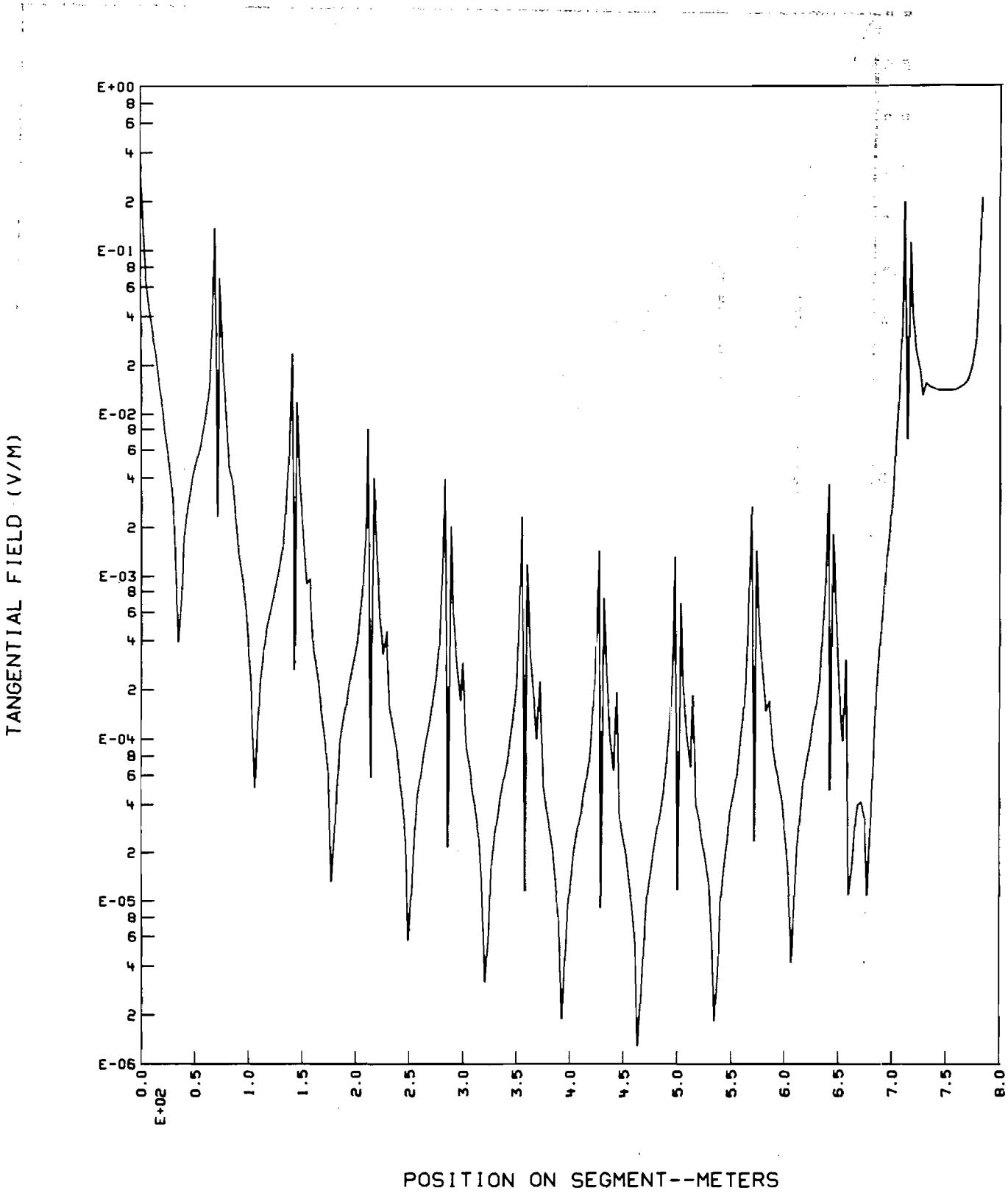

FIGURE 10c Magnitude of tangential field along dipole (Ω = 15, N = 21).

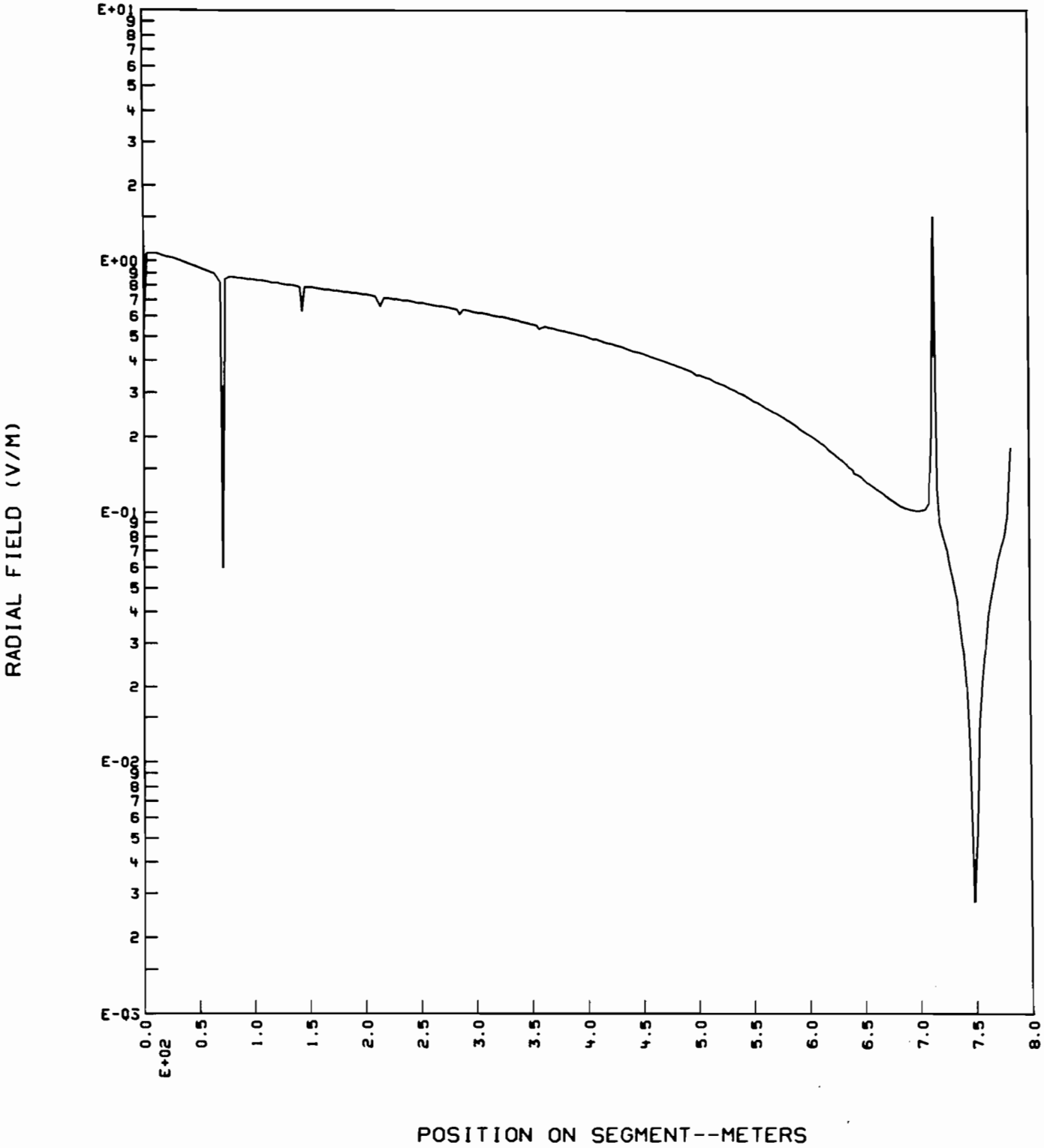

FIGURE 10c' Magnitude of radial electric-field along dipole (Ω = 15, N = 21).

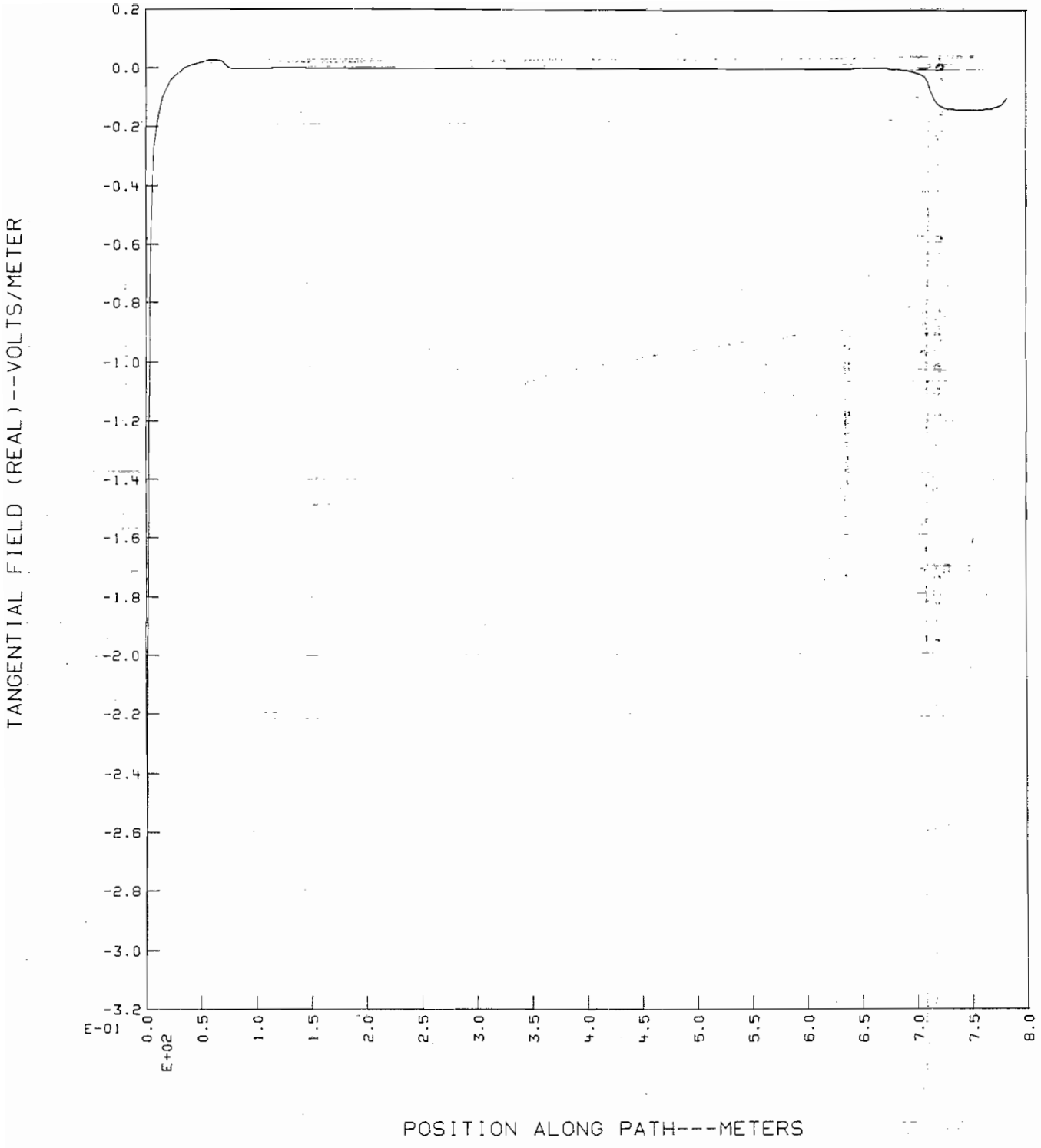

FIGURE 10d Tangential electric field along half of a half-wavelength dipole (Ω = 15, N = 21 segments) (Current amplitude, and derivative matched at segment junctions.

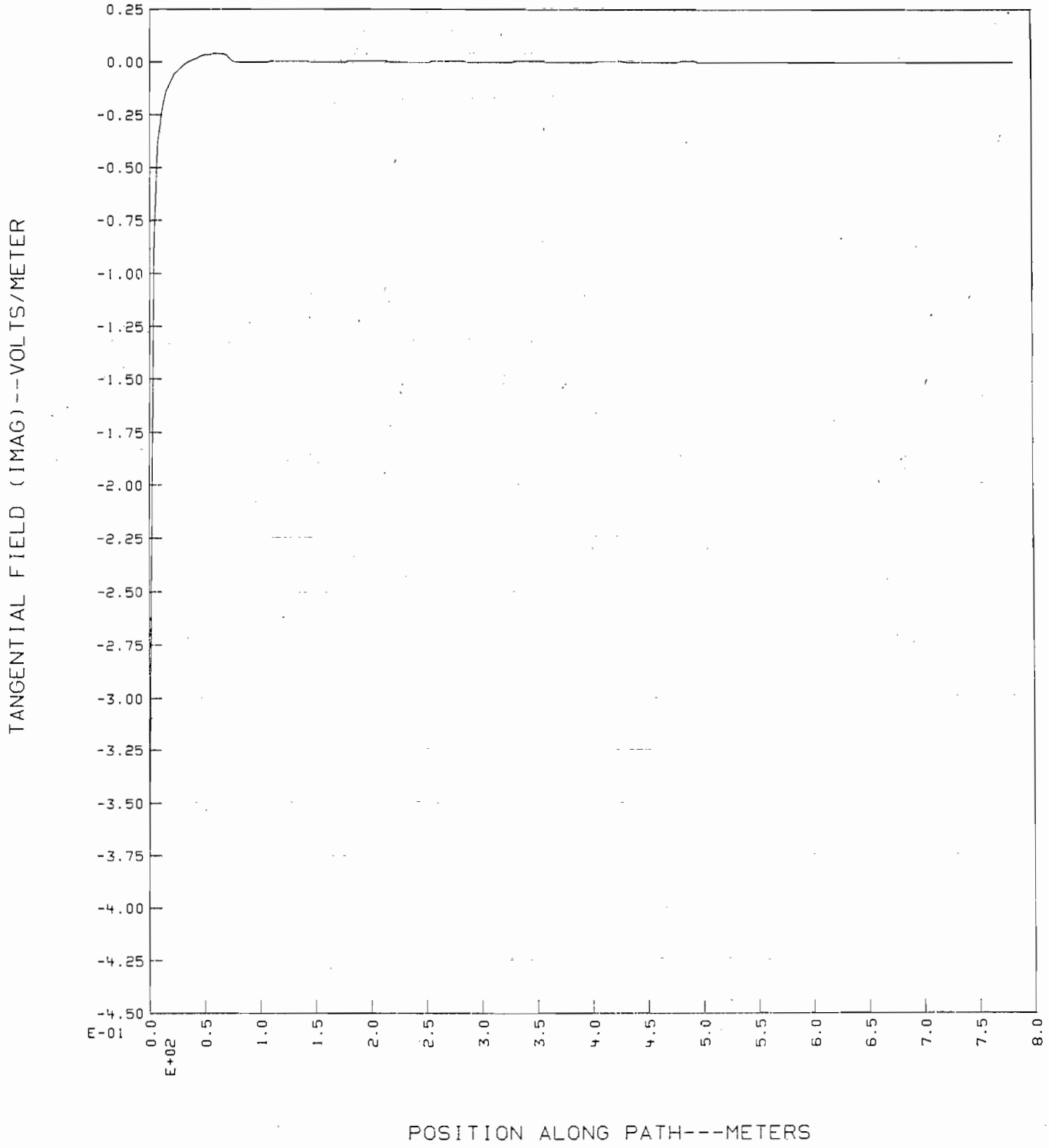

FIGURE 10d' Tangential electric field along half of a half-wavelength dipole (Ω = 15, N = 21 segments) (Current amplitude and derivative matched at segment junctions).

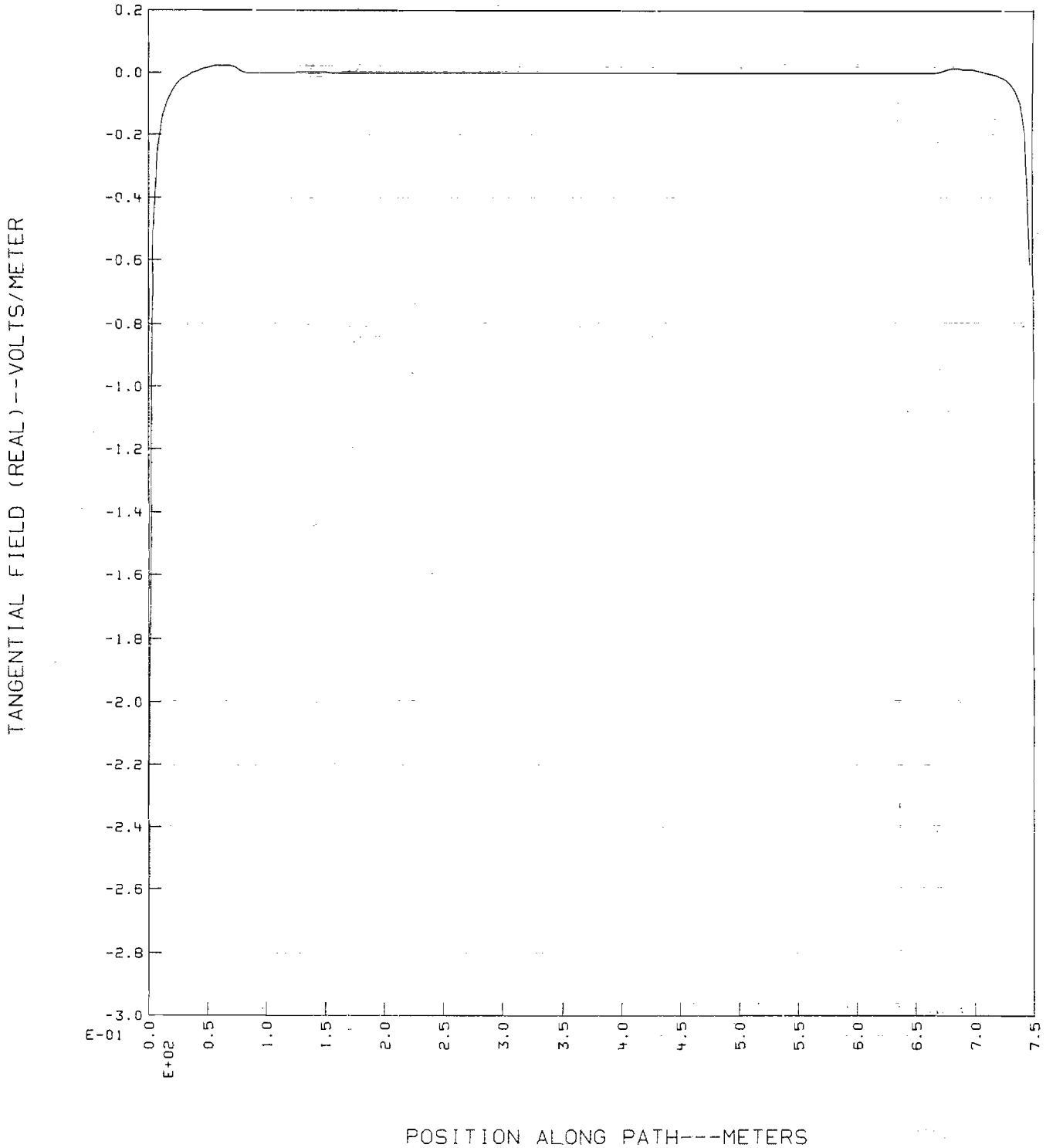

FIGURE 10e Tangential electric field along half of a half-wavelength dipole (Ω = 15, N = 20 segments) (Exciting source introduced as a slope current discontinuity).

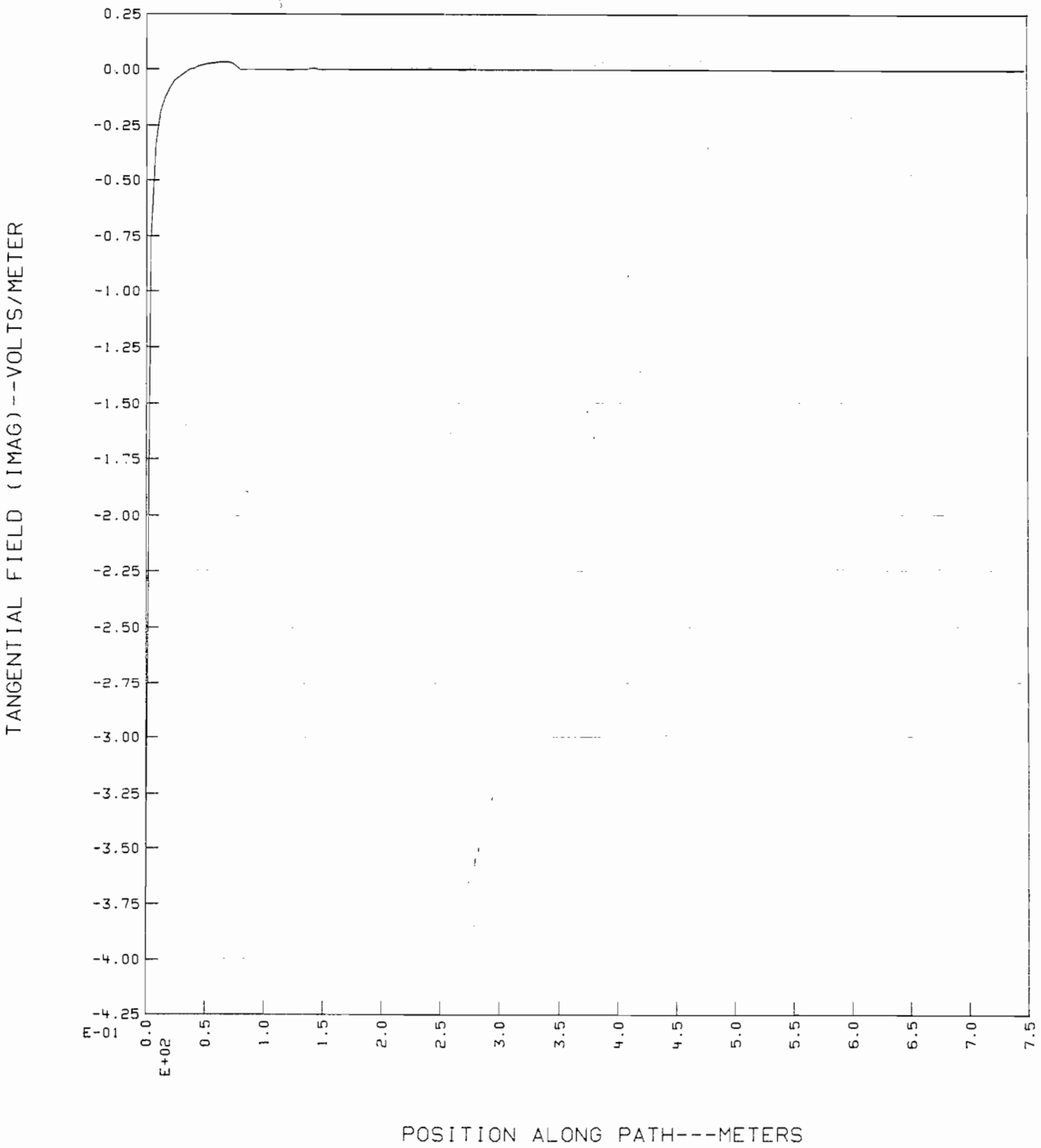

FIGURE 10e' Tangential electric field along half of a half-wavelength dipole (Ω = 15, N = 20 segments) (Exciting source introduced as a slope current discontinuity).

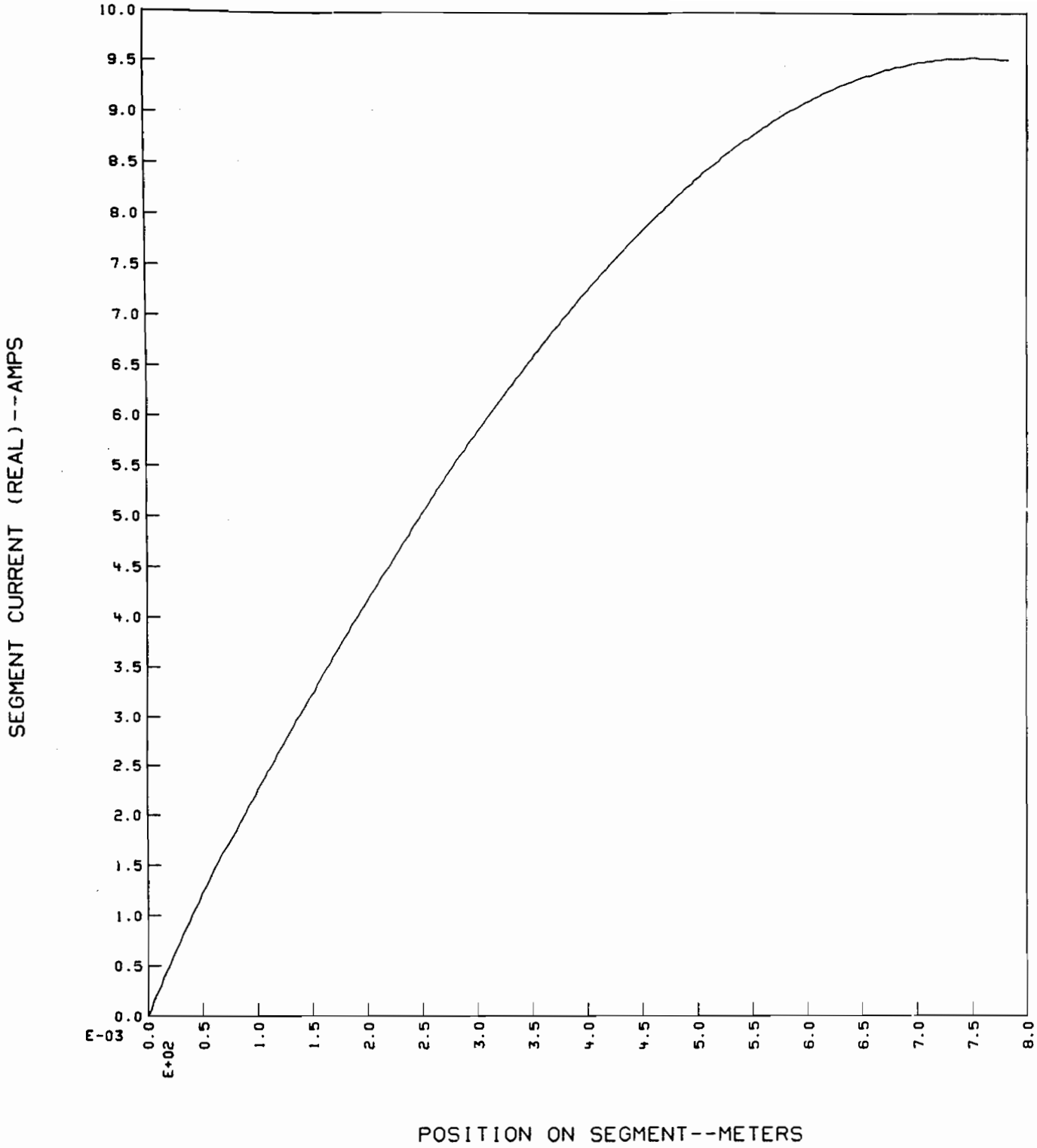

FIGURE 11a Current distribution along half of a dipole (Current extrapolation).

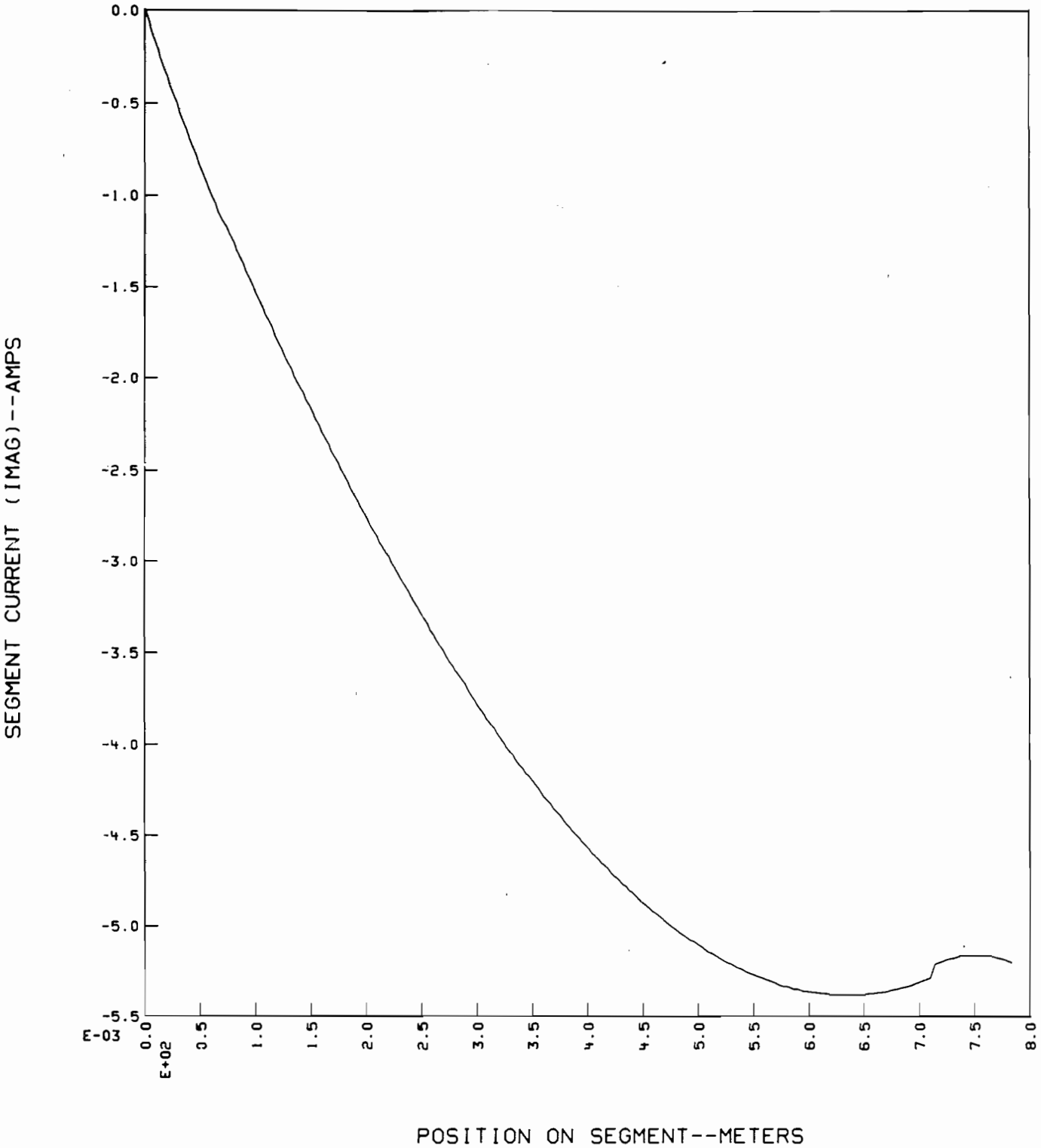

FIGURE 11b Current distribution along half of a dipole (Current extrapolation).

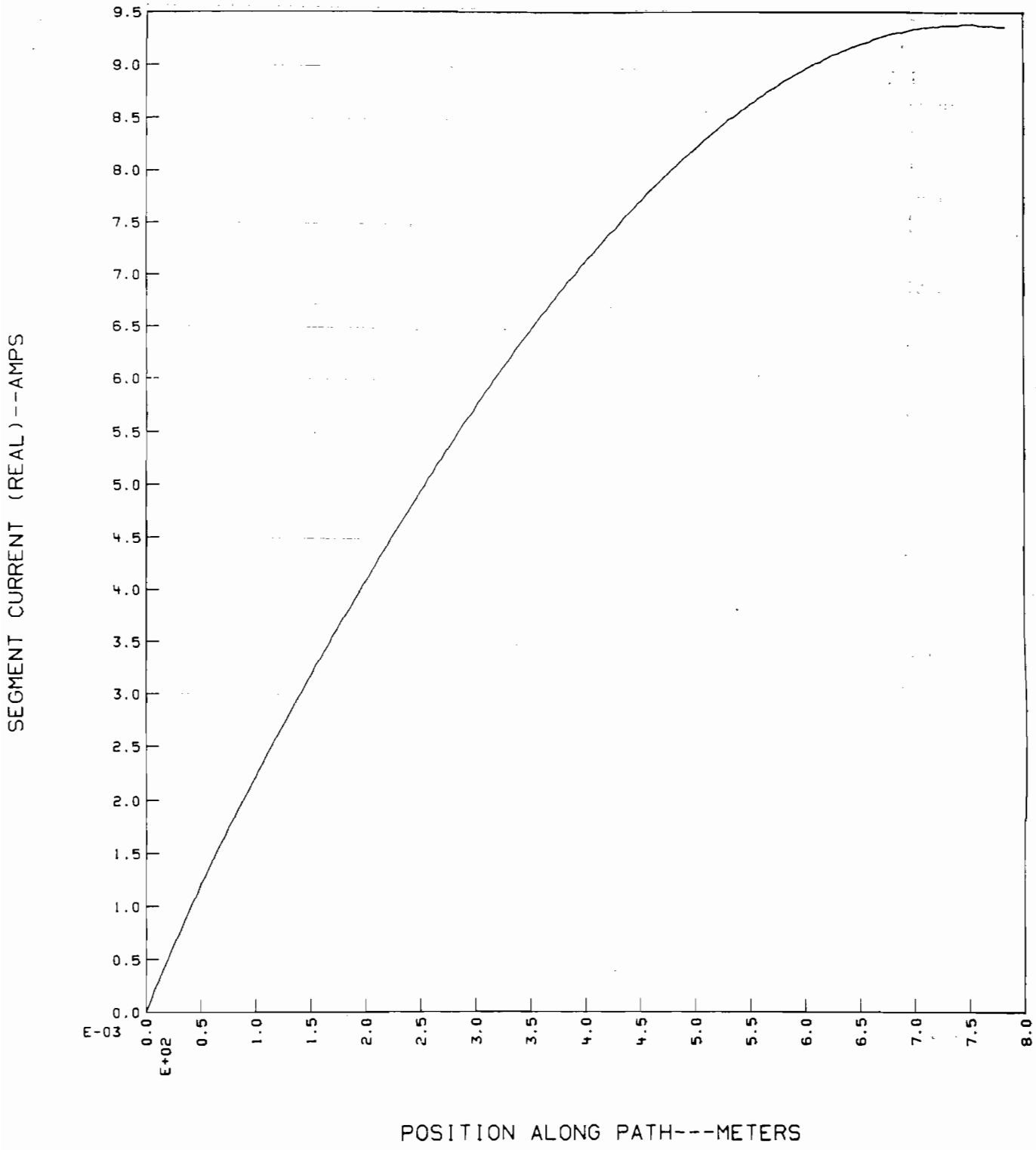

FIGURE 11c Current distribution along half of a dipole (Current amplitude and derivative matched at segment junctions).

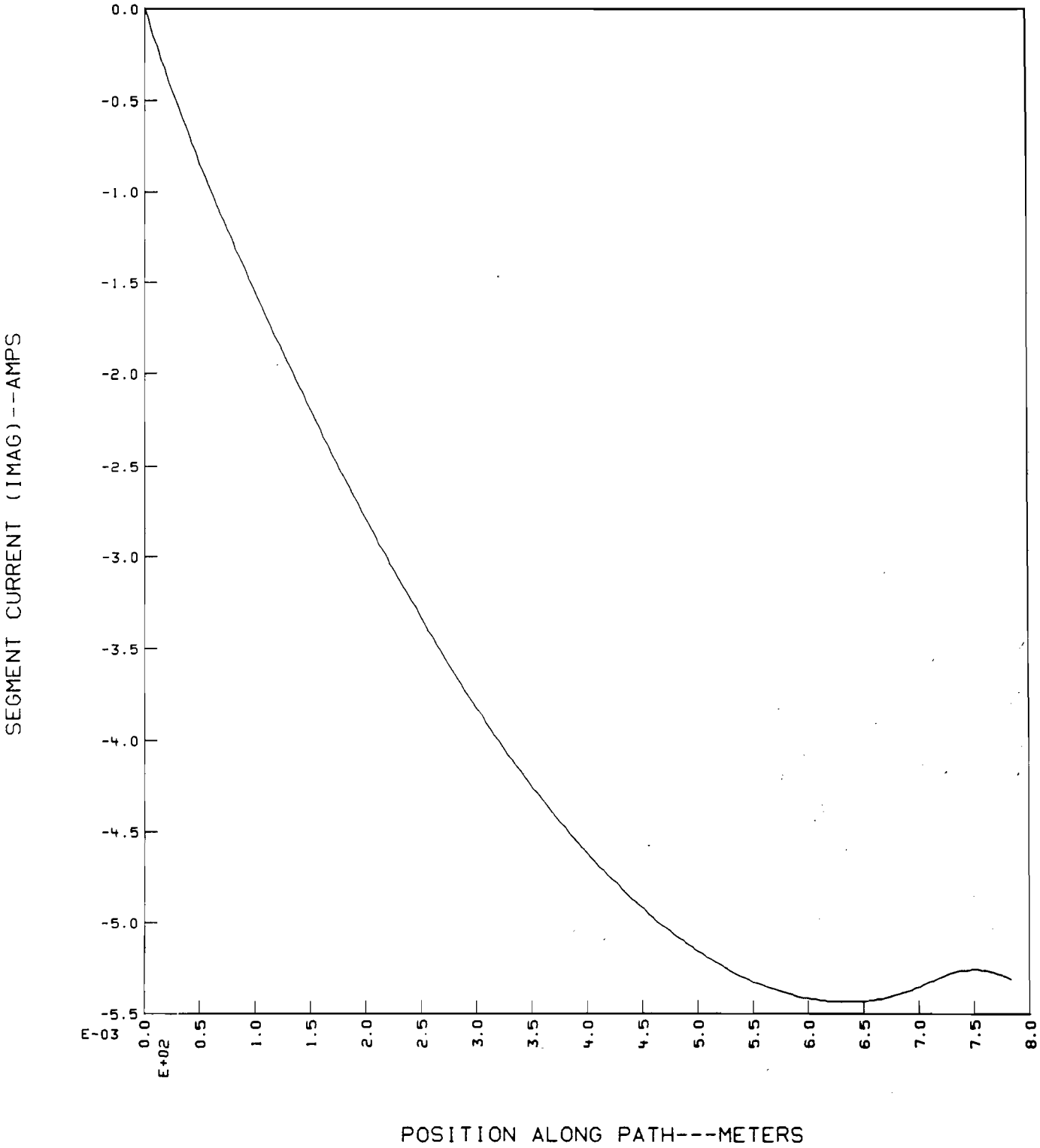

FIGURE 11d Current distribution along half of a dipole (Current amplitude and derivative matched at segment junctions).

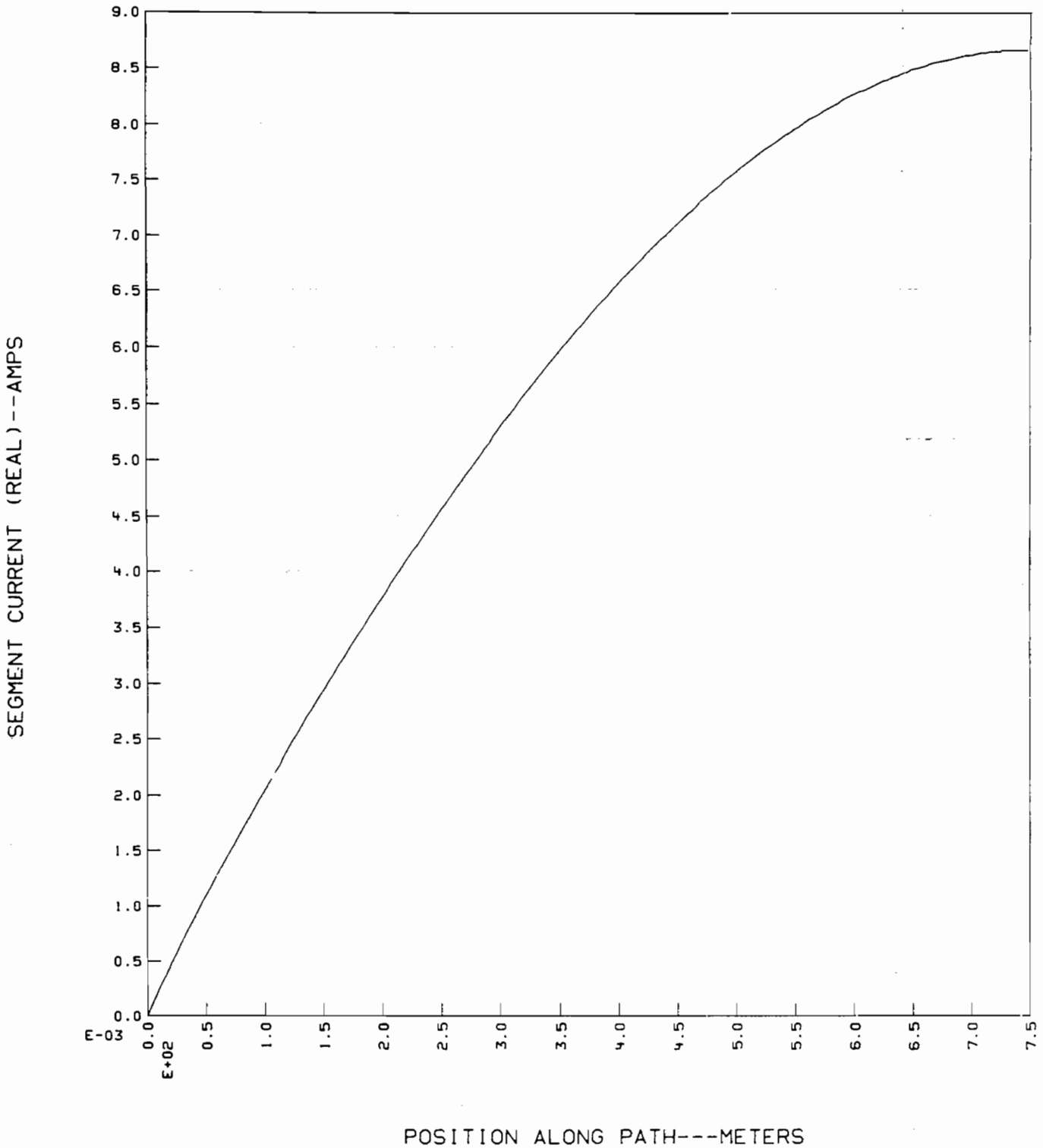

FIGURE 11e Current distribution along half of a dipole (Exciting source introduced as a slope discontinuity).

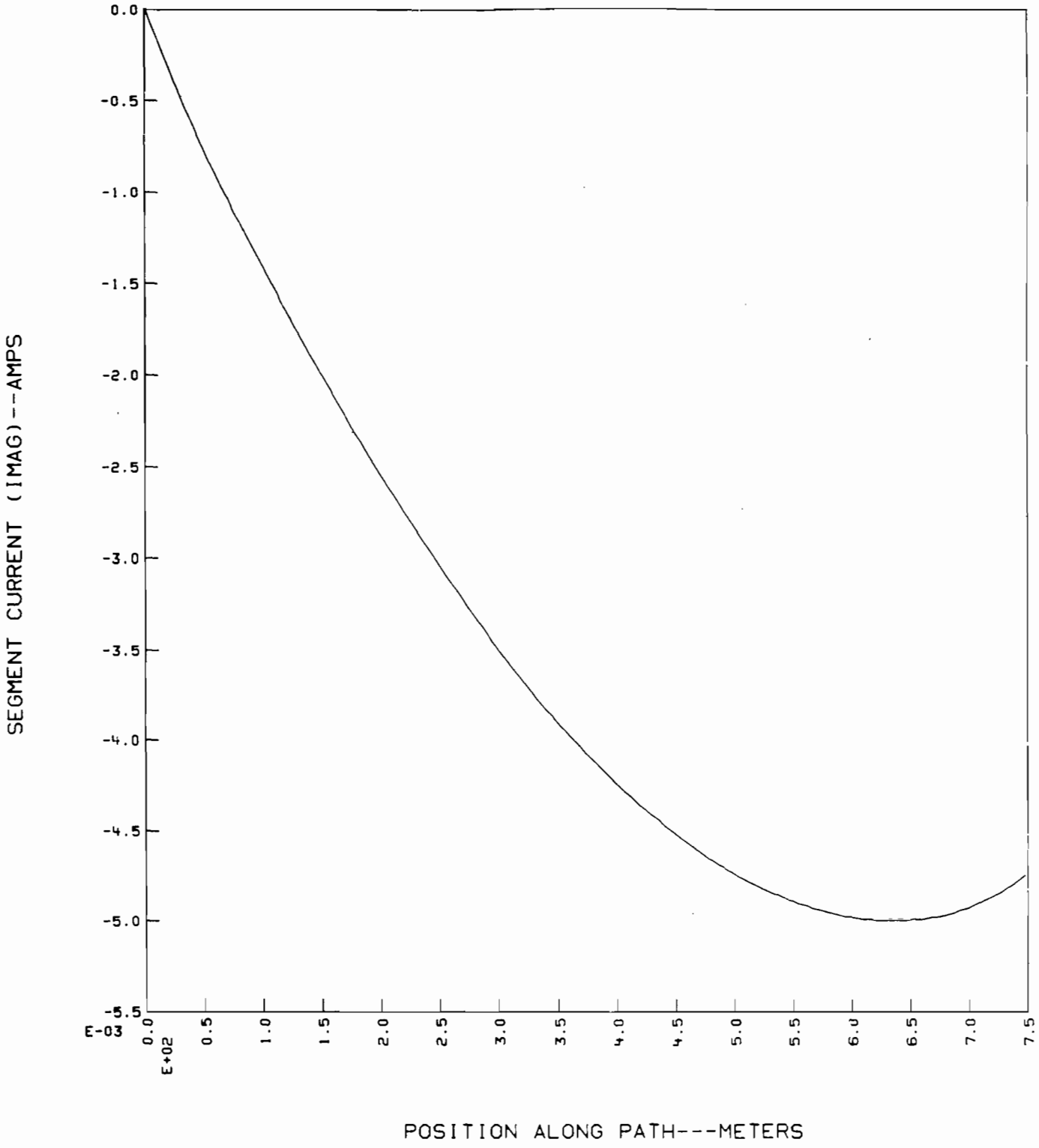

FIGURE 11f Current distribution along half of a dipole (Exciting source introduced as a slope discontinuity).

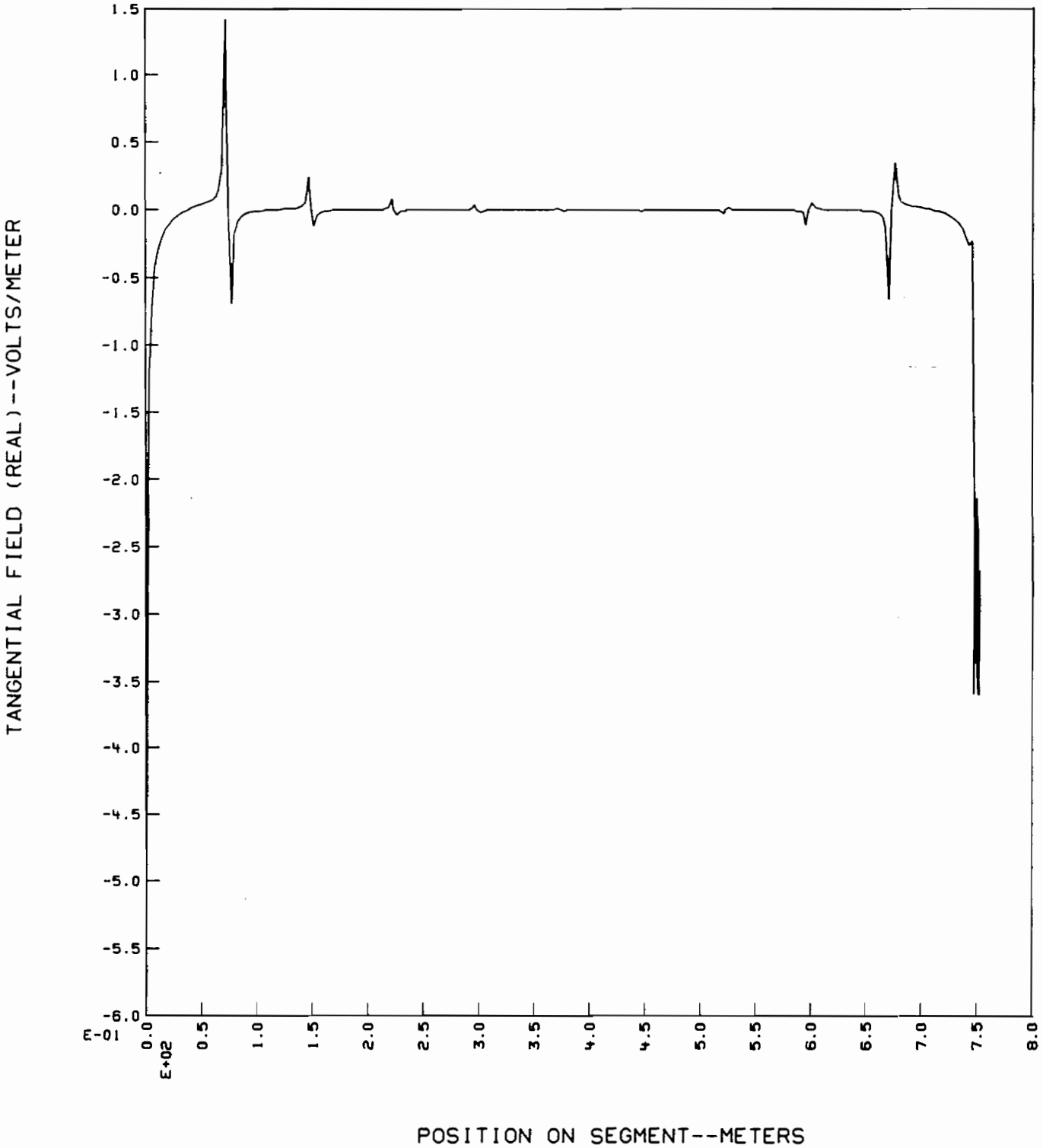

FIGURE 12a Tangential electric field for dipole where feed segment is 1/16 that of the other antenna segments.

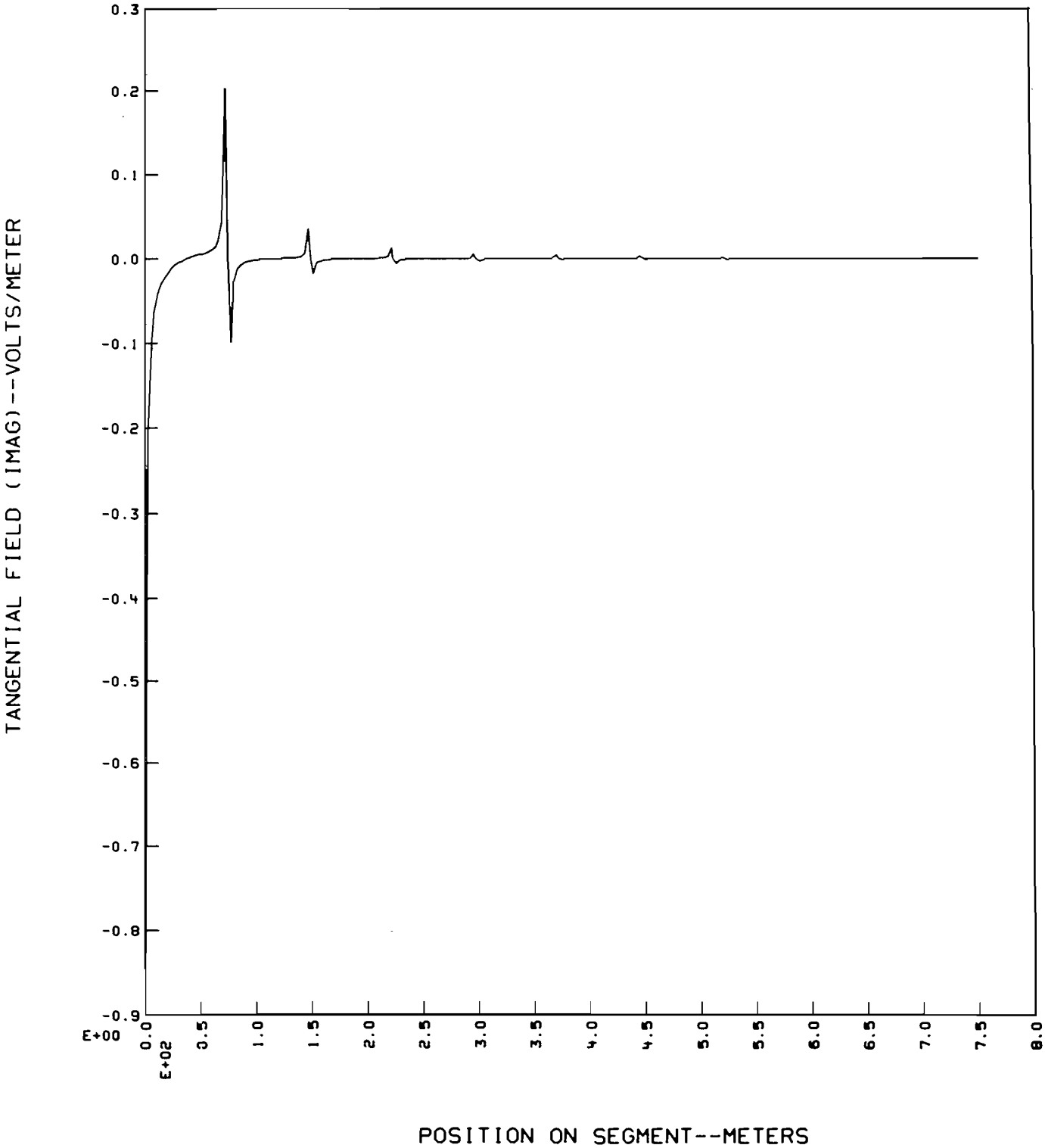

FIGURE 12a' Tangential electric field for dipole where feed segment is 1/16 that of the other antenna segments. Frequency = 100 kHz for all cases.

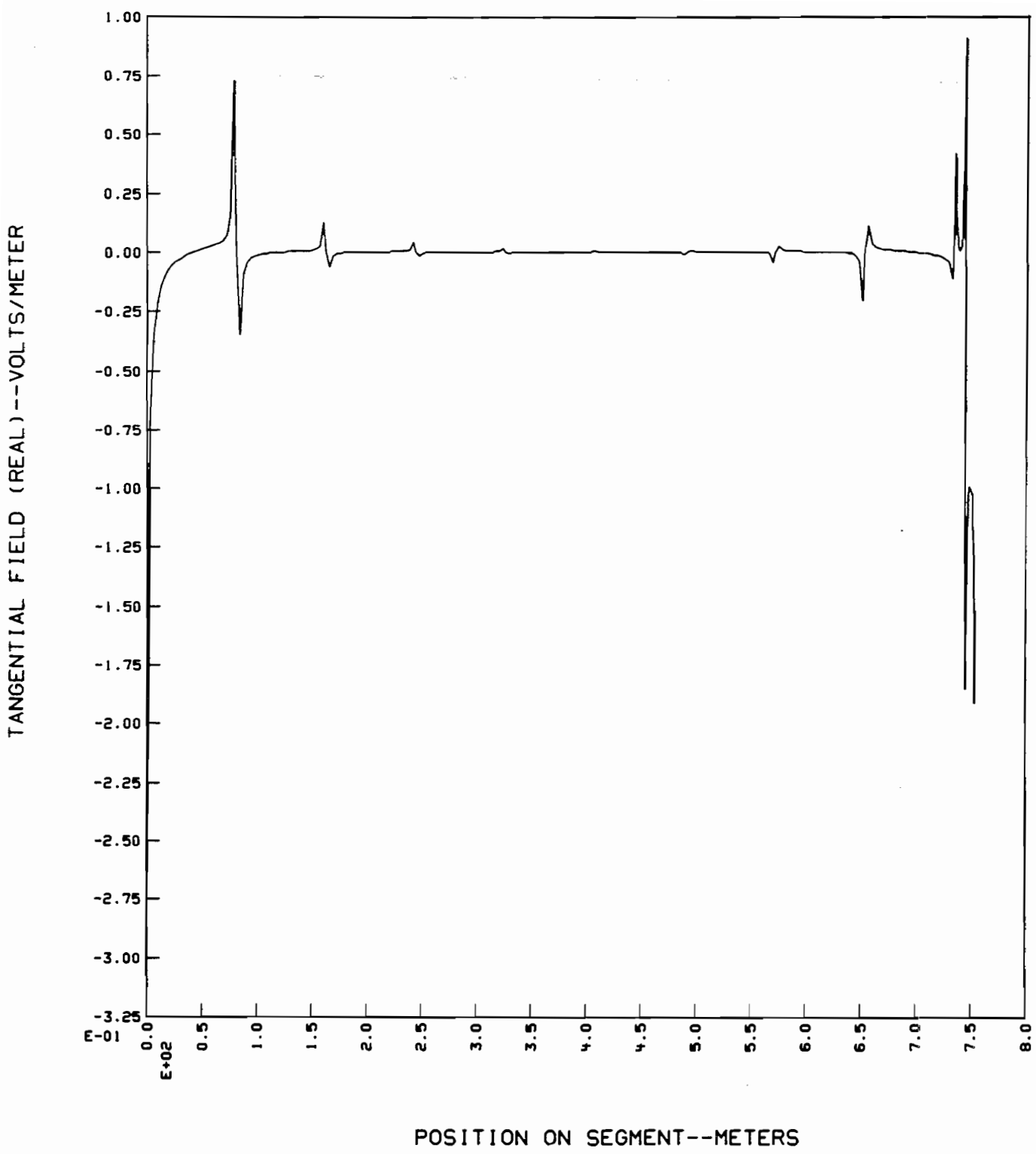

FIGURE 13a Tangential electric field for a 21 segment dipole (Ω = 15), where the three center segments are each 1/8 of the other segments, i.e. R = 1/8.

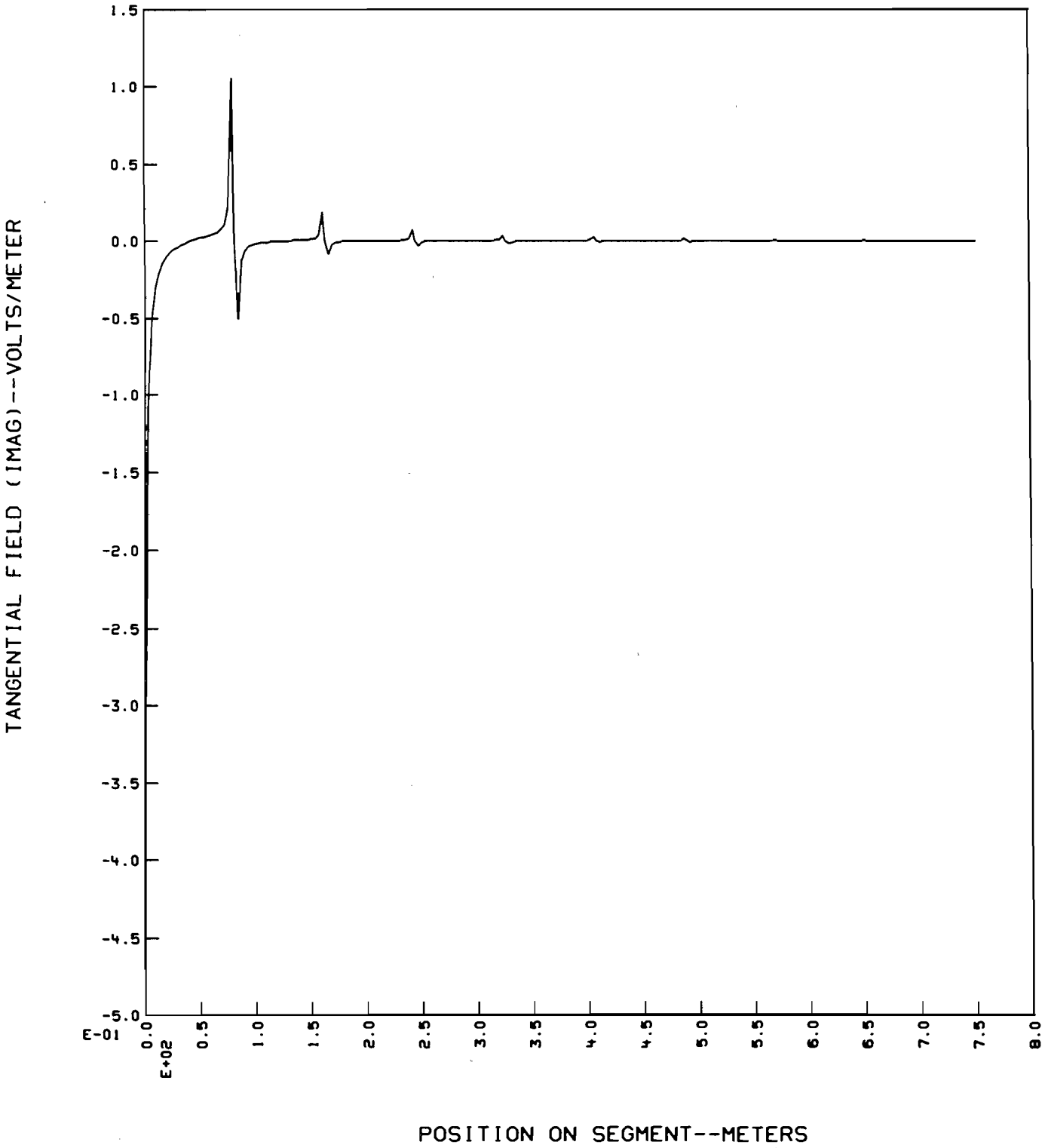

FIGURE 13a' Tangential electric field for a 21 segment dipole (Ω = 15), where the three center segments are each 1/8 of the other segments, i.e. R = 1/8, frequency = 100 kHz.

segment multiplied by the segment length itself. A worthwhile extension of this study would be to examine the influence of independently varying the boundary condition match points and the segment lengths on the linear antenna.

Calculations similar to these just presented have also been performed for the fields along the V-dipole antenna previously discussed in Section C above. We present in Figures 14a-14c below the tangential field along the nominal V-dipole model and various models containing unequal segment lengths in the source region. These results demonstrate that even for the nominal case where all segment lengths are equal there are significant non-zero tangential fields in the vicinity of the V-junction. These tangential fields become even more pronounced when there is a discontinuity in length between the segments on the center section and those on the V-arm as shown by Figure 12b. When however, the shortened segments are confined to the source region itself while maintaining equal length segments at the V-junction, the near field anomonaly is not as nearly pronounced, as shown by Figure 12c. As in the case of the linear antenna, it is the tangential fields shown in these plots which are integrated to obtain the effective driving voltage and to subsequently define the input admittance for the V-dipole antenna. For completeness we also present in Figure 12d the current distribution along one-half the V-dipole antenna for the nominal geometry case. There we see as expected, the halving of the current flowing along one of the symmetric V-arms relative to that on the center section, as required by Kirchoff's Law at the multiple junction.

The multiple junction results presented for the V-dipole antenna demonstrate the extreme variation which may be encountered in both the tangential and radial electric field components near a multiple wire junction. While we have demonstrated that the tangential field variation itself, may, when integrated, provide in some cases a numerically stable value for the input admittance, it is not clear that the radial field, which is in general much larger, is meaningful in terms of determining the propensity for corona discharge of the antenna. There are many practical applications of course where it is very important to obtain an accurate indication of the near field especially in the vicinity of wire bends, multiple junctions, etc. to determine whether precautions are required to eliminate corona discharge, which can of course have a significant negative impact on antenna performance. We therefore require a reliable indication of the radial electric field along the antenna, particularly in the vicinity of multiple junctions, if the computed near field results are to be at all useful.

In order to study this problem we have performed some calculations in the vicinity of a simple multiple wire junction. For convenience we have chose to use a dipole having a linear center section and a perpendicular wire connected at each end so that one-half the dipole resembles

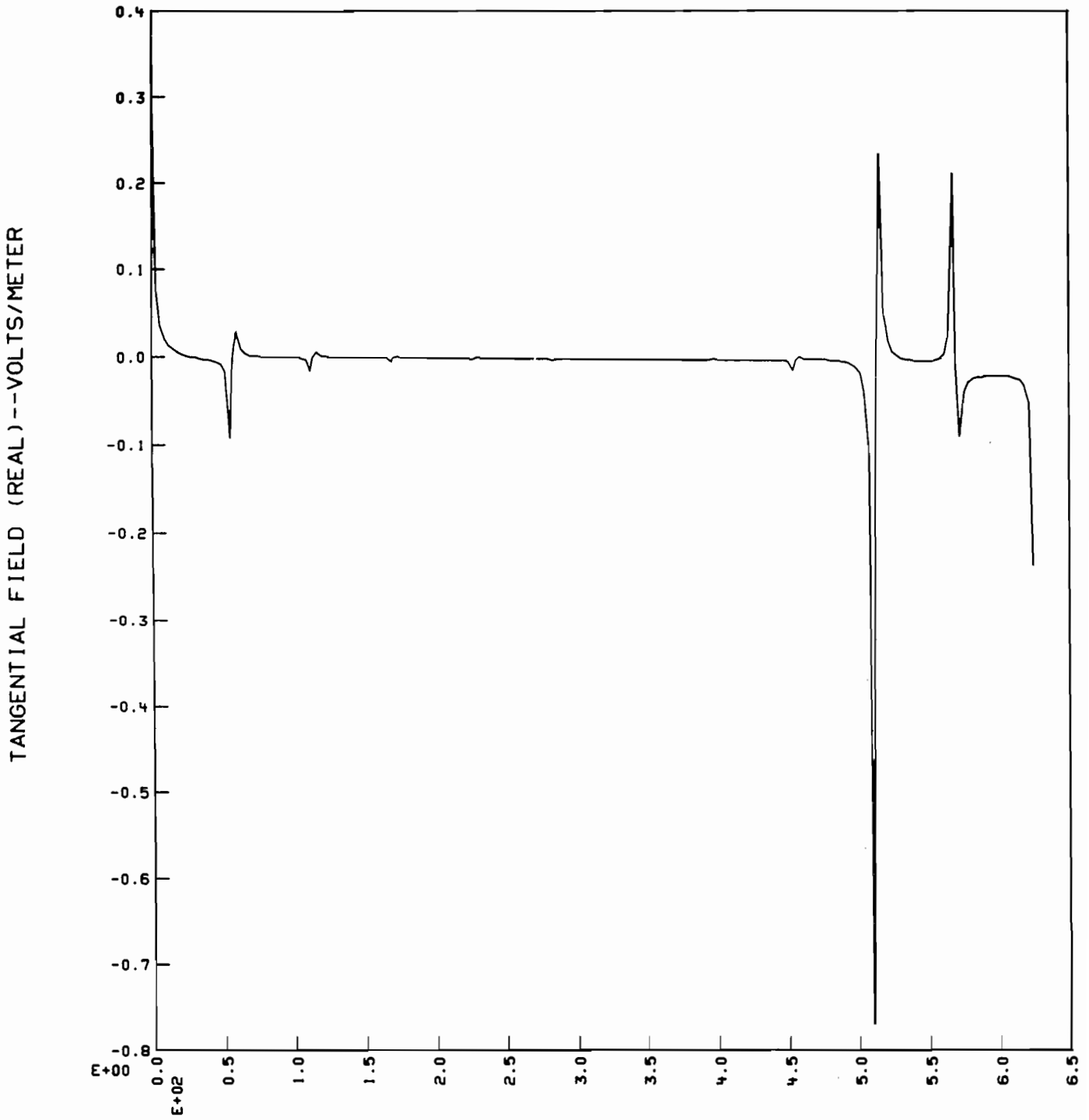

FIGURE 14a Tangential electric field for V-dipole antenna ($\delta/\Delta = 1$)

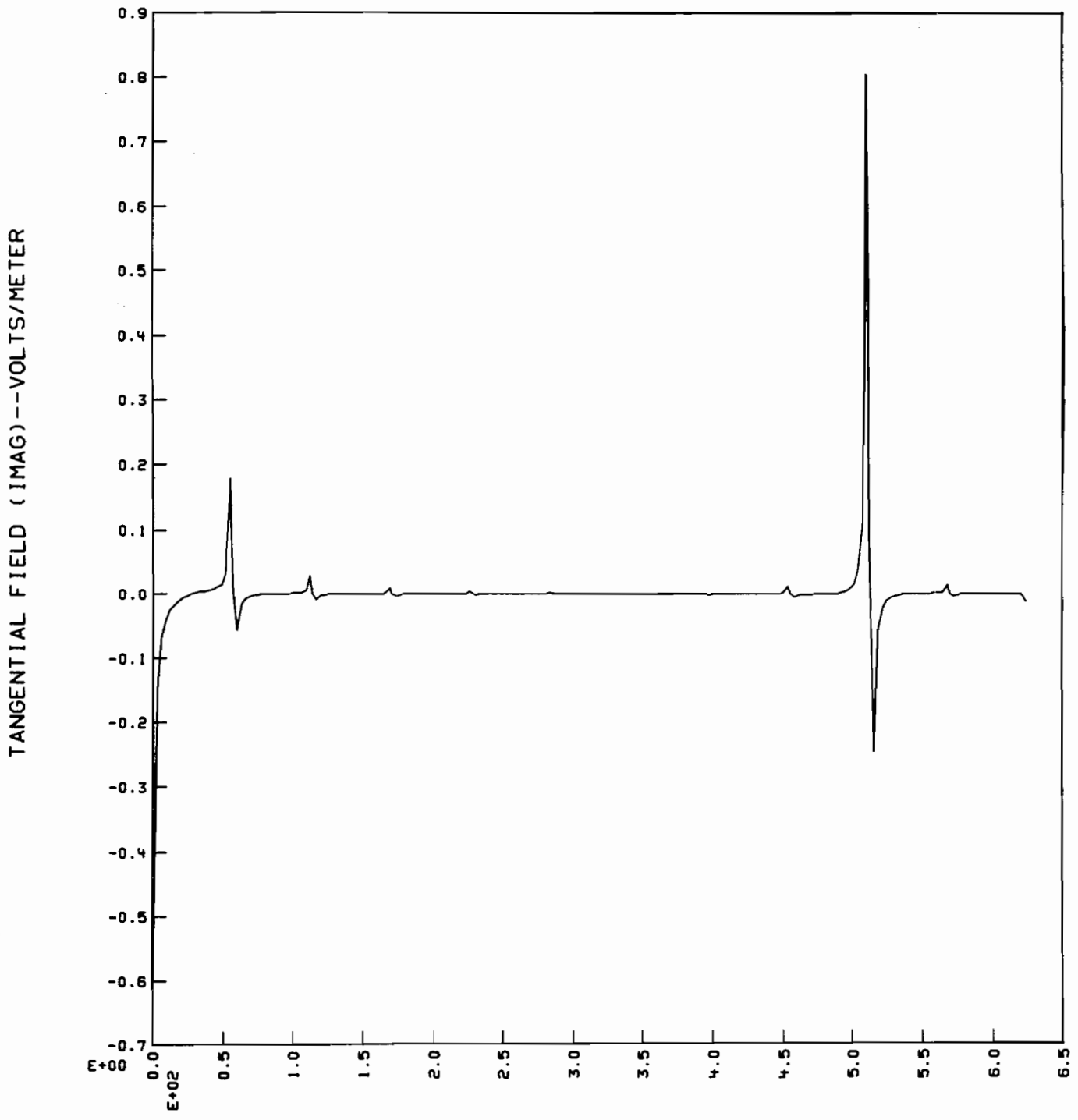

FIGURE 14a' Tangential electric field for V-dipole antenna ($\delta/\Delta = 1$)

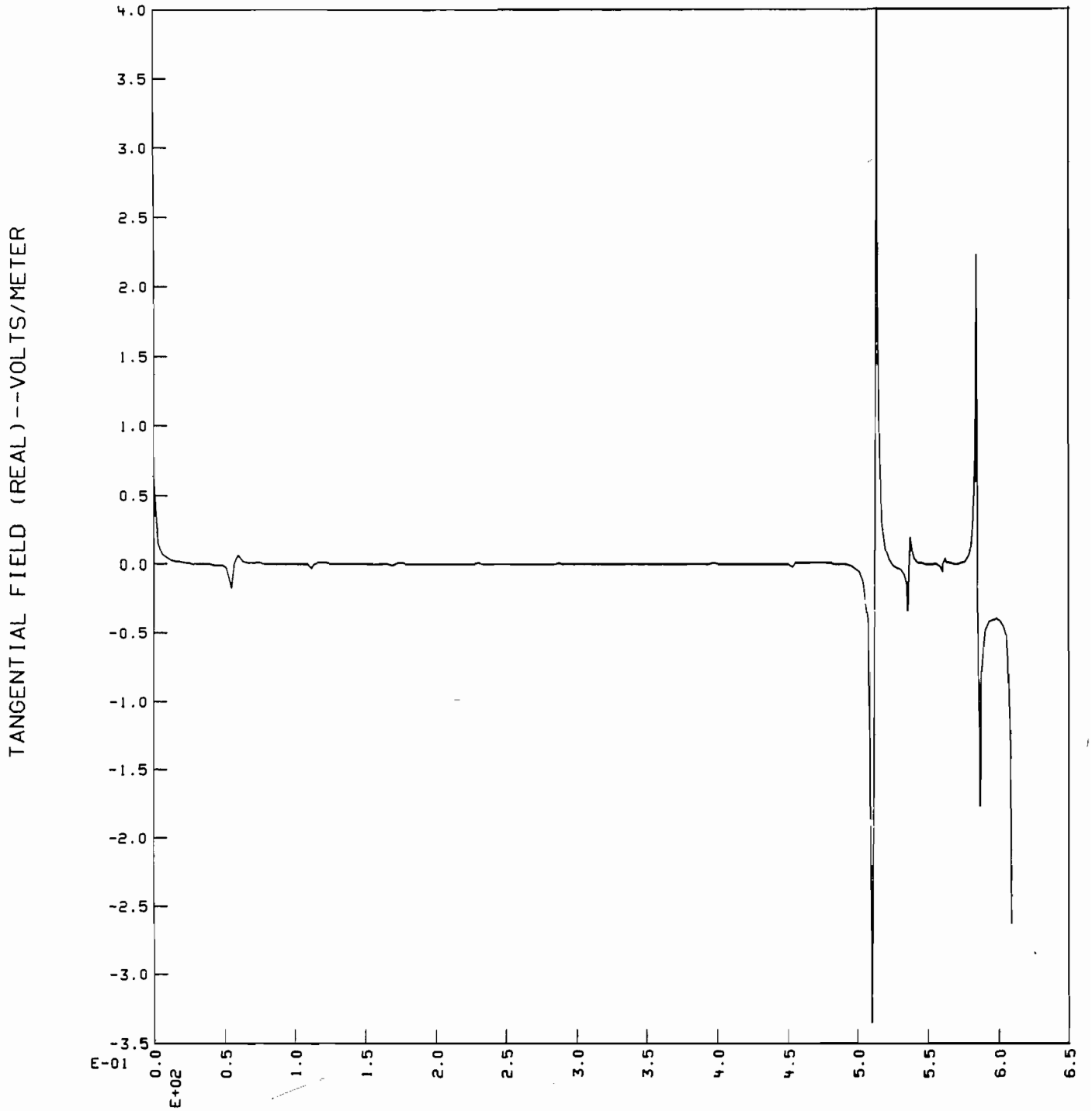

FIGURE 14b Tangential electric field for V-dipole (δ/Δ = 3/7)

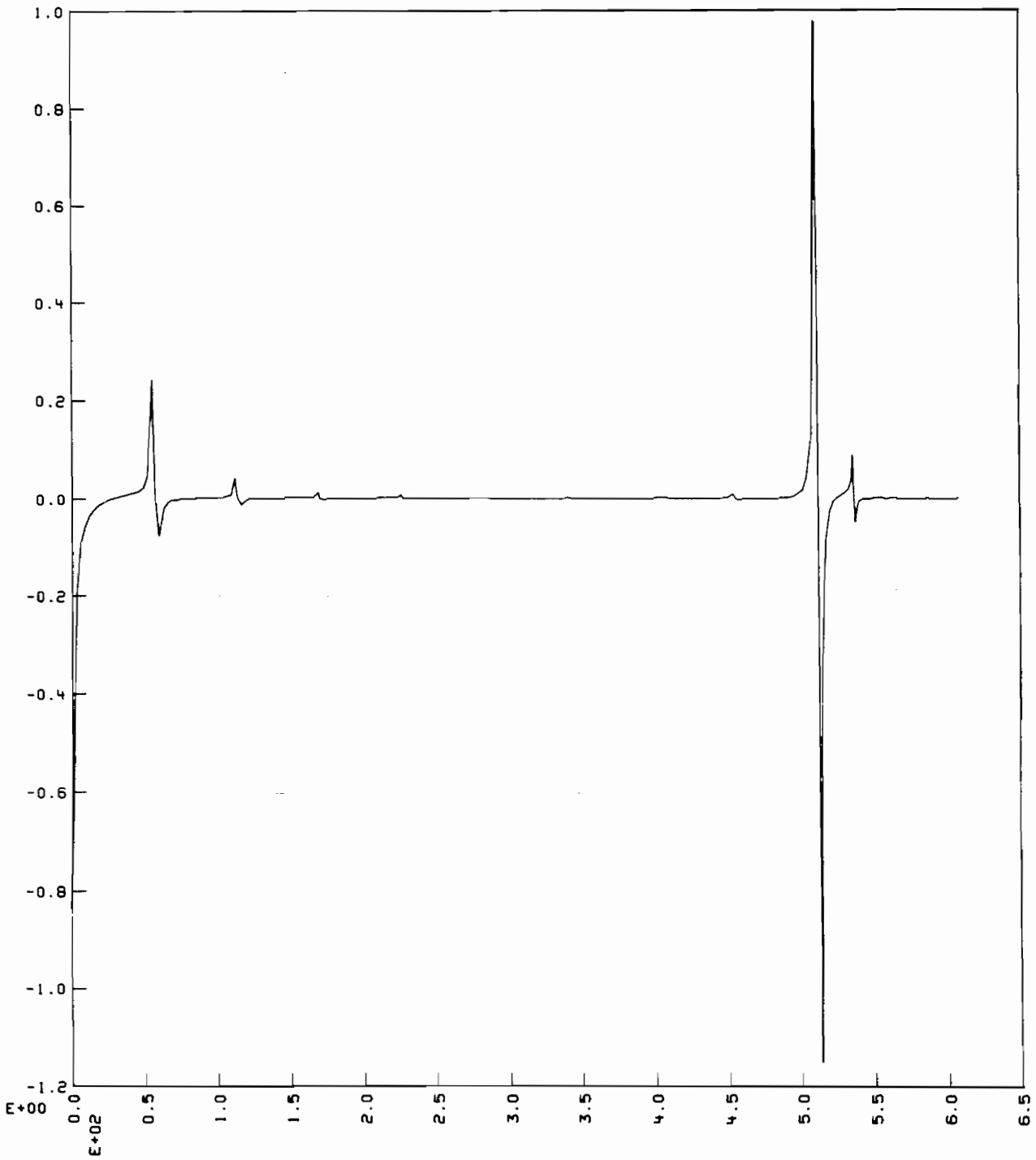

FIGURE 14b' Tangential electric field for V-dipole (δ/Δ = 3/7)

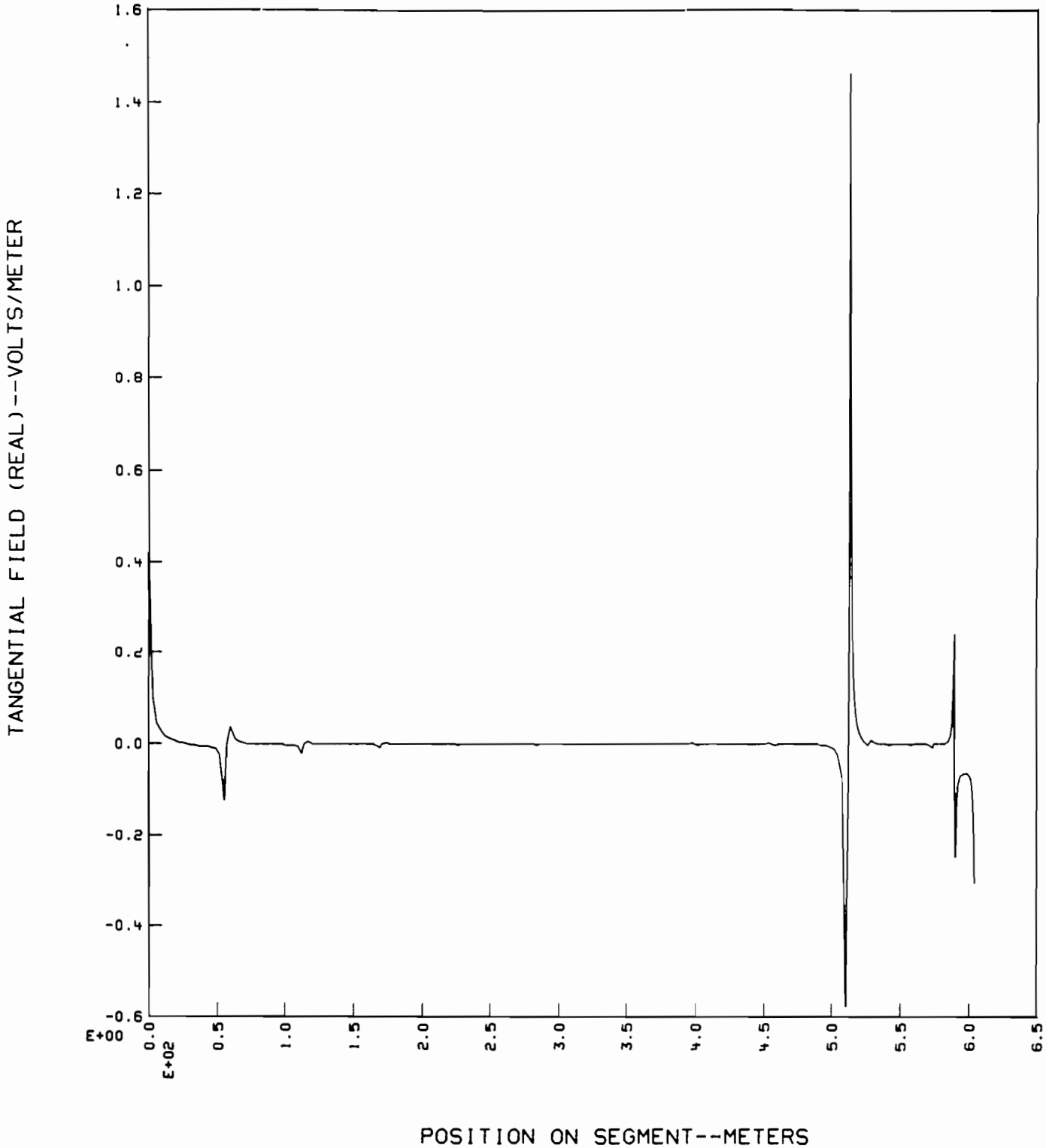

FIGURE 14b'' Tangential electric field for V-dipole (δ/Δ = 3/11)

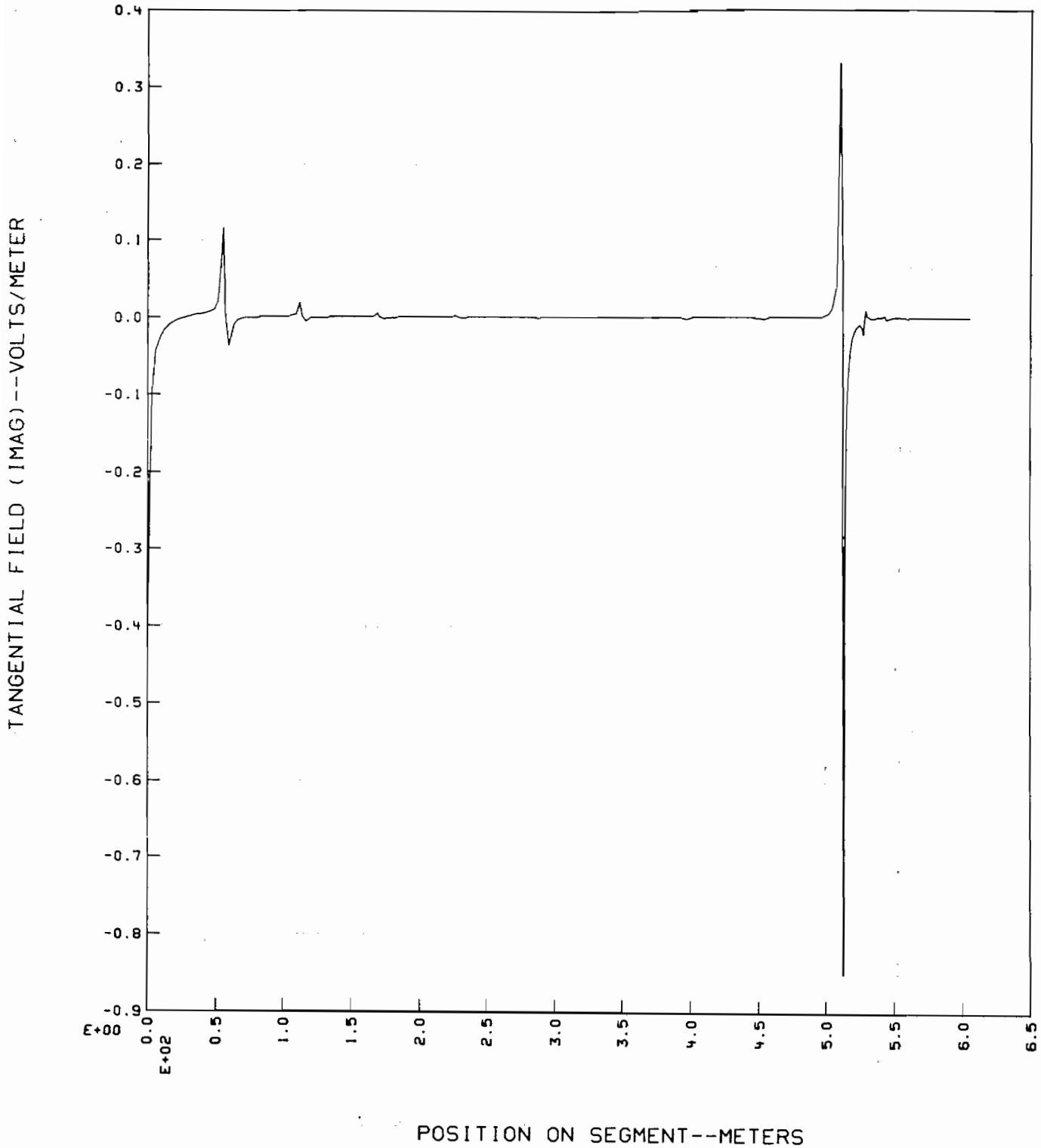

FIGURE 14b''' Tangential electric field for V-dipole (δ/Δ = 3/11)

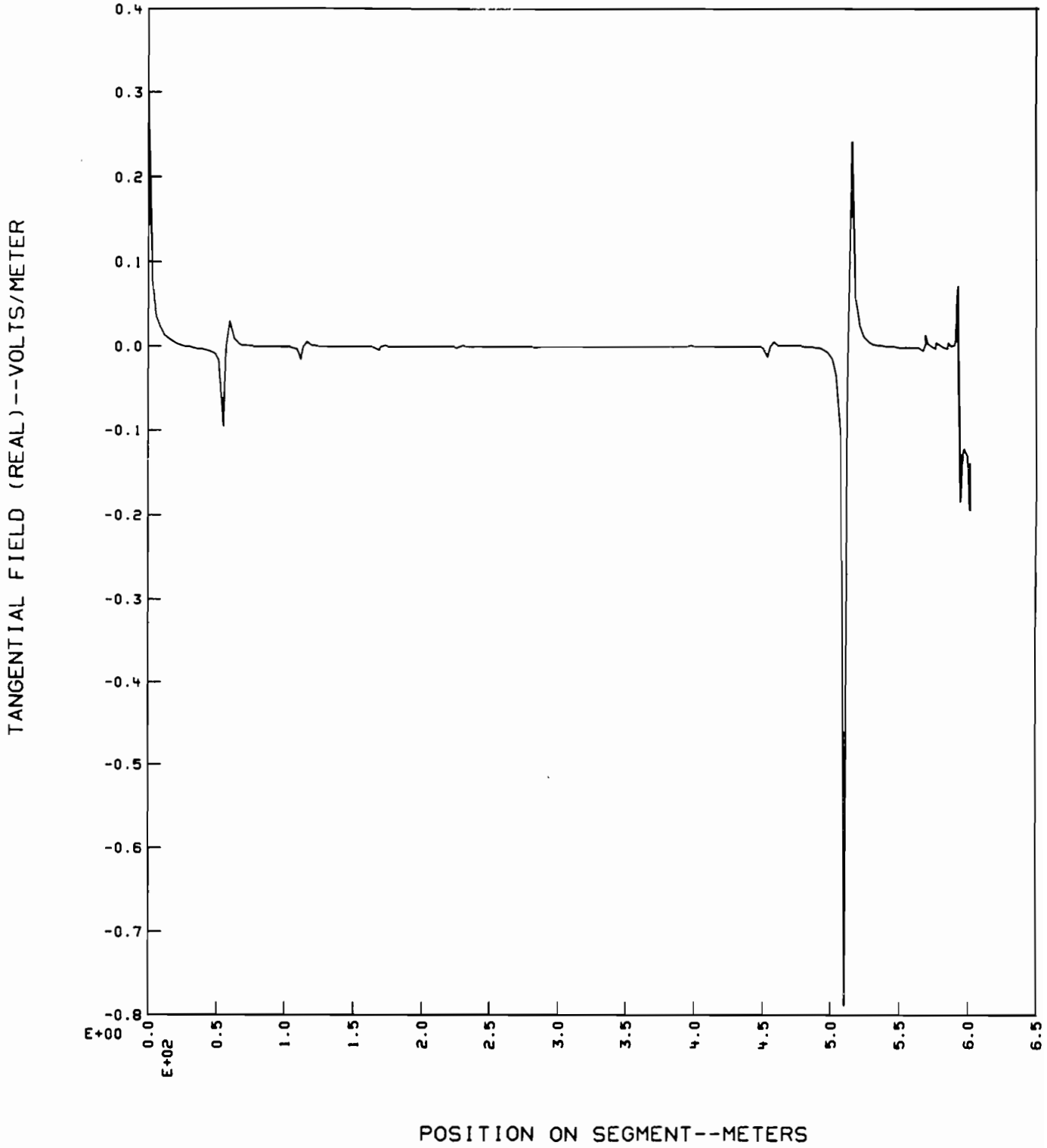

FIGURE 14c Tangential electric field for V-dipole (δ/Δ = 1/7)

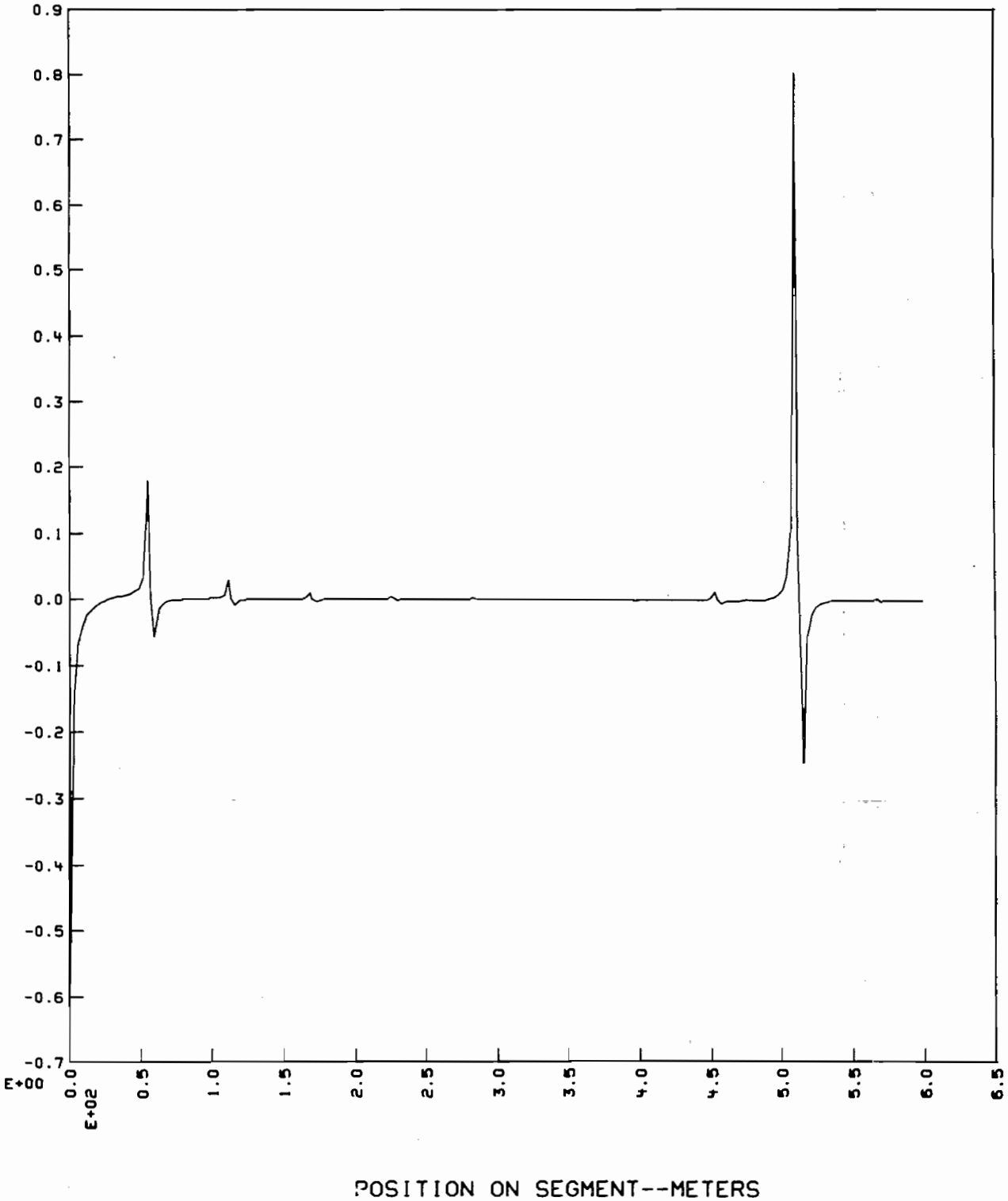

FIGURE 14c' Tangential electric field for V-dipole ($\delta/\Delta = 1/7$)

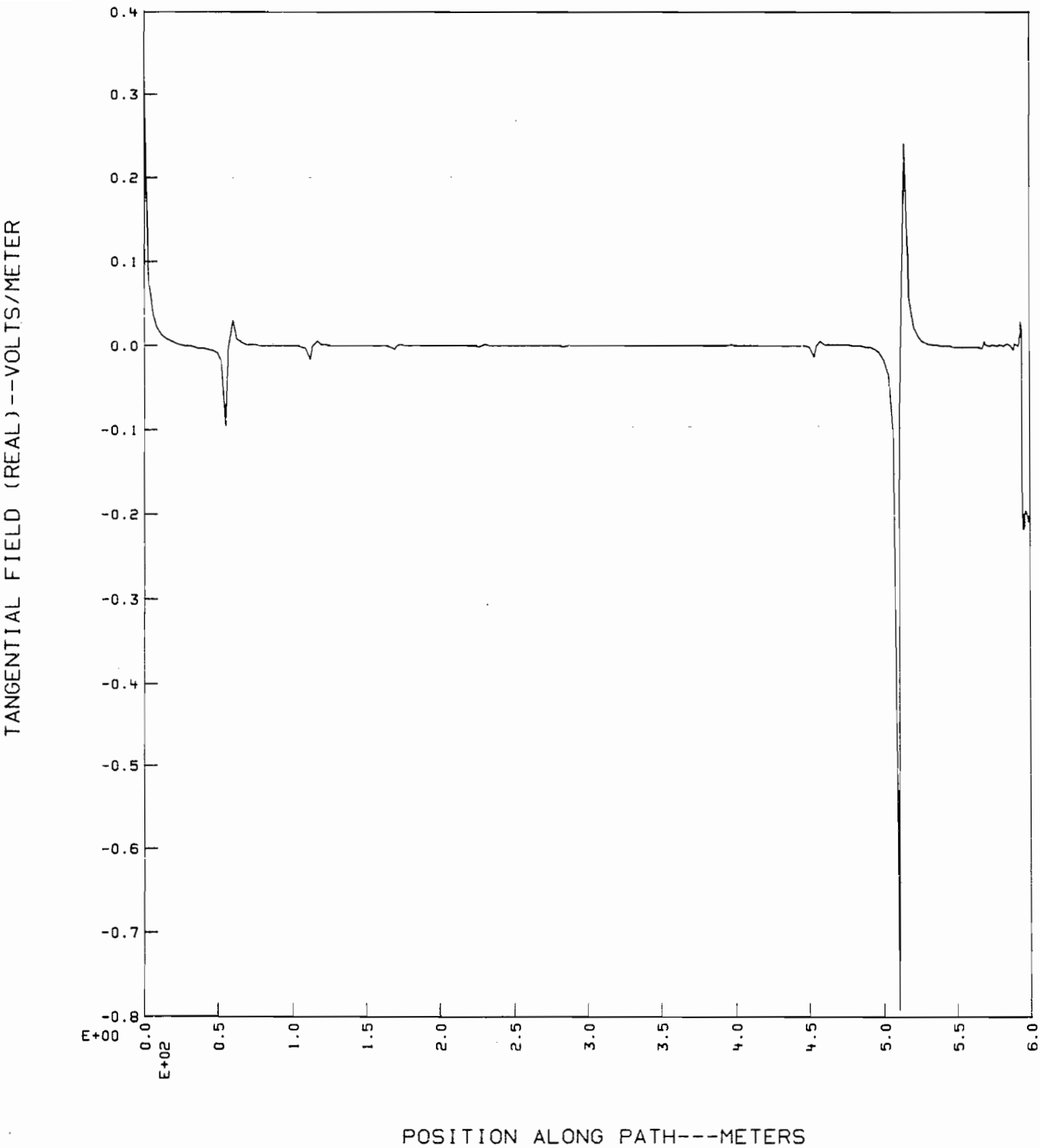

FIGURE 14c'' Tangential electric field for V-dipole (δ/Δ = 1/11)

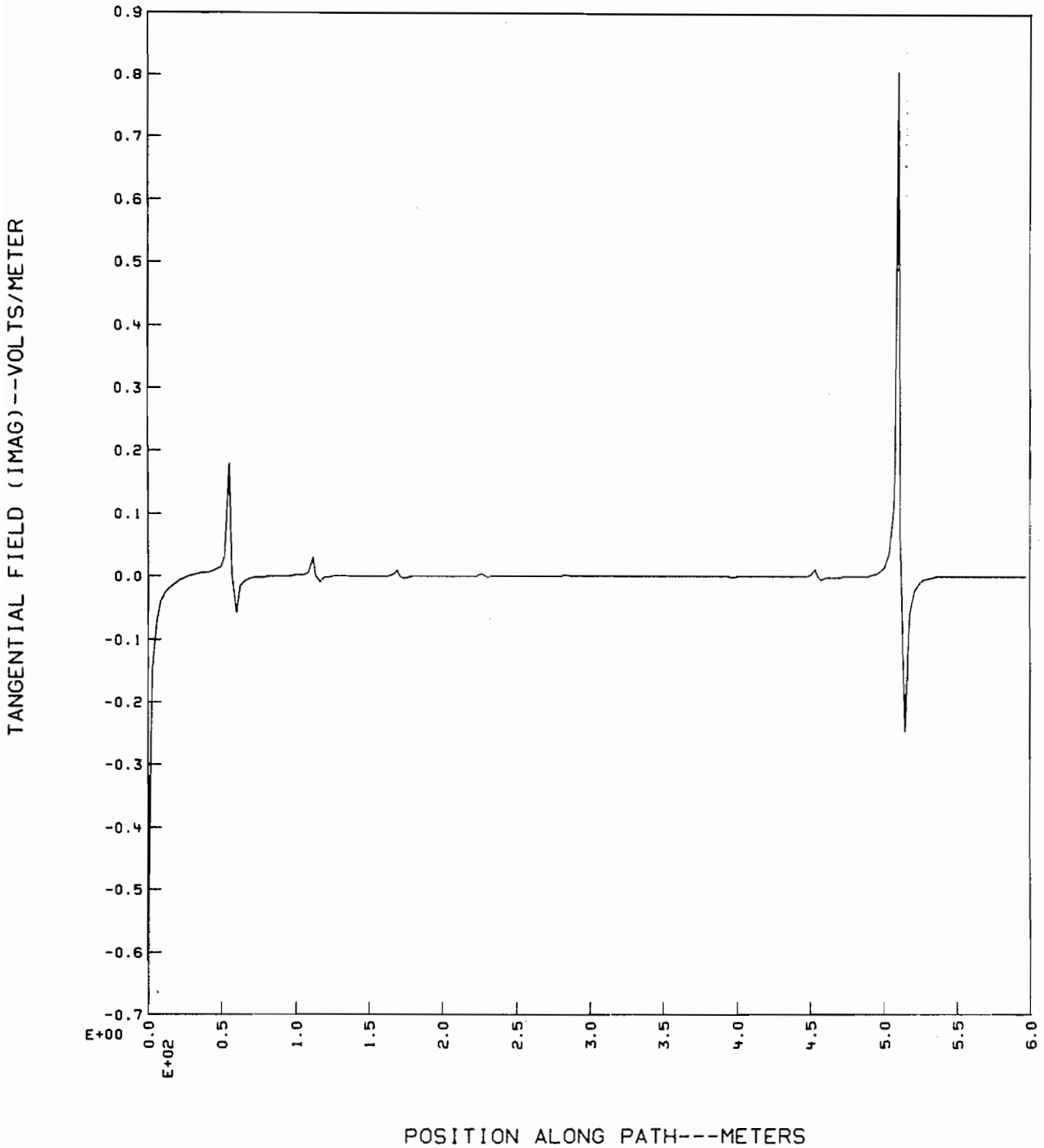

FIGURE 14c''' Tangential electric field for V-dipole (δ/Δ = 1/11)

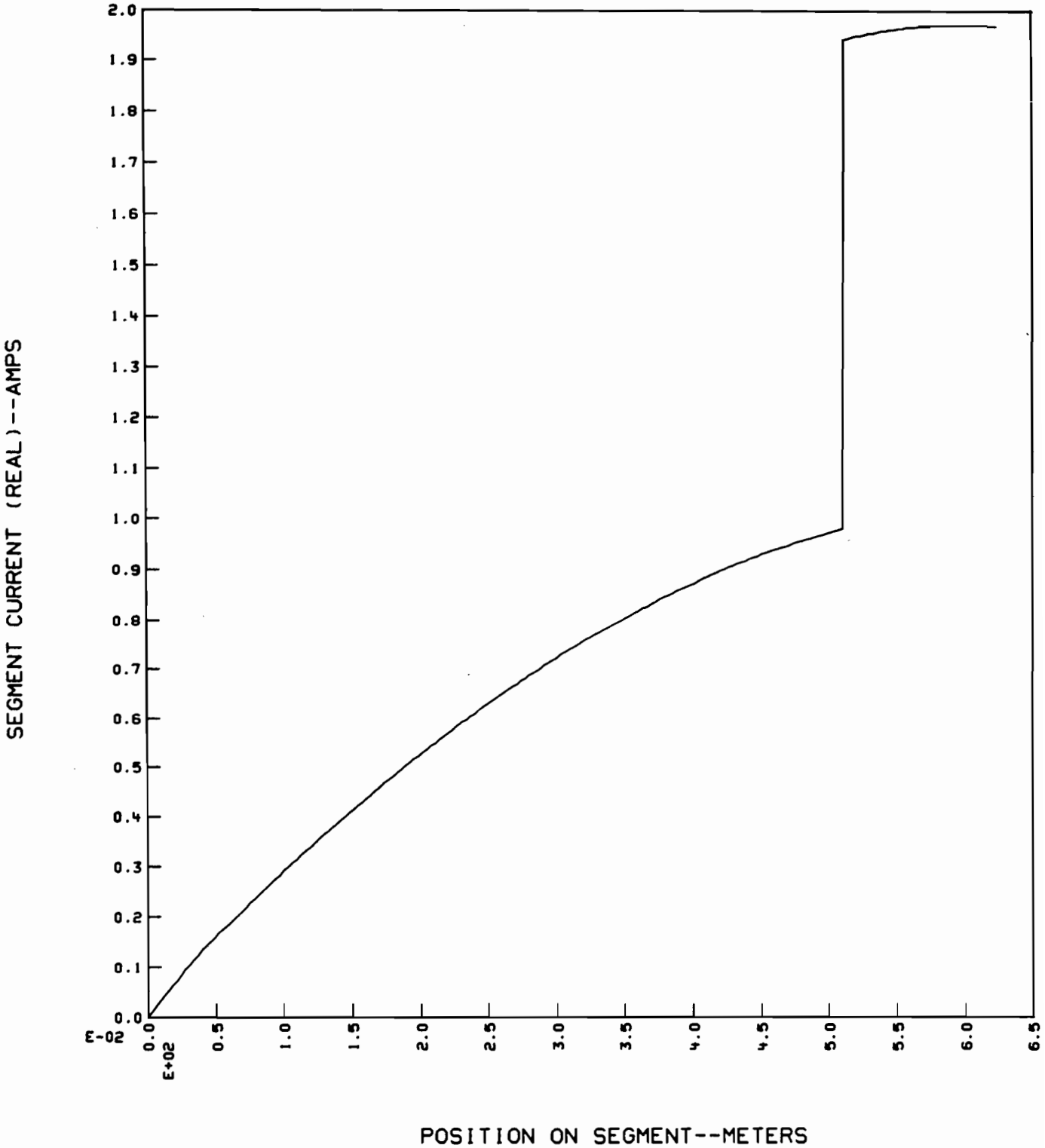

FIGURE 14d Current on V-dipole ($\delta/\Delta = 1$)

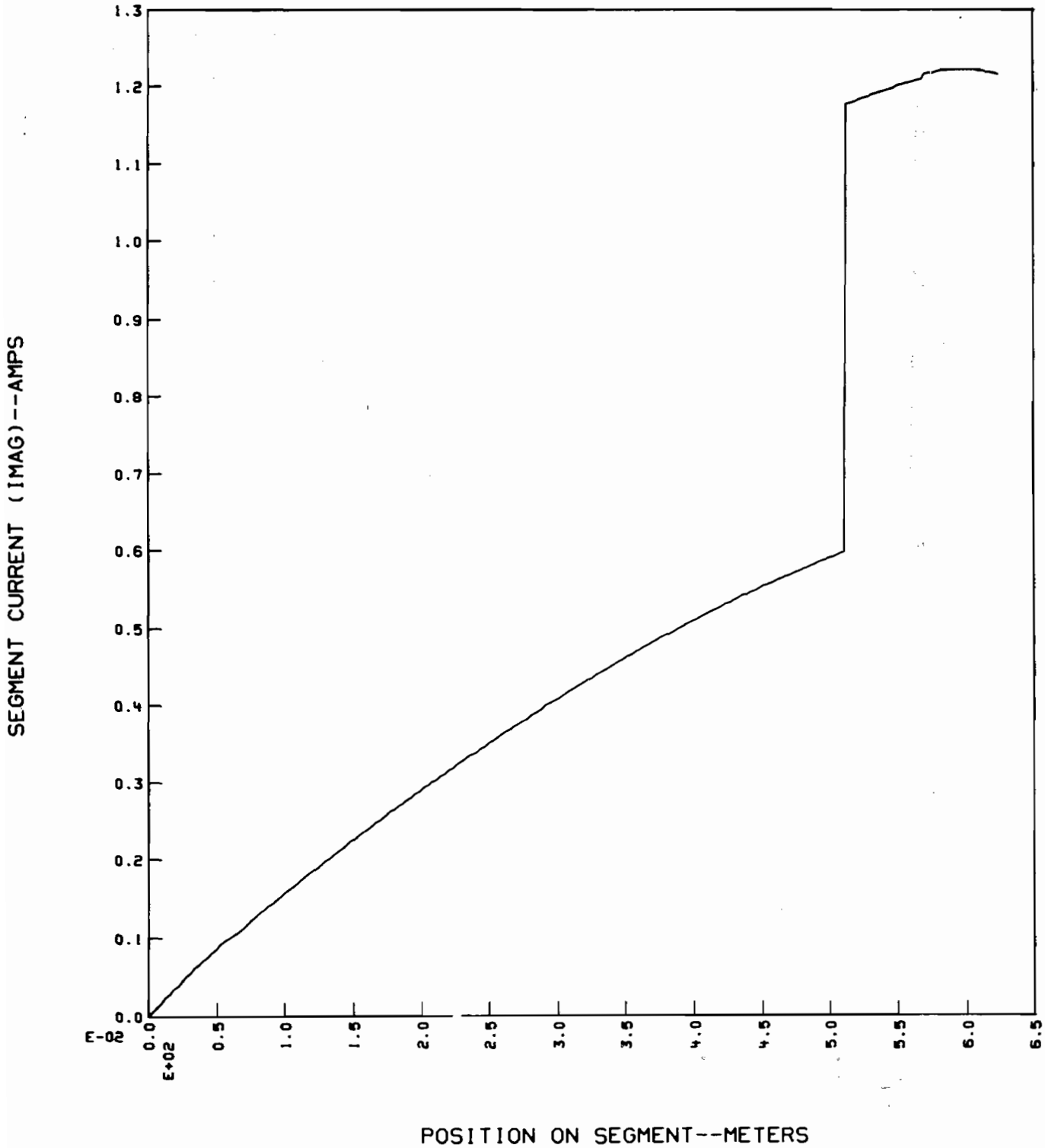

FIGURE 14d' Current on V-dipole (δ/Δ = 1), frequency = 100 kHz for all cases.

a tee. A sequence of calculations were performed for this geometry to obtain the normalized electric field intensity as a function of position along the wire in the vicinity of the junction equally spaced match points were used but with their separation distance a parameter. Results for the nominal geometry case are shown in Figure 15a, where 60 segments were used to model the entire antenna giving a segment length (Δ) to wire diameter (d) ratio of 100. The fields are evaluated along the top of the tee (as shown in the Figure) and extended ± 10 wire radii along the tee or cross wire. The uppermost line corresponds to a path along the wire surface with each successive line occuring at one radius step from the surface to a maximum distance of 20 radii. We see that the fields can increase by several orders of magnitude between the junction and the nearest match point,

A question we now wish to consider is to determine whether these field variations in the vicinity of the junction are real or are numerically generated because of the current basis function expansion or point matching procedure used in the program from which these results were obtained. A possible approach to answer this question is to segment the antenna more finely so that the match points can be brought arbitrarily close, within a wire diameter or so, of the junction. However, the small wire radius used to obtain these results in order to emphasize the near-field behavior in the vicinity of the junction precludes our using the number of segments this would require if the entire antenna were to be modeled with such short segments. Therefore, as a compromise, we have chosen to examine smaller and smaller portions of the antenna near the tee junction by successively decreasing the segment length and total wire length while maintaining a constant wavelength and wire diameter. In order to remove the near field dependence upon the changing impedance this procedure leads to, we again plot field intensities normalized to the maximum value, as in Figure 15 . Results for the two cases where $\Delta/d = 10$ and 1 are shown in Figures 15 and 15 .

We find that the region of large field value is always confined to within a half-segment length of the multiple junction. Furthermore, as the segment lengths themselves become smaller relative to the wire size the growth of the fields in the vicinity of the junction is reduced. When the segments become one wire diameter in length the field no longer significantly increases even in the vicinity of the junction and is thus seen to be reasonably well behaved.

From these results we can conclude that in the vicinity of either two wire or multiple wire junctions there is no significant increase in field value on approaching the junction until within a wire radius or so of the junction itself, a region in which our numerical results based on our thin wire model do not apply. But we also might hypothesize that it is permissible to smoothly extrapolate across the junction to determine the approximate near field behavior along the wire and to thus avoid the anomaly associated with the current discontinuity in the vicinity of the junction itself.

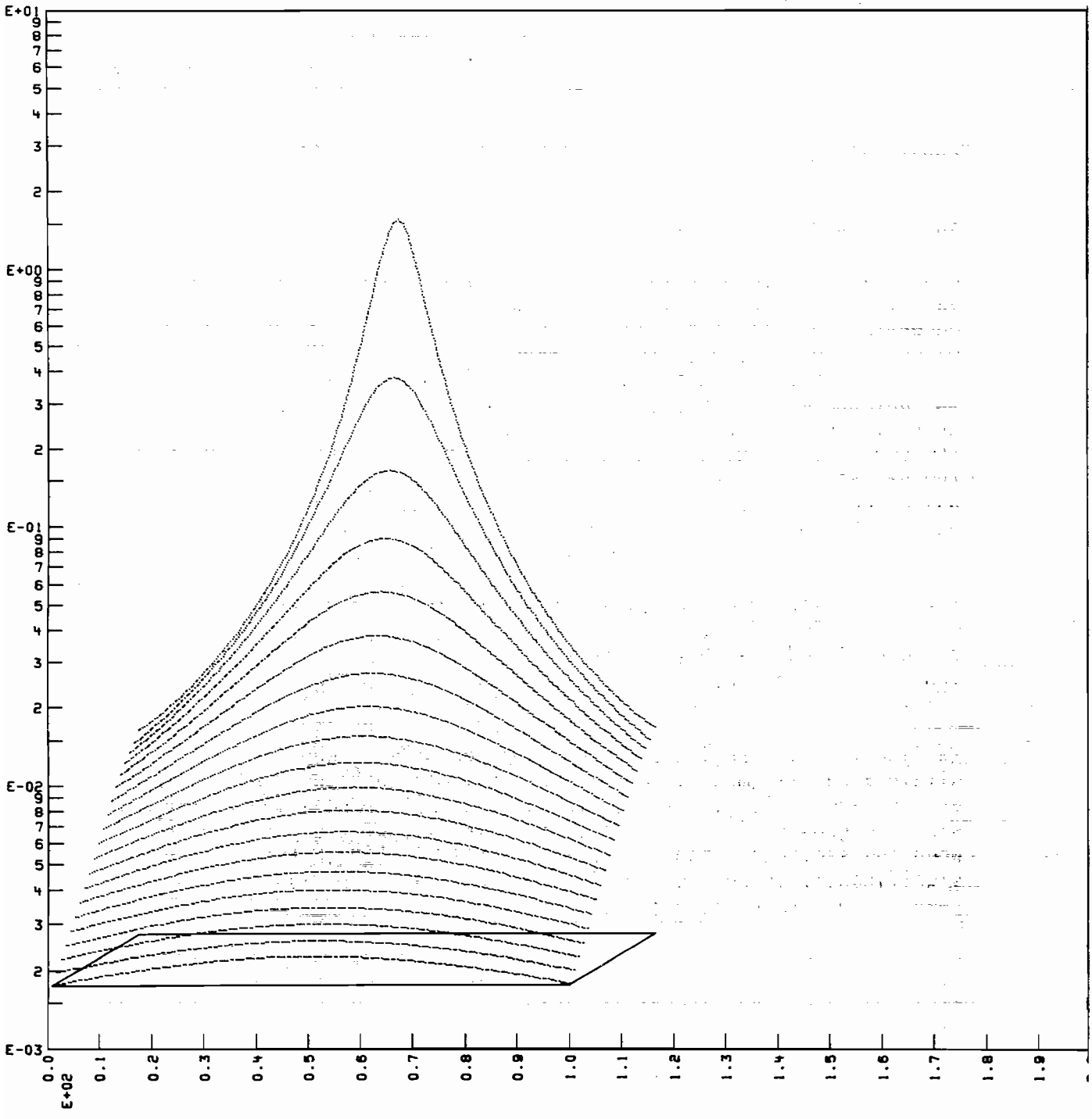

FIGURE 15 Near field on tee antenna segment length/diameter = 100

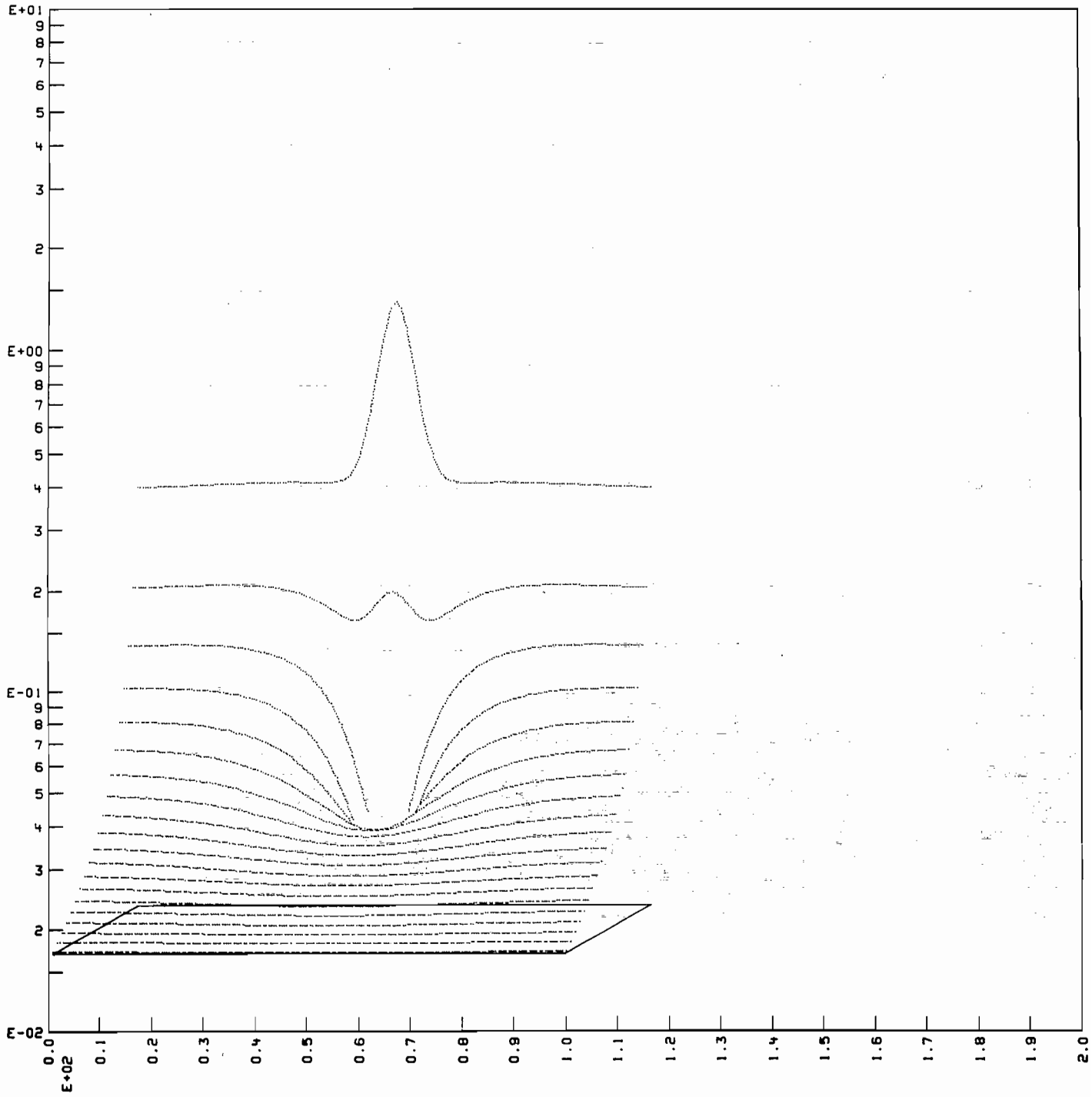

E-FIELD FRONT VIEW

FIGURE 15b Near field on tee antenna segment length/diameter = 10

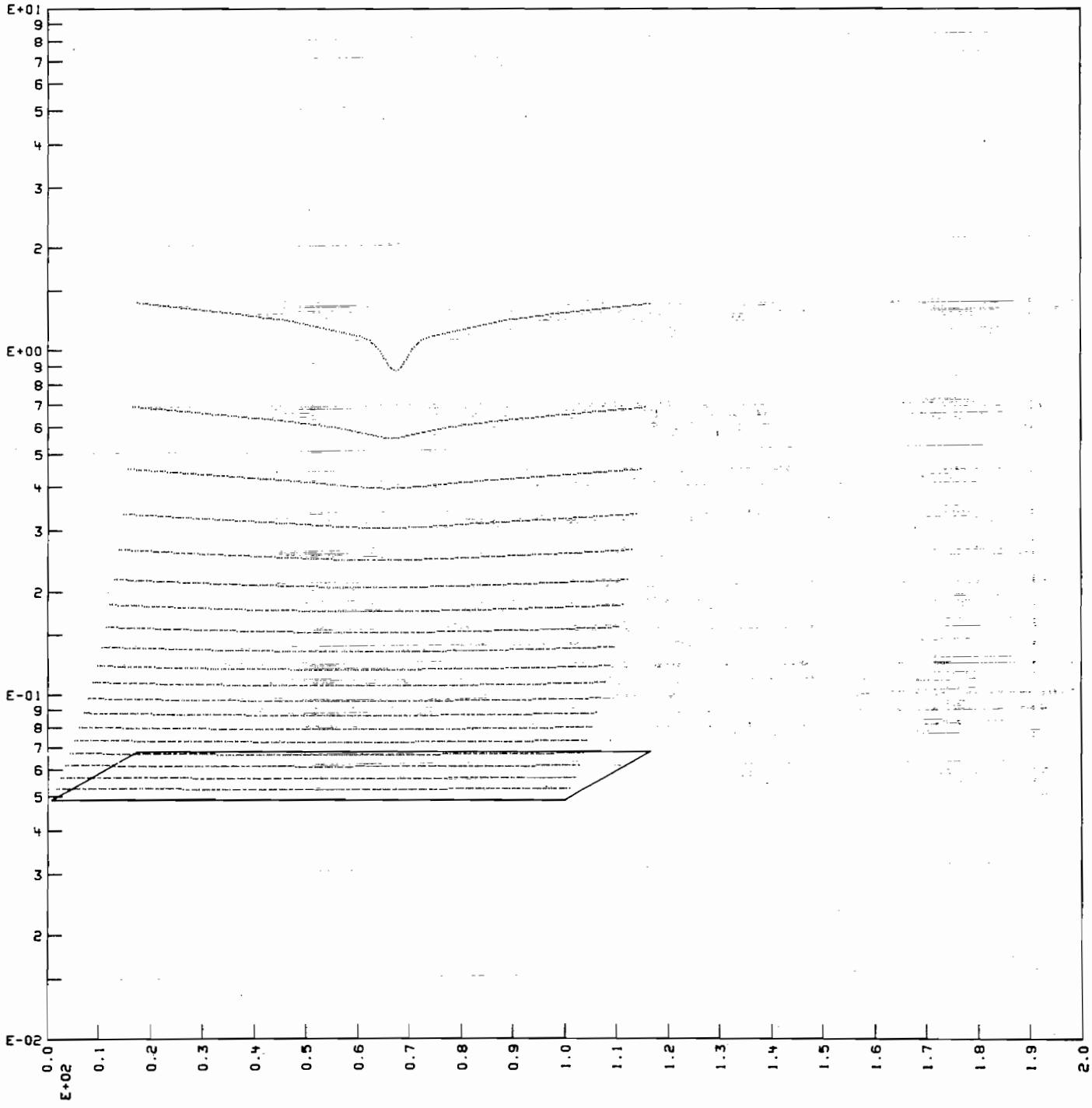

E-FIELD FRONT VIEW

FIGURE 15c Near field on tee antenna segment length/diameter = 1.

To conclude, we present a simple expression for determining the volumetric extent of the current discontinuity perturbation. The anamalous field due to the current discontinuity at a junction may exceed the actual field within a spherical volume of radius R given by [Miller and Deadrick (1973)].

$$R \sim \left[\frac{\Sigma I}{\Sigma |I|}\right]^{1/2} \Delta$$

where Δ is the length of the segments connected at the junction and the bracket term represents the normalized current discontinuity at the junction.

G. Wire Grid Modeling

Wire grid meshes find many uses in applications where the effect of a solid conducting surface is required but the weight and/or wind resistance of the latter must be avoided. They may be used, for example, to fabricate radar antenna reflectors, and as shields to screen sensitive equipment from stray fields. Their successful substitution for the solid surface depends upon the fact that as the mesh size becomes smaller relative to the shortest wavelength of concern; the mesh supports a surface current distribution which approaches that on the continuous surface. This phenomena occurs because of the transverse nature of electromagnetic fields, and does not hold for an acoustic field, which is longitudinal, for example.

Exploitation of wire grids as substitutes for solid surfaces need not be confined to actual practice, however, but can also be advantageous for the analytical study of certain problem types. Many problems of practical interest, for example radar cross-section studies, antenna analysis and EMP interactions, involve hybrid geometries which have features of both solid surface and wire-like structures. As such, these geometries are not well suited for treatment via the magnetic field integral equation (MFIE) (although this equation is apparently superior to the electric-field type for structures consisting only of solid surfaces). Furthermore, the magnetic field integral equation is not suited for the analysis of shell-like solid surfaces, such as thin plates and spherical shell sections. The thin wire approximation to the electric field integral equation (EFIE) however, offers a formulation which can in principle be used for treating all these geometries, by modeling the solid surface parts of such structures with wire grids. By extension of course, wire grids might then be used as well for the computer modeling of solid surface structures which might normally be treated via the MFIE.

As a matter of fact, wire grid models have already been quite widely used for a variety of problems and geometries. Richmond (1966) was apparently

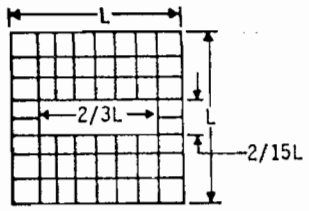

After Miller & Morton
(1970)

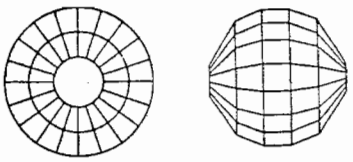

After Richmond
(1966)

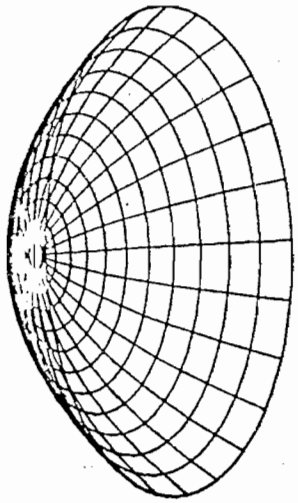

After Poggio & Miller
(1970)

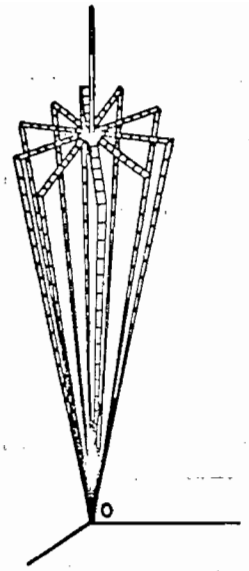

After Theile
(1970)

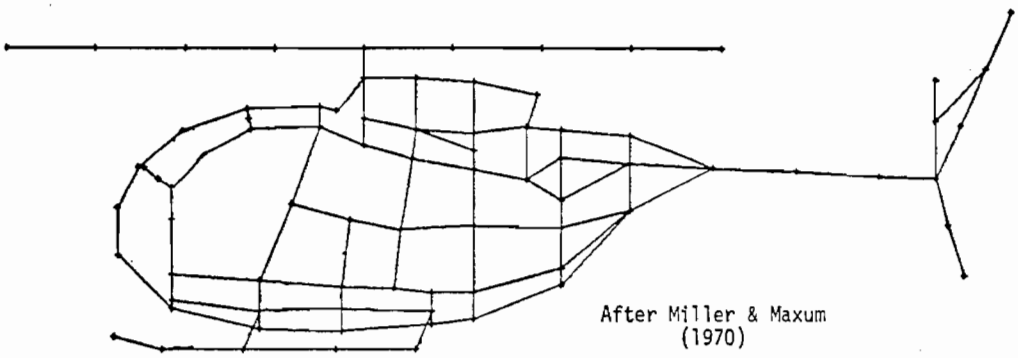

After Miller & Maxum
(1970)

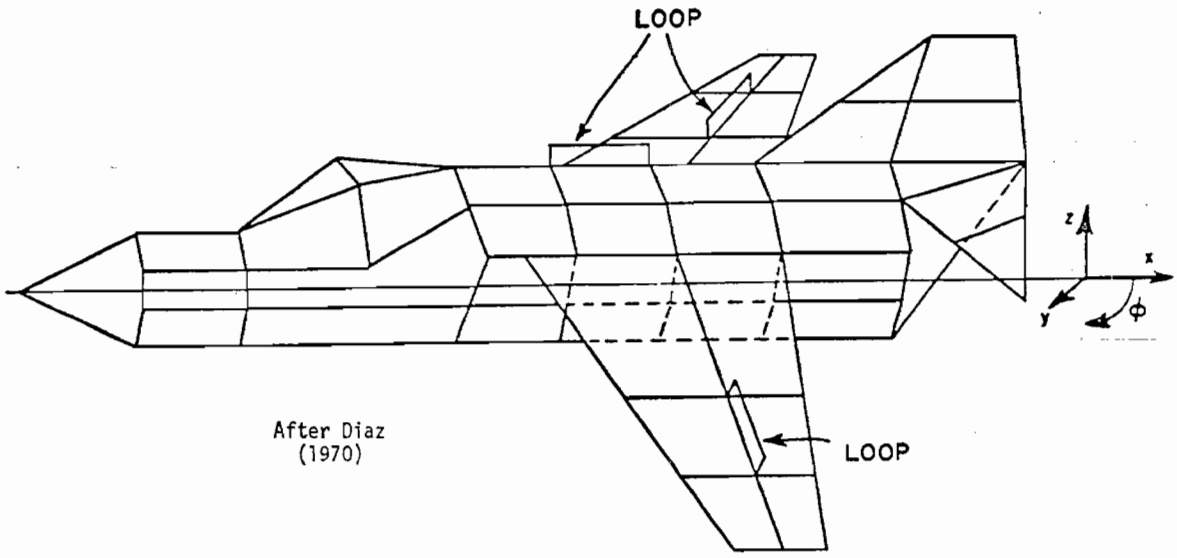

After Diaz
(1970)

FIGURE 16 Representative wire grid model structures.

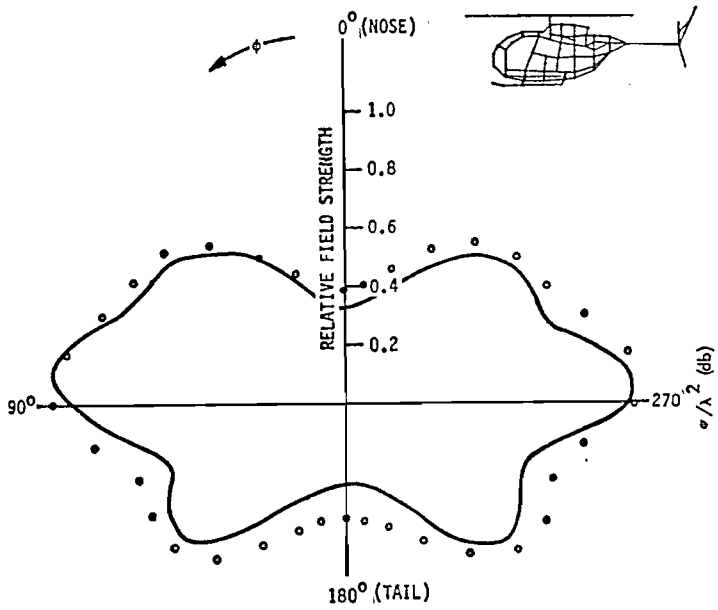

MEASURED* ——————

COMPUTED °

FREQUENCY = 41.75 MHz

*MICRONETICS, SAN DIEGO, CALIFORNIA

After Miller & Maxum (1970)

NUMERICAL-EXPERIMENTAL COMPARISON OF THE SCATTERED FIELD PATTERN OF AN OH-6A HELICOPTER WIRE GRID MODEL

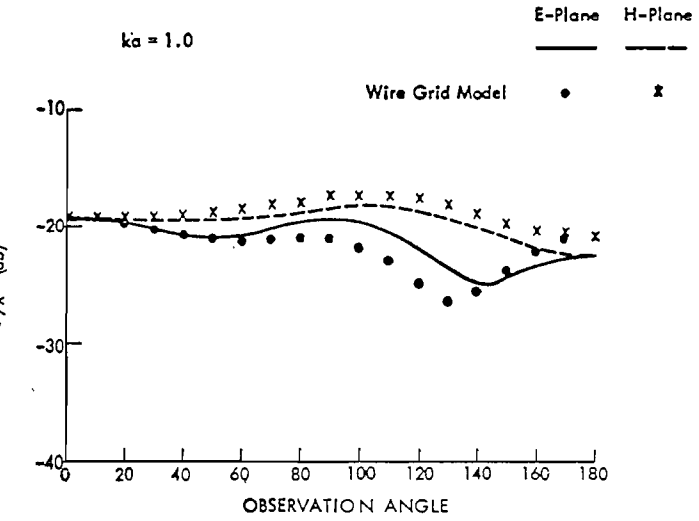

After Poggio & Miller (1970)

CONE-SPHERE BISTATIC SCATTERING PATTERN FOR TIP INCIDENCE (30 DEGREE INCLUDED CONE ANGLE) AS COMPUTED USING A WIRE GRID MODEL

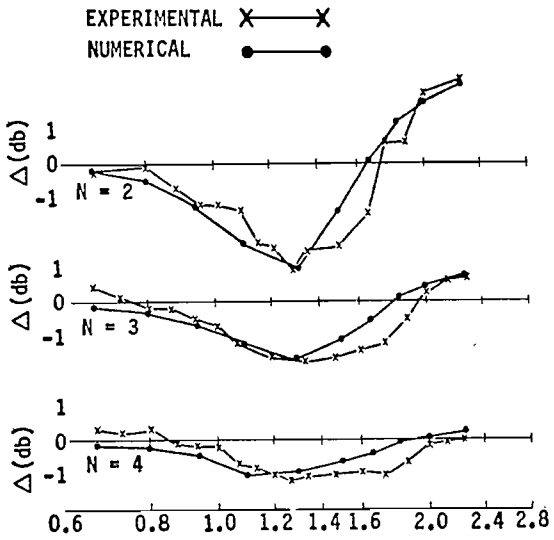

After Miller & Maxum (1970)

Backscatter RCS deviation of an N x N wire grid from that of a flat solid plate

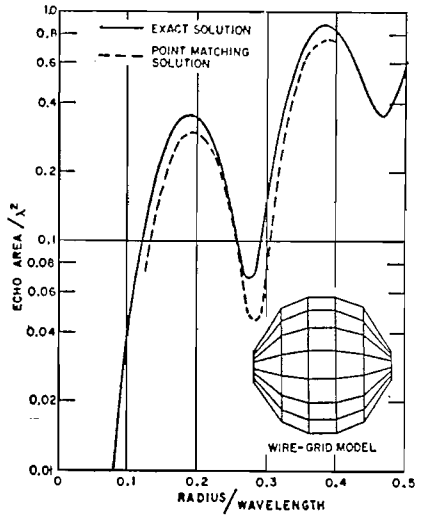

After Richmond (1966)

FIGURE 17a Numerical/Experimental Scattering Results for Wire Structures.

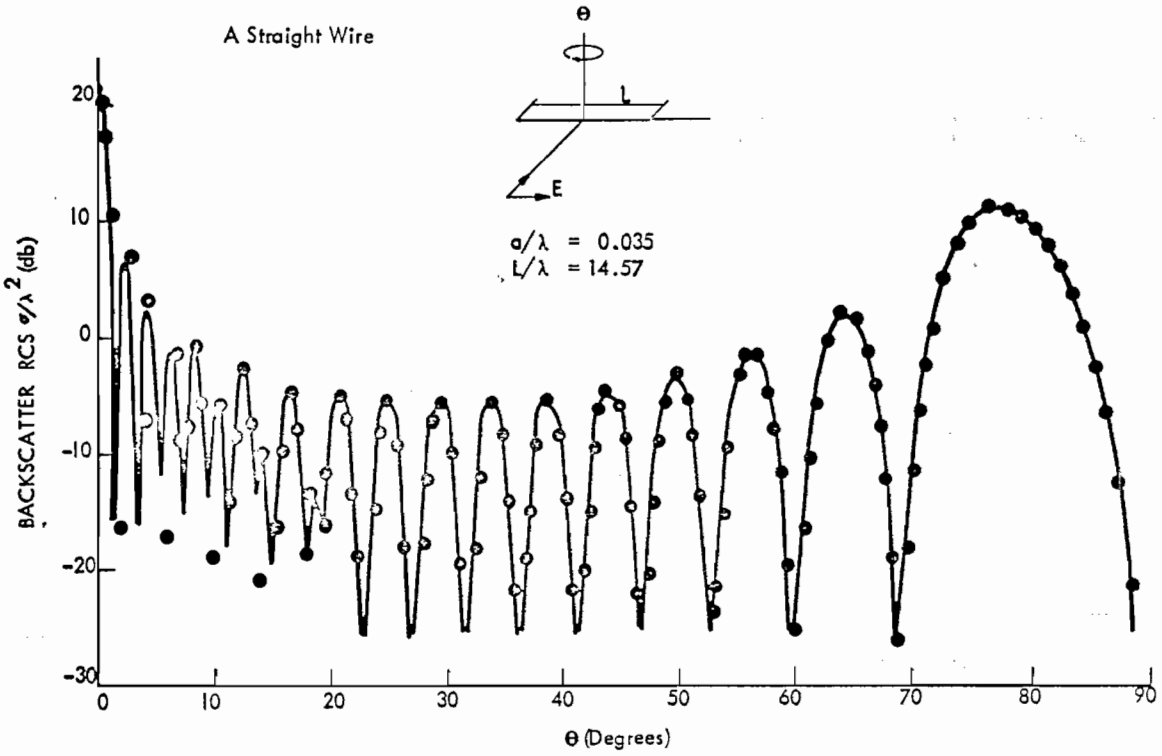

Comparison With Experiment of the Calculated (...) RCS of a Straight Wire vs Aspect Angle
After Poggio & Miller (1970)

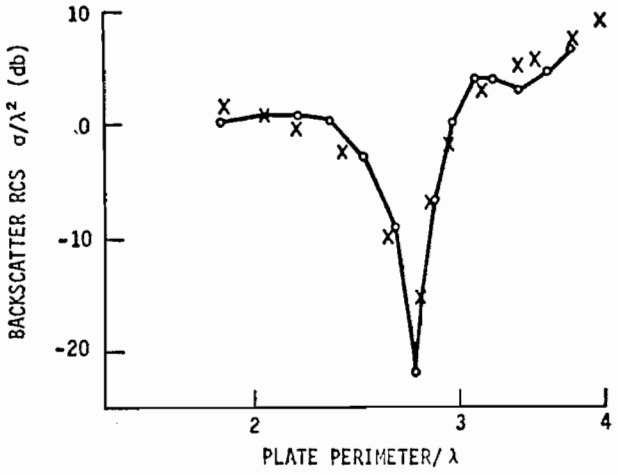

Frequency Variation of the RCS of a Slotted Wire Grid Calculated From the Thin-Wire Electric Field Integral Equation Compared with Measured Results.

After Miller & Morton (1970)

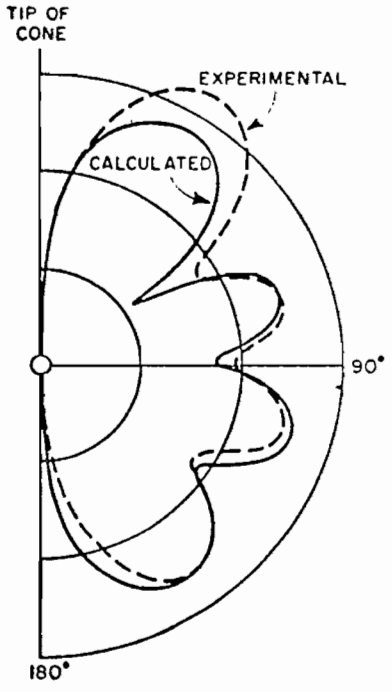

Calculated and Measured Patters for Single Slot Excitation of Cone

After Thiele (1970)

FIGURE 17b Numerical/Experimental Scattering Results for Wire Structures.

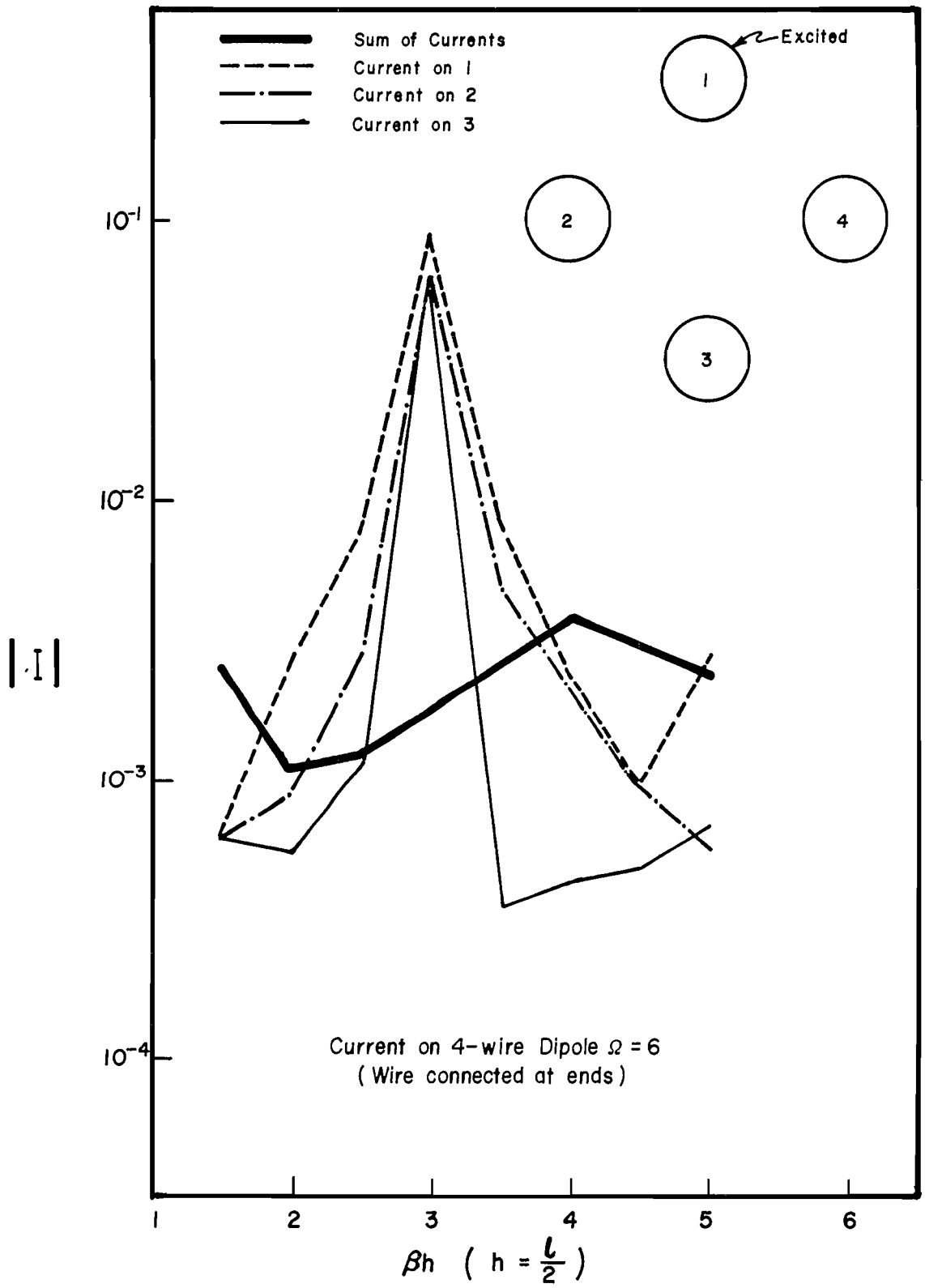

FIGURE 18a (After Burke and Selden, 1972)

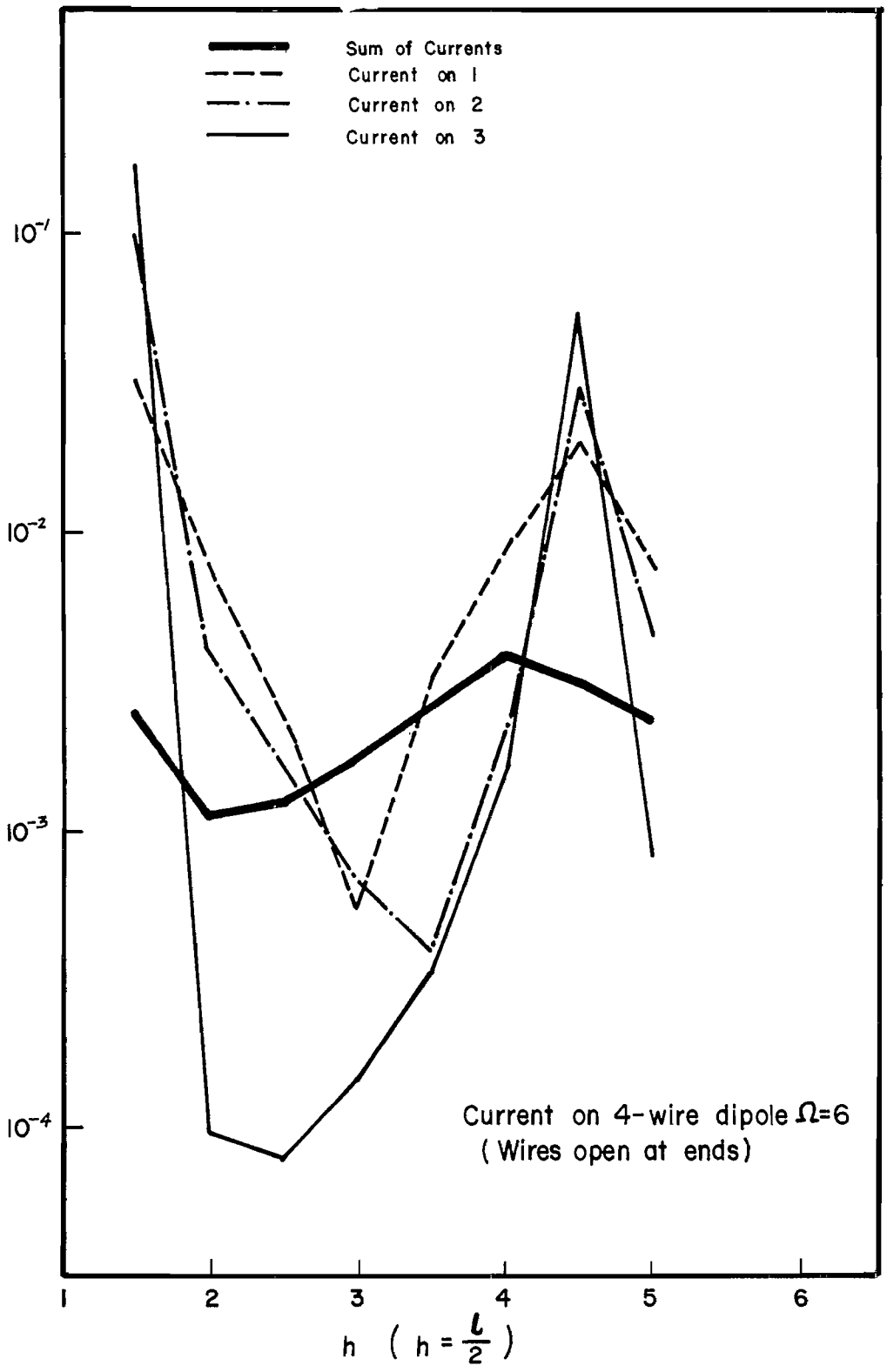

FIGURE 18b (After Burke and Selden, 1972)

the first to report on the application of the thin-wire EFIE to the analysis of wire grid models for circular disks and spheres. He demonstrated satisfactory agreement between his wire grid results and independent analytical or experimental back-scatter cross-section data presented as a function of frequency.

Subsequently, other wire grid results have been described by Tanner and Andreason (1967), Miller and Maxum (1970), Miller and Morton (1970), Thiele (1970), Diaz (1970), and Poggio and Miller (1970). These studies included the modeling of airplanes and helicopters, (Tanner and Andreason, Miller and Maxium and Diaz), a flat-backed cone, (Thiele), and flat plates, (Miller and Morton). Representative wire-grid model structures are depicted in Figure 16, with sample numerical results shown in Figure 17. In all cases, there was generally found to be reasonable agreement between theory and experiment for a far-field quantity such as the radar cross-section or antenna radiation pattern with the agreement relatively independent of the excitation (e.g., flat plate scattering was equally good for edge-on and broadside incidence).

These studies, while illustrating the applicability of wire grid meshes as models for solid surfaces in terms of their far field electromagnetic behavior, are not entirely convincing as to the use of wire grid models to determine near field quantities, such as charge density and surface current distributions. Preliminary studies in this regard to compare the results obtained with analytical models like spheres and circular disks with their wire grid counterparts are not yet conclusive. Such comparisons should do much to more clearly define the areas of application and limitations of wire grid models.

One particular test case which has been investigated and which does shed some light on the potential problems inherent in using wire grid models concerns a simple linear dipole antenna. The dipole antenna considered had an Ω value of 6 and is thus not suited to treatment via the thin wire integral equation because of the dipole's thickness. Therefore, Burke and Seldon (1972) have developed a simple wire model of this particular antenna by representing it with four equispaced, parallel wires, whose centers lie on the dipole's circumference. In order to determine the sensitivity of the results to the end of the antenna two sets of calculations were performed; one with the thin wires open-ended and the other with the wires cross connected at the ends of the dipole.

The input impedance was obtained as a function of frequency for the two models, results for which are presented in Figure 18. These impedance values were obtained for two different kinds of excitation, symmetric and asymmetric. In the former, the center segments on all four wires were excited with the same electric field, corresponding to a one volt source. For the asymmetric excitation only one of the four wires was excited, again with the field corresponding to a one volt source. The input admittance in each case was defined to be the sum of the currents on the center segment of the four wires. Both models yielded the value

for input impedance shown by the solid curve on the figures. This result is in fairly good agreement with that presented by King, whose values are also shown.

A significant difference is seen however in the individual wire currents for the two excitations. The variation with frequency of the individual currents on the three wires as indicated on the figure differs markedly from their sum. As a matter of fact that individual wire currents can become as large as two orders of magnitude greater than the resultant current for the four center segments. This situation evidently arises because the two pairs of wires effectively act as transmission lines whose currents are thus oppositely directed and of nearly the same magnitude. In order that the sum be that for the symmetrically excited configuration the individual wire currents can consequently become very large. Since the impedance characteristics of open and short-circuited transmission lines are phase shifted by $\lambda/4$, the wavelength region where this large excursion in individual wire currents occurs differs by half a wavelength for the two models. This result indicated that asymmetric excitation of the wire grid model for a solid surface may produce individual wire currents which are significantly different from those which would occur on a solid conducting surface itself. While in this case the composite effect did not exhibit a significant error, such happy circumstances can of course not always be guaranteed. A similar behavior has been found on other kinds of wire grid models for solid surfaces, e.g. by large circulating currents which are found to occur on the interior wire loops or mesh of wire grids (Burke and Seldon 1972).

H. Computer Time

In prior discussion we have not dealt in any specific way with the actual computer time requirements, or what is equivalent, the expense of performing a given calculation. Results such as those presented above in Section C are useful to demonstrate the convergence rate of a numerical solution as a function of the number of segments and to develop application guidelines. Such results do not in general however, indicate what method might offer the greatest efficiency to obtain a given accuracy in any particular application. The reason for this is that while the number of samples required per wavelength to achieve a given accuracy is one indicator of numerical efficiency, that alone does not provide a complete basis for comparison with other methods. In addition to the convergence rate itself, we must be concerned with the computer time required to compute the matrix, since it is this factor together with the convergence rate which determines the overall efficiency of a particular method.

The computer time associated with the moment method or matrix solution of an integral equation for a wire or surface structure can be obtained from the following equation:

$$t = AN^2 + BN^3 + CN^2N_i + DNN_iN_a$$

where N is the order of the linear system, or the number of unknowns, N_i is the number of incident fields or source configurations, and N_a is the number of observation points in the far field. The corresponding coefficients A, B, C, and D, represent the computer time associated with computing the impedance matrix, factoring or inverting it, computing the currents from the specified incident field and computing the far field, respectively. Obviously, a comparison of two different methods for solving a given problem is incomplete without considering both the number of samples, N, required to obtain a given accuracy from each and the timing coefficients associated with their use, i.e., we must compare t_1/t_2 rather than N_1/N_2 alone. Note that the coefficients A, B, C, and D, depend upon the method used and are thus both algorithm and computer dependent.

It is thus necessary when comparing alternative methods to have available the timing coefficients associated with their application referred to a common computer. Unfortunately such data is not easy to obtain. The various programs have generally been developed for use on different computers, have not been optimized and have not been used to analyze the same set of problems, information required to form a valid basis for comparison. We have however, been able to extract from published literature matrix fill time data for the program developed by Chao and Strait (1970) at Syracuse and that developed by Richmond (1969) of Ohio State. Let us further assume that the matrix factorization times will be generally comparable since there is relatively little variation associated with this particular operation, and that the current computation and far field evaluation times are relatively minor in terms of the overall computer time. We then obtain the following computer (CDC-6600) time requirements for the programs mentioned, and for the program utilized in obtaining the results presented in this report. These results are shown in Table IX below.

For convience, we have given the matrix fill time coefficient, A, for each of these methods and in addition the representative computer time required to solve a problem with N = 50, 100, and 200 segments. Generally speaking, there is not a substantial amount of difference between these various methods. It must be recognized that these computer programs are probably not optimized and that furthermore the details of the computation and consequent relative running times may vary from structure to structure. These data however do provide some indication of the computer times involved in using such programs.

Before concluding it is worthwhile to comment on the impact which symmetry has on the overall computational efficiency. Symmetry may be exploited in both the computation and storage requirements associated with an integral equation solution. Two distinct types of symmetry exists, mirror symmetry and rotational symmetry. Mirror symmetry may involve from one to three mutually othogonal planes about which structural symmetry occurs and can be characterized by

TABLE IX
Some Typical Calculation Times (seconds)
on a CDC-7600

	Matrix Fill Time			Matrix/Solve
N	3 Term $A = 4.1 \times 10^{-4}$	Piecewise Linear (Syracuse) $A = 2.6 \times 10^{-4}$	Piecewise Sinusoidal (Ohio State) $A = 3.7 \times 10^{-4}$	$B = 2.2 \times 10^{-6}$
50	1.0	0.7	0.9	0.3
100	4.1	2.6	3.7	2.2
200	16.0	11.0	15.0	18.0

the parameter $M = 2^m$ where $m = 1, 2,$ or 3 is the number of planes of othogonal symmetry. Rotational symmetry can be either discrete or continuous. Continuous symmetry is exhibited by a circular ring whereas discrete symmetry of order n is exhibited by an n sided regular polygon. It is possibly more useful to exploit discrete rotational symmetry over continuous rotational symmetry since the former can be employed for structures which are both continuously or discretely rotationally symmetric, whereas continuous rotational symmetry can of course be rigorously used only for structures with continuous symmetry. Note furthermore that discrete rotational symmetry is identical to mirror symmetry with $m = 1$ or 2. A structure can of course possess at the same time both mirror and discrete rotational symmetry, e.g. a square having an even number of segments per side. Discrete symmetry is characterized by $n = 2\pi/\alpha_n$ with α_n the minimum angle through which the structure must be rotated to reproduce itself.

The solution time exhibited by the equation above becomes, for a symmetric structure,

$$t \cong AN^2/M + BN^3/M^2 + CN^2N_I/M + DNN_IN_A/M$$

where

$$M = n2^m$$

and the $\cong$ is used since the actual time reductions realized depend upon the particular problem. Matrix storage requirements can furthermore be reduced by the factors m and n respectively for mirror and rotational symmetry. Taken together the effects of symmetry can significantly reduce the expense associated with a given computation and greatly enlarge the scope of applicability of the numerical solution procedure.

The mathematical aspects of symmetry exploitation are briefly summarized below. The symmetric matrices encountered using the moment method are called circulant, and are special forms of the more general Toeplitz matrix. A Toeplitz matrix has the form

$$Z = \begin{bmatrix} Z_1 & Z_2 & \cdot & \cdot & Z_n \\ Z_{n+1} & Z_1 & Z_2 & \cdot & \cdot \\ \cdot & Z_{n+1} & Z_1 & Z_2 & \cdot \end{bmatrix}$$

i.e., all entries in a given diagonal are equal. Straight wires yield Toeplitz matrices and can consequently be very efficiently modeled [Lytle and Lager (1973)]. The individual elements Z_1, Z_2, ... may themselves be matrices in which case Z is called block Toeplitz.

When the matrix is circulant, then it takes the form

$$Z = \begin{bmatrix} Z_1 & Z_2 & \cdot & Z_n \\ Z_n & Z_1 & Z_2 & Z_{n-1} \\ Z_{n-1} & Z_n & \cdot & Z_1 \end{bmatrix}$$

so that not only are the diagonals composed of equal entries, but the rows are repeated as well, though sequentially shifted from row to row. This property of course reduces the storage by 1/n. The inverse of a circulant matrix is also circulant. It is by making use of this fact, that we can reduce the number of computations to find the general inverse or factored form of Z by $1/n^2$. This is possible since the matrix product

$$ZZ^{-1} = I_N$$

with I_N the unit matrix of order N, can be written

$$Z_1 Z_1' + Z_2 Z_2' + \ldots + Z_n Z_n' = I_{N/n}$$

$$Z_N Z_1' + Z_1 Z_2' + \ldots + Z_{N-1} Z_n' = 0$$

.

.

.

$$Z_2 Z_1' + Z_3 Z_2' + \ldots + Z_1 Z_n' = 0$$

where the inverse matric elements are denoted by the primes. Note that this set of equations occurs n times in the product ZZ^{-1}

Upon systematically combining the product equations it is possible to express each Z_i' in terms of a linear combination of the Z_i. Since this equation is of order N/n, it can be factored (or inverted) in, $\sim (N/n)^3$ operations. But there are n of the Z_i so that the total operations are $\sim n(N/n)^3$ or N^3/n^2.

The procedure may be summarized as follows:

Let $S_{jk} = \exp[i(2\pi/n)(j-1)(k-1)]$; j, k = 1, ..., n

Form the matrix product (with $\sim$ denoting the complex conjugate of the transpose).

$$SZZ^{-1}\tilde{S} = I_N$$

from which we define the submatrices

$$S_i = \sum_{j=1}^{n} S_{ij}Z_j \qquad i = 1, \ldots, n$$

We can then show that

$$Z_i' = \frac{1}{n} \sum_{j=1}^{n} \tilde{S}_{ij}S_j$$

Note this operation is similar to a fast Fourier transform. Each of the S_i matrices corresponds to a single discrete mode. The source and current vectors can be similarly factored in terms of the same modes.

OBSERVATIONS AND CONCLUSION

The preceding discussion was intended to not only demonstrate some of the capabilities inherent in wire integral equation analysis, but also to emphasize some of the pitfalls and problems which can be only too easily encountered in its use. Some numerical anamolies such as negative input resistance for an isolated antenna, a current oscillation related to the sampling interval rather than the wavelength, or the divergence of a numerical result with increasing sample density, are obvious enough to alert even the inexperienced used to question a given result, although their rectification may not be equally obvious. The more subtle the problem however, the more difficult identification of its occurence and estimation of its impact on the validity of the calculated data. Consequently as a necessary adjunct to the sequence of operations involved in the overall modeling

procedure: (1) theoretical formulation, (2) mathematical manipulation; and (3) numerical computation, is (4) validation of the calculated result. It is probably safe to say that this last step may absorb as much time in the course of using a given program as the former three.

If it is concluded that validation is a key element in permitting a numerical method to be reliably and confidently used, we must then ask how this can best be realized. There are two obvious approaches: (1) experimental--comparison of the calculated results with measured data; and (2) numerical--comparison with independent theoretical results and/or internal numerical consistency checks.

Experimental validation is generally the most convincing, but measurement has its own difficulties which quite often frustrate its effectiveness in this role. While comparison of experimental and computed data in an absolute sense is probably preferable, much can be done on a relative basis, by for example, comparing the difference between calculations for two numerical models with corresponding measured data obtained from two similar experimental models. Also on a relative basis, two experimental models might be measured. The first should correspond as closely as possible to the numerical model, to provide a check on the numerical validity of the calculation. The second should resemble the real problem as closely as possible, to provide a check on the physical validity of the numerical model, which for all but the simplest problems will incorporate some degree of approximation, or which due to the formulation may completely alter the problem description. As an example of the former, we might use circular cylinders and flat planes to model an aircraft, while in the latter instance we might instead use a wire grid model.

As an addition or alternative to experimental validation we might choose a numerical route. Comparisons with independent theoretical results can involve quite similar steps to those discussed above in connection with experimental validation. We might for example compare wire grid results with analytical solutions for disks, spheroids, etc. The other area is that of internal consistancy checks. Some possibilities are:

1) Determine whether the bistatic scattered fields and mutual admittances satisfy reciprocity.
2) Evaluate the degree to which energy is conserved.
3) Insert the numerical solution into the original linear system.
4) Increase sampling density.
5) Plot current and charge distributions.
6) Examine the tangential fields to see the degree of boundary condition accuracy between match points.

Of the above, (1) and (2) are necessary but not sufficient conditions for solution validity. The third provides a check on possible matrix roundoff while (4) should provide an indication of the numerical convergence. Item (5) may indicate faulty results through obviously non-physical current and charge distributions. The sixth could probably be the most definitive, but

at the same time, most expensive to use. In addition, as has been shown above, the fields along the structure can exhibit obvious errors while the solution retains good accuracy.

An additional check we have not mentioned is physical intuition, a sometimes useful resource, but one unfortunately of uneven quality. It all too frequently happens that suspicious looking numerical (or for that matter experimental) data can after a time be explained on plausible physical grounds, followed then by discovery of the computational (experimental) error which was really the culprit.

In spite of the various kinds of checks to which the validation of computer produced results can be subjected, perhaps the best check of all is careful attention to detail in computer useage, both in the development of an algorithm and its subsequent application. A commonly heard truism in computing is "garbage in – garbage out". Certainly, the computer can provide no better output than the instructions and input which are given it. It is then extremely important to keep an open mind if the computer is to be most effectively exploited, both to question results which appear wrong, and to seek an explanation for results which conflict with our preconceptions.

REFERENCES

Andreasen, M. G. and F. B. Harris, Jr. (1968), Analysis of Wire Antennas of Arbitrary Configuration by Precise Theoretical Numerical Techniques, Contract DAAB07-67-C-0631, Tech. Report ECOM 0631-F, Granger Associates, Palo Alto, California.

Bacmain, K. G. (1969), "Dipole Admittance for Magneto Plasma Diagnostics," IEEE Transactions on Antennas and Propagation, AP-17, pp. 389-392.

Burke, G. J. and E. S. Selden (1972), Private Communication.

Cassidy, E. A. and J. Fainberg (1960), "Backscattering Cross Sections of Cylindrical Wires of Finite Conductivity," IRE Transactions on Antennas and Propagation Vol. AP-8, pp. 1-7.

Chao, H. H. and B. J. Strait (1970), "Computer Programs for Radiation and Scattering by Arbitrary Configurations of Bent Wires," Scientific Rept. No. 7 on Contract No. F19628-68-C-0/80; AFCRL-70-0374; Syracuse University, Syracuse, N.Y., September 1970.

Curtis, W. L. (1972), Private Communication.

Diaz, M. (1970), Figure 2-47 from Chapter 2 of "Computer Techniques for Electromagnetics and Antennas," Short Course Notes, U. of Illinois, September 28 - October 1, 1970.

Harrington, R. F. (1968), "Field Computation by Moment Methods," MacMillan, New York.

Landt, J. (1973), Private Communication.

Lytle, R. J. and F. V. Schutz (1969), "Prolate Spheroidal Antennas in Isotropic Plasma Media," IEEE Transactions on Antennas and Propagation, AP-17, pp. 496-506.

Lytle, R. J. and D. L. Lager (1973), "Application of Toeplitz Matrix to the Problem of a Dipole in a Warm Plasma," Northern California GAP Symposium, May 15, 1973.

Miller, E. K. (1967), "Admittance Dependence of the Infinite Cylindrical Antenna Upon Exciting GAP Thickness," Radio Science, Vol. 2, pp. 1431-1435.

Miller, E. K. and J. B. Morton (1970), "The RCS of a Metal Plate with a Resonant Slot," IEEE Transactions on Antennas and Propagation, AP-18, p. 290.

Miller, E. K. (1970), "A Variable Interval Width Quadrature Technique Based on Romberg's Method," Journal of Computational Physics, V. 5, No. 2, April 1970.

Miller, E. K. and B. J. Maxum (1970), "Mathematical Modeling of Aircraft Antennas and Supporting Structures," Final Report, ECOM Contract ADDB07-68-C-0456, Report No. ECOM-0456-1.

Miller, E. K., G. J. Burke, and E. S. Selden (1971), "Accuracy Modeling Guidelines for Integral-Equation Evaluation of Thin-Wire Structures," IEEE Transactions on Antennas and Propagation, AP-19, No. 4.

Miller, E. K. and F. J. Deadrick (1973), "Computer Modeling of LORAN Antennas," UCRL 51464, Lawrence Livermore Laboratory.

Mitzner, K. M. (1967), "An Integral Equation Approach to Scattering From a Body of Finite Conductivity," Radio Science, 2 (New Series) p. 1459.

Neureuther, A. R., B. D. Fuller, G. D. Hakke, G. Hohmann, et al., "A Comparison of Numerical Methods for Thin Wire Antennas," presented at the 1968 Fall URSI meeting, Department of Electrical Engineering and Computer Sciences, University of California, Berkeley.

Poggio, A. J. and E. K. Miller (1970), "Integral Equation Solutions of Three-Dimensional Scattering Problems" MBA Report No. MB-TM-70/20.

Richmond, J. H. (1965), "Digital Computer Solutions of the Rigorous Equations for Scattering Problems," Proc. IEEE, 53, p. 796.

Richmond, J. H. (1966), "A Wire-Grid Model for Scattering by Conducting Bodies," IEEE Transactions on Antennas and Propagation, AP-14, p. 782.

Richmond, J. H. (1972), Private Communication.

Richmond, J. H. (1969), "Computer Analysis of Three Dimensional Wire Antennas," Ohio State U., ElectroScience Lab., Technical Report 2708-4.

Sayre, E. P. (1973), "Junction Discontinuities in Wire Antenna and Scattering Problems," IEEE Transactions on Antennas and Propagation, AP-21, pp. 216-217.

Schelkenoff, A. A. (1952), "Advanced Antenna Theory," John Wiley & Sons, N. Y.

Sneior, T. B. A. (1960), "Impedance Boundary Conditions for Imperfectly Conducting Surfaces," Appl. Sci. Res., Sec. B, 8.

Strait, B. (1973), Private Communication.

Tanner, R. L. and M. G. Andreasen (1967), "Numerical Solution of Electromagnetic Problems," IEEE Spectrum, 4, No. 9, p. 53.

Thiele, G. A. (1969), "The Maximum Echo Area of Imperfectly Conducting Dipoles," IEEE Transactions on Antennas and Propagation, AP-17, pp. 379-381.

Thiele, G. A. (1970), "Wire Antennas," Chapter 2 of "Computer Techniques for Electromagnetics and Antennas," Short Course Notes, U of Illinois, September 28 - October 1, 1970.

Yeh, Y. S. and K. K. Mei (1967), "Theory of Conical Equiangular Spiral Antennas: Part I - Numerical Techniques," IEEE Transactions on Antennas and Propagation, AP-15, p. 634.